

**MODELING OF LOW SALINITY ENHANCED OIL RECOVERY
APPLYING ARTIFICIAL INTELLIGENCE**

A thesis submitted to the
UPES

For the award of
Doctor of Philosophy
In
Petroleum Engineering

BY
Tony Thomas

July 2024

Supervisor
Dr Pushpa Sharma
Distinguished Professor

Co-Supervisor
Dr. Dharmendra Kumar Gupta
Professor



Department of Petroleum Engineering & Earth Sciences
Energy Cluster
School of Advanced Engineering
UPES
Dehradun – 248007: Uttarakhand

**MODELING OF LOW SALINITY ENHANCED OIL RECOVERY
APPLYING ARTIFICIAL INTELLIGENCE**

A thesis submitted to the
UPES

For the award of
Doctor of Philosophy
In
Petroleum Engineering

BY
Tony Thomas
(SAP ID 500065488)

Supervisor
Dr. Pushpa Sharma
Distinguished Professor
Department of Petroleum Engineering & Earth Sciences
Energy Cluster
UPES, Dehradun

Co-supervisor
Dr. Dharmendra Kumar Gupta
Professor
Sustainability Cluster
UPES, Dehradun



Department of Petroleum Engineering & Earth Sciences
Energy Cluster, School of Advanced Engineering
UPES

Dehradun – 248007: Uttarakhand
July 2024

JULY 2024

DECLARATION

I declare that the thesis entitled ‘Modeling of Low Salinity Enhanced Oil Recovery Applying Artificial Intelligence’ has been prepared by me under the guidance of Dr. Pushpa Sharma, Distinguished Professor and Dr. Dharmendra Kumar Gupta, Professor. No part of this Thesis has formed the basis for the award of any degree or fellowship previously.



Tony Thomas

SAP ID 500065488

Department of Petroleum Engineering & Earth Sciences,
Energy Cluster, School of Advanced Engineering,
UPES,
Dehradun– 248007, Uttarakhand

THESIS COMPLETION CERTIFICATE

This is to certify that the thesis entitled “**Modeling of Low Salinity Enhanced Oil Recovery Applying Artificial Intelligence**” submitted by **Mr. Tony Thomas** (SAP ID: 500065488) in fulfilment of the requirements for the award of the degree DOCTOR OF PHILOSOPHY in Petroleum Engineering is an original work carried by him under our supervision and guidance.

It is certified that the work has not been submitted anywhere else for the award of any other diploma or degree of this or any other University.

Supervisor



Dr. Pushpa Sharma
Distinguished Professor
Department of Petroleum Engineering & Earth Sciences
Energy Cluster
School of Advanced Engineering,
UPES
Dehradun -248007, Uttarakhand
Date: **19/07/2024**

Co-Supervisor



Dr. Dharmendra Kumar Gupta
Professor
Sustainability Cluster
School of Advanced Engineering,
UPES
Dehradun -248007, Uttarakhand
Date: **19/07/24**

ABSTRACT

The different major reservoirs around the world are past their peak primary production and many of them are on ‘secondary’ production and/or ‘tertiary’ production schemes. Enhancement of the Recovery of hydrocarbon (‘EOR’) is the tertiary production scheme that has been applied with reasonable success in improving the hydrocarbon production rate, the recovery factor and extending the life of the hydrocarbon reservoirs. Different types of enhanced methods of hydrocarbon recovery are currently employed depending on the different reservoir parameters. The ‘EOR’ methods can be categorised as chemical, thermal, gas (miscible/immiscible) and microbial. One of the ‘EOR’ methods that has been gaining increasing focus and investigation in the last decades is Different Composition waterfloods (DCWF) which is also known by different trademark names of low salinity waterflood, smart waterflood, bright water and local flooding. DCWF is waterflooding with a different constituent and salinity of the water as compared to the insitu water. The claim to fame of this DCWF EOR technique is its ease of implementation due to water being used as the displacing phase and from the minimal requirement from surface and subsurface facilities perspective.

DCWF though facilitates ease to implementation, the governing mechanisms behind a successful DCWF is yet to be understood. Decades of research have highlighted that the mechanisms behind the success of DCWF depend on multiple parameters related to the rock, brine/water, hydrocarbon/oil and system/reservoir and their interactions/interplays. This research performs a meta-analysis of the various experiments to understand the critical parameters and mechanisms and develops a critical screening system that helps to provide fast and efficient screening of reservoirs for its suitability towards DCWF. This research then analyses and applies the different artificial intelligence and machine learning algorithms towards modelling and prediction of the performance of recovery factor from the DCWF which hasn’t been investigated before. Furthermore, research experiments from multiple reservoirs from across the world from the north sea sandstones to the middle east carbonates are analysed and incorporated into the meta-analysis. This research work is further augmented through use of physics based models utilized into the data set and application of AI/ML techniques towards the screening and prediction of the performance is performed with high level of accuracy as reported through this research work.

ACKNOWLEDGEMENT

I would like to thank my supervisor Dr Pushpa Sharma and co-supervisor Dr Dharmendra Kumar Gupta for their continuous guidance, support, encouragement, advise and blessings in completing my academic journey. Without their presence this wouldn't have been possible and for that I will be forever appreciative.

My sincere appreciation to the petroleum engineering department faculty who have been a source of support and guidance especially Dr Vamsi Krishna Kudapa. I would also like to express my appreciation to the research administration and leadership team at UPES for their supporting processes in place, their timely reminders and their support in clarification and progression of this research journey. My gratitude also goes out to Dr Devesh Kumar Avasthi, Dean – R&D, Dr Pankaj Kumar, Dr S M Tauseef, Mr. Rajeev Kumar Attari, Mr. Yogesh Kumar Sharma and other members of the FRC/SRC. My gratitude also goes out to Dr Nilanjana Banerjee, Head, Energy Cluster for her encouragement and support. This has been a multi-year journey and I know there are many more who have helped me to reach this stage and to all of them your support and timely guidance is appreciated.

Appreciative of having the support of family and friends, especially my wife Sharon , my sons Marc and Luke, my parents Thomas and Veena, my parents-in-law Sebastian and Josephine, my sisters Tina and Pamela, my friends John, Riadh, Djamel, Ahmed El-Banbi, Razzik, Lucy, Marina, Rita, Sonia. There are many more of you who truly prayed for me, stuck with me through all the struggles, at various points in this journey, without you all I wouldn't be here.

Finally, above all, grateful to God, for being able to experience this academic journey and to reach this stage.

(Tony Thomas)

TABLE OF CONTENTS

DECLARATION	iii
ABSTRACT	i
ACKNOWLEDGEMENT	ii
TABLE OF CONTENTS	iii
LIST OF TABLES	v
LIST OF FIGURES	vi
CHAPTER 1 : INTRODUCTION & RESEARCH OBJECTIVES	1
CHAPTER 2: LITERATURE REVIEW	5
2.1 Water Flooding Process And Evaluation Methods.....	5
2.1.1 Microscopic Efficiency	9
2.1.2 Macroscopic Displacement Efficiency	10
2.2 Low Salinity Water Flooding Process, Mechanisms and Evaluation Methods	11
2.3 Modeling of DCWF At Different Scales	25
2.4 Operational Aspects and Monitoring	36
2.5 Economic Considerations.....	40
CHAPTER 3 : UNDERSTANDING OF THE CRITICAL MECHANISMS FOR DIFFERENT COMPOSITION/SALINITY EOR ASSOCIATED SIMULATION	42
3.1 Mechanisms of Different Composition/Salinity EOR	43
3.2 Modeling and Simulation of Different Composition/Salinity (Eclipse).....	49
CHAPTER 4 : ARTIFICIAL INTELLIGENCE METHODS APPLIED IN EOR	55
4.1 Overview Of Various Artificial Intelligence Methods And Algorithms	58
4.2 Selection Of Approach For Different Composition/Salinity EOR.....	67
CHAPTER 5: EOR SCREENING METHODOLOGY AND MODELING APPLYING ARTIFICIAL INTELLIGENCE	76
5.1 Screening Matrix.....	76
5.2 Screening Methodology (AI/ ML).....	79

CHAPTER 6 : DATA SELECTION FOR DIFFERENT COMPOSITION/SALINITY FLOODING AND COMPARISON BETWEEN DIFFERENT METHOD.....	91
6.1 Corefloods	91
6.2 Single Well Data.....	95
6.3 Sector Models 2D and 3D	97
6.4 Validation and Application of Optimum Model.....	99
CHAPTER 7 : SUMMARY, CONCLUSIONS AND RECOMMENDATIONS	108
REFERENCES	113
Appendix A.....	124
LIST OF PUBLICATIONS.....	138

LIST OF TABLES

Table 2-1: Reject stream options for onshore project. The choices in red are least favourable (Sorop et al., 2013).....	39
Table 3-1: Summary of the critical DCWF mechanisms	44
Table 4-1: Summary of AI/ML Challenges.....	66
Table 4-2: Input features with removal of features of low variance.....	68
Table 5-1: Expert system results with different cases.....	77
Table 5-2: Key input and output parameters for DCW physics based model	80
Table 5-3: Statistics of the parameters for DCW EOR physics based model	80
Table 5-4: Training performance scores from multi-variate linear regression.....	81
Table 5-5: Testing performance scores from multi-variate linear regression	82
Table 5-6: Prediction Results and the Error % from multi-variate linear regression	82
Table 5-7: Statistical Summary of the Various Input Parameters from DCW Experiments... 84	
Table 5-8: Random Forest Training performance scores.....	87
Table 5-9: Random Forest Testing performance scores.....	88
Table 5-10: Random Forest Prediction Results and Error%	88
Table 5-11: AdaBoost Training performance.....	89
Table 5-12: AdaBoost Testing performance	89
Table 5-13: AdaBoost Prediction and Error%.....	90
Table 5-14: Performance metrics comparison between various AIT/ML models	90
Table 6-1: Parametric Summary through physics based modeling	97
Table 6-2: Data Matrix of different parameters impacting the DCWF.....	100
Table 6-3: Random Forest Training Metrics	102
Table 6-4: Random Forest Testing Metrics.....	103
Table 6-5: Random Forest Feature Importance	103
Table 6-6: Gradient Boosting Training Metrics	104
Table 6-7: Gradient Boosting Testing Metrics	105
Table 6-8: Gradient Boost model Feature Importance.....	105
Table 6-9: Comparison of Recovery Factor between lab/field work and AI/ML models	106
Table 6-10: RF% Prediction Vs Original Simulation	107
Table 6-11: RelPerm Kromax.....	107

LIST OF FIGURES

Figure 2-1: Zeta Potential definition in electrical double layer of the particle.....	14
Figure 2-2: Interaction of PDIs (a) Calcium and Sulphate interaction (b) Magnesium and Sulphate at high temperature interaction.....	14
Figure 2-3: Crude to surface attraction involving divalent cations (Lager et al., 2007).....	16
Figure 2-4: Crude oil attachment to the rock surface by ionic assistance.....	17
Figure 2-5: Candidate Well Selection Criteria (Yousef, Liu, et al., 2012)	19
Figure 2-6: Core flooding experimental setup (Hadia et al., 2013).....	21
Figure 2-7: Comparison of recovery of oil versus synthetic brine injection(PV) at different wettability conditions (Hadia et al., 2013)	21
Figure 2-8: Pressure differential transversing the core-plugs for different wettability conditions during synthetic brine injection	22
Figure 2-9:Relation between secondary waterflood oil recovery and initial core wettability at high and low salinity brines injection (Hadia et al., 2013).....	22
Figure 2-10: Effects of injection brine salinity on saturation of residual oil for varying wettability post secondary waterflooding (Hadia et al., 2013).....	23
Figure 2-11: (a) Representation of the core plug with oil and connate water saturation in the Amott glass container. Produced oil is collected in the measuring cylinder (b) A schematic representation of the Amott test (Romanuka et al., 2012).....	24
Figure 2-12: EtF (Ethyl Formate) and EtOH (Ethanol) flow	25
Figure 2-13: Integrated workflow to improve understanding of DCW (Suijkerbuijk et al., 2013)	26
Figure 2-14: Experimental set up of Micromodel investigation (Schumi et al., 2020)	27
Figure 2-15: a) Oil and Water saturations depicted by the grey and red colours respectively (b) Formation of oil bank depicted by the white arrows (Schumi et al., 2020).....	28
Figure 2-16: Coreflooding experimental set up schematic	29
Figure 2-17: RF Vs PV injected for a various coreflood experiments. A refers to Alkali, P to polymer and C to cosolvent.....	29
Figure 2-18: Sor vs effective molar Gibbs free energy (Al-Shalabi et al., 2016).....	31
Figure 2-19: Oil end point relperm as a function of effective molar Gibbs free energy (Al-Shalabi et al., 2016).....	32
Figure 2-20: Corey's exponent for oil as a function of effective molar Gibbs free energy (Al-Shalabi et al., 2016).....	32

Figure 2-21: Cumulative Oil Recovery history matching (Al-Shalabi et al., 2016).....	33
Figure 2-22: Pressure drop history matching (Al-Shalabi et al., 2016)	33
Figure 2-23: Heat Map indicating Collinear features	36
Figure 2-24 Sandstone and Carbonate Models showing evolution of fraction of water to total liquid and hydrocarbon recovery factor with respect to heterogeneity.....	38
Figure 2-25: Membrane Desalination Integration into waterflood facilities.....	39
Figure 3-1: Elements and their interactions which impact the recovery of oil in DCW.....	43
Figure 3-2: pH changes Vs Pore Volume Injected	46
Figure 3-3: Analysis of DCW Recovery for sandstones and carbonates	48
Figure 3-4: Dynamic Simulation model set up.....	51
Figure 3-5: Simulation sensitivity for different salt injection	53
Figure 3-6: Corey Parameters Uncertainty Input.....	53
Figure 3-7: Uncertainty and Sensitivity Parameters	54
Figure 3-8: Cumulative Oil Production Vs Time for the various sensitivities.....	54
Figure 4-1: Illustration of Data Collection Procedure and Workflow (Kang et al., 2014)	55
Figure 4-2: Box Plots of Reservoir Properties Vs EOR methods (Ramos, 2017).....	56
Figure 4-3: Interaction between the different models.....	57
Figure 4-4: Sigmoid function	60
Figure 4-5: Confusion Matrix.....	60
Figure 4-6: ROC- AUC curve.....	61
Figure 4-7: Illustration of an example Decision Tree	62
Figure 4-8: Impurity Measures in DTs.....	63
Figure 4-9: Schematic representation of ANN	65
Figure 4-10: Collinear features with Pearsons correlation.....	69
Figure 4-11: Relative Deviation (RD _i) distribution for (a) Linear Regression (b) Multilayer Perceptron (c) Support Vector Machine (d) CMIS. The CMIS distribution is closer to normality compared with the other AI/ML models	71
Figure 4-12: Feature importance of DT model with (a) 35 number of independent features/parameters (b) 11 number of independent features.	72
Figure 4-13: RMSE variation for models built using varying number of parameters/features.....	73
Figure 4-14: Predicted vs experimental final recovery factor	73
Figure 4-15: Training data and Testing data relative deviation.....	74
Figure 4-16: Error comparison between the models.....	74

Figure 4-17: Illustration of predicted values and experimental values (a) training (b) testing data	75
Figure 5-1: Application of Expert System in DCW.....	76
Figure 5-2: Expert System Workflow based on the meta-analysis.....	78
Figure 5-3: Correlation Matrix of the parameters for the 3D Physics based model.....	81
Figure 5-4: Matrix illustration of parameters in experiments reported and missing	83
Figure 5-5: Matrix Illustration of Positive and Negative Parameter Correlations.....	85
Figure 5-6: Sustainable Workflow for AI/ML Application in DCWF	86
Figure 5-7: Pair Grid Analysis of the different parameters from the physics based model. ...	87
Figure 6-1: Coreflood Setup.....	93
Figure 6-2: Plot of Displacement Efficiency on primary y-axis and Differential Pressure on secondary y-axis vs Pore Volume of Brine/Water Injection (Awolayo et al., 2014)	93
Figure 6-3: Plot of Effluent active ions at normalized concentrations(Awolayo et al., 2014) 94	
Figure 6-4: Oil Recovery at different dilutions and temperature (Boussour et al., 2009)	94
Figure 6-5: Matching of historical observation points of oil recovery and observed difference in pressure.....	95
Figure 6-6: SWCTT Surface Layout (Skrettingland et al., 2011)	96
Figure 6-7: Measured tracer concentrations and profiles modeled(Skrettingland et al., 2011)	96
Figure 6-8: Comparison of observed (in maroon colour) and simulated (in green colour) water cut for two wells (Mahani et al., 2011)	98
Figure 6-9: Recovery Factor Vs Pore Volume Injected from different cases around the world	99
Figure 6-10: Parameter Matrix	99
Figure 6-11:Correlation Matrix	101
Figure 6-12: Random Forest Workflow.....	102
Figure 6-13: Gradient Boosting Workflow	104
Figure 6-14: ANN Training & Validation.....	106

CHAPTER 1

INTRODUCTION & RESEARCH OBJECTIVES

Different Composition Waterflooding (DCWF) is injecting water of a distinct composition makeup from the formation water insitu, into the formation reservoir for sweeping and displacing the oil for enhanced oil recovery. The results that are seen on the reduction in the residual oil saturation (Sor) and consequently the improved recovery of oil puts this type of recovery method in top contention with other forms of 'EOR' methods. The lower complexity of injection of the displacement injectant, its corresponding lower costs, surface facility requirements and environmental footprint makes this DCWF mechanism worth serious consideration as an 'EOR' methodology to maximize the reservoir hydrocarbon recovery.

DCWF impacts the recovery not just from the displacement of the hydrocarbon in the reservoir from the physical aspect, but there are chemical aspects to it leading to the change in the system wetness from either an oil wetting or mixed wetting to a more water wetting system as shown in the findings from the various research carried out at different scales from pore, core, single well to reservoir levels.

Additional oil recovery of 1-10% (Al-Harrasi et al., 2012; Yousef et al., 2011) were reported in laboratory research on carbonate samples from the middle east. The extensive work done on the Omar Field in Syria shows DCWF related incremental recovery of 10-15% for Sandstone reservoir at the field level(Vledder et al., 2010) while little or no incremental recovery was reported from both corefloods and single well chemical tracer tests in the Snorre field (Skrettingland et al., 2011). The mixed results obtained with DCWF highlights the need to perform detailed and efficient screening, modelling and predictions before proceeding to detailed study of the DCWF EOR and its subsequent reservoir/field implementation.

DCWF has been researched and studied for the past decades to understand the underlying mechanisms and its effectiveness in different reservoirs. Many of the studies and experiments have demonstrated varied results and cited varied mechanisms (wettability alteration, interfacial tension [IFT] reduction, saponification, multi-component ion exchange[MIE], electric double layer[EDL] expansion, salting-in effect, fines migration and osmotic effect) behind the success of DCWF. The different studies initially started with coreflood tests as early

as in 1960s(Bernard, 1967) and then progressed from cores, micromodels to single well tests and pilot studies. This was followed by advances in modelling which entailed using single component function to model the impact of low salinity to coupling of geochemistry and flow simulation. More recently the application of Artificial Intelligence (AI) has found its way into the screening and modelling of DCWF. The research initially started with sandstones and then progressed to carbonates. The diversity of the interaction parameters necessitates the need for research to identify the critical parameters and the critical mechanisms that impact the DCWF. This research aims at identifying the critical parameters and mechanisms while developing a workflow for screening and application of ML/AI for faster modelling.

DCWF evolved from coreflood experiments where the impact of the chemical composition of the water was observed in addition to the physical impacts of the water flood in terms of the volumetric sweep efficiency and the displacement sweep efficiency. Core based experiments in the form of corefloods were commonly conducted to investigate the effectiveness of DCWF, where varied results were observed. Many experimentation and measurement techniques were developed to understand the interaction mechanisms. The corefloods are carried out on 3” long and 1.5” diameter core plugs taken from reservoir whole cores. The detailed cleaning process of the core plugs was performed before they were placed in the laboratory setup consisting of a core holder, injection pump and sensors for measurement of temperature, pressure, saturation, effluent properties. The coreflooding process entails flooding with the insitu brine followed by oil to restore to the initial water saturation and this is followed by flooding with reservoir brine and then subsequently with different composition waterflood. The core plugs (1” – 2.5” long) are subjected to spontaneous imbibition (SI) experiments primarily for rapid understanding of wettability alteration at the core level through replacing the insitu brine with different salinity brine and measuring the amount of spontaneous imbibition. The spontaneous imbibition experiments are used for fast screening of low salinity processes. The core samples are prepared for the experiments, and they are cleaned, dried and saturated with oil to simulate the reservoir conditions. The samples are then placed inside the imbibition cell and closely monitored for the imbibition process including the injection of water with altered lower salinity. The monitoring entails using NMR, ultrasonic measurements and other imaging techniques for fluid saturation and oil production. This enables understanding the hydrocarbon recovery with respect to parameters like wettability, fluid salinity and rock properties. In the corefloods the cumulative oil produced and oil rates versus timing of the injection of the different water salinity is measured. Also, the pressure changes and the effluent properties in terms of

composition analysis, rock saturation pre and post flooding and the rock properties through CT scans pre and post flooding are measured.

Micromodels are small scale representations of the porous media built to understand the interactions of the different components in DCWF and consequently an improved understanding of the underlying mechanisms and dynamics. This modelling helps to understand the rock-fluid interactions, wettability, complex nature of oil recovery like clay induced flow diversion, impact of water salinity contrast on oil mobilization through diffusion and osmosis and finally the mechanisms of improved sweep efficiency. Overall micromodel modelling enables understanding the underlying mechanisms at the pore scale leading to improved optimization of the process.

On a larger scale compared to cores and micromodels, there were many tests at well level, pilots and reservoir wide study of the impact of the DCWF. The single well tests consisted of the log inject log test which encompassed running saturation and production logs in the well before and after the injection to determine the change in the saturation and the production/injection (Rotondi et al., 2014). The single well chemical tracer tests (SWCTT) consist of tracer injection to understand the residual oil saturation (Sor) change by measuring the movement and concentration of the tracers with time. It requires adequate well set up for injection and production and a reservoir specific compatible tracer. The SWCTT provides information about the tracer concentration, reservoir characterization through understanding of the fluid flow and connectivity in the reservoir, fluid flow and finally assessing the 'EOR' potential through better understanding of the displacement process and the remaining fluid saturation. The pilots consisted of observing the production/injection pair and their performance. The field wide study included changes in the oil rate and water cut as different salinity water break through was observed in the producer wells.

Different experiments have emerged as important to closely monitor and understand the different effects of the different interaction parameters. These experiments can be classified based on understanding the rock system, the fluid system, the interactions between the rock and fluid systems, the interaction within the fluid systems and finally the state of the overall system including its conditions.

The various research carried out cite various contrasting and contradicting mechanisms behind the success of DCWF. These lead to uncertainty in understanding what are the critical mechanisms and hence what are their corresponding critical parameters. This research work aims at identifying the critical mechanisms and their critical parameters. Furthermore, due to the intensity of the resources involved the screening of DCWF through an artificial intelligence based method would provide for better utilization of the resources through an early fast and efficient screening of the viability of DCWF. This research employs the use of sustainable workflows for fast screening and modelling for DCWF before proceeding to the next stage of resource intense experimentation and investigation.

The Research aims at understanding the fundamental mechanisms of DCWF through evaluating various research work carried out in different environments at different scales and different labs to provide a meta-analysis based on which key critical parameters and mechanisms (at the interfaces of crude oil, brine and rock) are identified. It aims to investigate and understand the different scales of modelling techniques employed. Further the research aims at developing a sustainable workflow for qualitative screening of the DCWF under different variables. This results in the application of the AI/ML based tools for fast modelling and hence screening of the DCWF. The applications of this research work would then be used for better modelling and gaining insight into the reservoir engineering aspects of this emerging 'EOR' technique and hence screening of this 'EOR' technique.

The thesis will be structured as follows Chapter 1 will be about the Introduction & Research Objectives; Chapter 2 on the Literature Review which covers the concept of water flooding and its evaluation mechanisms followed by low salinity water flooding its concept, mechanisms, modelling, operational and economical aspects. Chapter 3 deals with the understanding of the critical mechanisms of low salinity and its impact on modelling the same. Chapter 4 covers the various AI techniques and methods applied for 'EOR'. Chapter 5 covers 'EOR' screening methodology and modelling applying AI. Chapter 6 covers data selection for modelling DCWF and comparison between the different methods. Final Chapter 7 covers the summary, conclusions, and recommendations.

CHAPTER 2

LITERATURE REVIEW

This chapter reviews the literature connected to waterflooding and different composition waterflooding an enhanced oil recovery technique.

The water flooding process entails water injection to displace hydrocarbon from the injector well to the producer well and during the process to sweep the hydrocarbon through the reservoir. There are though many factors that impact the effectiveness of the sweep which include the reservoir heterogeneity, the rate of injection, the location and ratio of the injector to producer, the wettability of the reservoir and the fluid PVT properties of the insitu hydrocarbon and water injected.

Hydrocarbon recovery from waterflooding as it produced a second hydrocarbon peak production after a field was depleted by primary recovery is termed secondary recovery. The different composition waterflood is a tertiary recovery as it is implemented after the secondary recovery. The methods of evaluation of the different recovery processes is crucial to understanding the effectiveness of these processes.

2.1 Water Flooding Process And Evaluation Methods

The water flooding process involves water injection into the subsurface reservoir in order to move hydrocarbon from the injection well towards the producer well. It also provides pressure support in the reservoir and hence improves the productivity and enables increased production. There are many aspects of the water flooding evaluation and these are detailed in the following sections.

One of the key factors that is an indication of the effectiveness of the waterflood is the recovery factor.

Recovery Factor (RF) is a product of three efficiency factors (displacement, areal and vertical) as generalised by the equation:

$$RF = E_D \times E_A \times E_V \qquad 2-1$$

The aforementioned equation can be expressed as

$$N_P = N_S \times E_D \times E_A \times E_V \quad 2-2$$

Where:

‘RF- Recovery Factor

N_s-Initial Oil in place at the start of the flood, STB

N_p-Cumulative Oil produced, STB

E_D- Displacement Efficiency

E_A- Areal Sweep Efficiency

E_V- Vertical Sweep Efficiency’

The fraction of movable oil that has been displaced from the swept zone at any given time or pore volume injected is defined as the displacement efficiency E_D. E_D is always less than 1, since an immiscible gas injection or waterflood will always leave behind some residual oil.

The fraction of the area of the pattern that is swept by the displacing fluid is areal sweep efficiency, E_A. The major factors determining areal sweep are:

Fluid mobilities (Mobility Ratio), pattern type, areal heterogeneity (directional permeability), total volume of fluid injected and pressure distribution between the injectors and producers.

The mobility ratio (M) can be expressed as the ratio of mobility of the displacing phase and the mobility of the displaced phase.

$$M = \frac{\lambda_{displacing}}{\lambda_{displaced}} \quad 2-3$$

For waterflooding it can be translated to

$$M = \frac{\lambda_{water}}{\lambda_{oil}} \quad 2-4$$

The vertical sweep efficiency E_V is the fraction of the vertical section of the pay zone that is contacted by the injected fluids. The vertical sweep efficiency is primarily a function of vertical heterogeneity, degree of gravity segregation, fluid mobilities and total volume of injection.

The product of the E_A and E_V is the volumetric sweep efficiency and represents the overall fraction of the flood pattern that the injection fluid contacts.

The following section is on estimating the different efficiency factors.

$$E_D = \frac{(S_{oi} - \bar{S}_o)}{S_{oi}} \quad 2-5$$

$$S_{oi} = 1 - S_{wi} - S_{gi}$$

$$\bar{S}_o = 1 - \bar{S}_w \text{ (under the assumption that there is no gas in the swept area)}$$

Where ‘ S_{oi} : Initial Oil Saturation

S_{wi} : Initial Water Saturation

S_{gi} : Initial Gas Saturation

\bar{S}_w : Average current water saturation’

E_D can be formulated as a function of water saturation.

$$E_D = \frac{(\bar{S}_w) - S_{wi}}{1 - S_{wi}} \quad 2-6$$

This shows that the E_D will continually increase with increasing water saturation. To find the \bar{S}_w change as a function of the cumulative water injection, Buckley Leverett developed the frontal displacement theory. The frontal displacement theory consists of the fractional flow equation and the frontal advance equation.

The fractional flow for oil and water are given as fractional flow of water (or the immiscible displacing phase) is the flow rate of water divided by the total flow rate. So,

$$f_w = \frac{q_w}{q_t} = \frac{q_w}{q_o + q_w} \quad 2-7$$

Where ‘ f_w : fractional flow of water (bbl/bbl)

q_w : water flowrate (bbl/d)

q_o : oil flowrate (bbl/d)

q_t : total flowrate (bbl/d)’

Considering steady state flow, Darcy’s equation can be applied:

$$q_o = -\frac{k_o A}{\mu_o} \left[\frac{\Delta P_o}{\Delta x} + \rho_o \sin \alpha \right] \quad 2-8$$

$$q_w = -\frac{k_w A}{\mu_w} \left[\frac{\Delta P_w}{\Delta x} + \rho_w \sin \alpha \right] \quad 2-9$$

Fractional flow formulation is depicted in field units as :

$$F_w = \frac{\left\{ 1 + \left(\frac{k_o A}{\mu_o q_t} \right) \left[\frac{\Delta P_c}{\Delta x} - g \Delta \rho_o \sin \alpha \right] \right\}}{\left(1 + \left[\frac{k_o \mu_w}{k_w \mu_o} \right] \right)} \quad 2-10$$

Where the units in bbl, cP, mD, ft²

The equation of frontal advance aids in determining the water saturation profile in the reservoir at any given time during the water injection. This equation has material balance as the basis, where the water entering a finite volume and the water leaving the same finite volume is equal to the water accumulation. Buckley leverett presented this formulation for a 2phase flow immiscible linear displacement.

And the final equation can be

$$(dx/dt)_{S_w} = (V)_{S_w} = \left[\frac{5.615 q_t}{\phi A} \right] \left(\frac{df_w}{dS_w} \right)_{S_w} \quad 2-11$$

Where :

‘(V)_{S_w} = Velocity of any specified value of S_w, ft/day

A= cross-sectional area, ft²

q_t= total flow rate (oil+water), bbl/day

$\left(\frac{df_w}{dS_w} \right)_{S_w}$ = slope of the f_w vs S_w curve at S_w’

The above equation indicates that the velocity of any specific water saturation is directly proportional to the slope of the fractional flow curve. Additionally, for two-phase flow, the injection rate i_w is equal to the total flow rate q_t.

The total distance advanced is an integration of the distance of the movement of the water front given by

$$(X)_{S_w} = \left[\frac{5.615 t q_t}{\phi A} \right] \left(\frac{df_w}{dS_w} \right)_{S_w} \quad 2-12$$

When the total flow rate is equal to the water injection rate (i_w) the above equation is reformulated as

$$(X)_{S_w} = \left[\frac{5.615 t i_w}{\phi A} \right] \left(\frac{df_w}{dS_w} \right)_{S_w} \quad 2-13$$

And the cumulative water injection is $Winj = i_w t$

$$(X)_{S_w} = \left[\frac{5.615 Winj}{\phi A} \right] \left(\frac{df_w}{dS_w} \right)_{S_w} \quad 2-14$$

Where:

' i_w ' = water injection rate, bbl/day

$Winj$ = cumulative water injected, bbls

t = time, day

$(X)_{S_w}$ = distance from the injection for any given saturation S_w , ft'

2.1.1 Microscopic Efficiency

The microscopic displacement efficiency is denoted by E_D and is defined as the stock tank oil recovered per unit PV (pore volume) contacted by water divided by stock tank oil in place at the waterflood start per unit contacted by water. E_D is expressed in terms of saturation changes by:

$$E_D = [(S_{o1}/B_{o1}) - (S_o/B_o)] / (S_{o1}/B_{o1}) \quad 2-15$$

Where:

' S_{o1} ': Volumetric average oil saturation at the waterflood start, where the pressure average is p_1 , fraction,

S_o : Volumetric average oil saturation at a particular point during the waterflood,

B_{o1} : Oil formation volume factor at p_1 , bbl/STB and

B_o : Oil formation volume factor at a particular point during the waterflood, bbl/STB'

E_D formulation at the residual saturation (S_{or}),

$$E_D = 1 - [(S_{or}/S_{o1})(B_{o1}/B_o)] \quad 2-16$$

Which becomes

$E_D = 1 - [(S_{or} / S_{oi})]$ when the formation volume factors for oil are equal and represents the maximum efficiency attainable.

2.1.2 Macroscopic Displacement Efficiency

Macroscopic efficiency describes the displacement efficiency of a waterflood in a specified volume of reservoir rock. The formulation of the macroscopic displacement efficiency is $(S_o - S_{or}) / (1 - S_{wi} - S_{or})$

This macroscopic displacement efficiency is a combination of the areal and vertical sweep efficiencies.

The two methods used to predict the displacement performance are the Buckley-Leverett (frontal advance) model and solving of PDE of two-phase flow. Several key parameters that impact the outcome of the waterflooding are as follows:

Capillary Pressure (P_c): is defined as the difference between the non-wetting (oil in this case) phase pressure and wetting phases (water in this case) pressures and is formulated as $P_c = P_o - P_w$.

Wettability: inclination to preferentially adhere to or wet the surface of a rock by a fluid is termed as the wettability of that fluid. The wetting fluid can be either oil or water or mixed, but gas doesn't wet the rock surface.

Interfacial Tension (IFT): Interfacial tension and wettability affects the performance of the waterflood. At high IFT between the oil and water leads to high P_c and causes unfavourable fluid-fluid interaction. Many 'EOR' techniques like surfactant injection is aimed at reducing the IFT between the fluids. DCWF is thought to lower the oil and water IFT.

2.2 Low Salinity Water Flooding Process, Mechanisms and Evaluation Methods

DCWF is an ‘EOR’ technique entailing water injection into the reservoir with a lower salt concentration vis-à-vis the insitu formation water. This process is based on the observation that injected water of low salinity results in enhanced oil recovery which was first tested and demonstrated in 1967 (Bernard, 1967). The mechanism behind this phenomenon is not yet fully understood, but it is believed to be related to the wettability alteration of the of the rock/mineral surface, which can lead to improved oil displacement and mobilization.

The low salinity waterflooding process typically involves several stages. First, the reservoir is flooded with high salinity water for hydrocarbon displacement and driving it towards the producer wells. Then, injection of the lower salinity/different composition water, compared to insitu water, into the reservoir is carried out to further the displacement of the remaining oil. The reduced water salinity is prepared by dilution of the formation water with fresh water or through a desalination process. The DCW waterflooding process effectiveness is impacted by several factors, including the rock and fluid properties, the injection rate, and the water injection salinity and composition (Jerauld et al., 2008; Morrow & Buckley, 2011a).

DCW waterflooding has several advantages over other ‘EOR’ techniques. It is a relatively simple and low-cost process that can be efficient in various kinds of reservoirs. It also has a lower environmental impact compared to other ‘EOR’ techniques, as it does not involve the use of chemicals or other additives. However, the effectiveness of the process can vary depending on the reservoir conditions, and further detailed investigation/research is needed to fully understand the underlying mechanisms and optimize the process parameters.

Overall, low salinity waterflooding is a promising ‘EOR’ technique that has gained increasing attention in recent years. While the mechanism behind the process is not yet fully understood, it has been efficient and effective in improving oil recovery in a wide range of reservoirs inclusive of both carbonates and sandstones. Expansive and in-depth research is needed to optimize the process and develop predictive models that can help operators design and implement low salinity waterflooding projects more effectively.

Implementing low salinity waterflooding operationally involves several steps. First, the reservoir must be characterized to determine its properties, such as the rock and fluid properties, the injection rate, and injection water salinity and composition. This information is used to design the low salinity waterflooding project, including the injection well location, the injection rate, and the water composition. The water composition can be adjusted through formation water dilution with fresh water or by using a desalination process.

Once the project is designed, injection into the reservoir of water with lower salinity takes place through the injection well. The injection rate and pressure are carefully controlled to ensure that the water is distributed evenly throughout the reservoir and that it does not cause any damage to the formation. This water injection of lower salinity displaces the remaining insitu oil and pushes it towards the production wells. The produced oil is then separated from the water and transported to the surface for further processing.

During the implementation of DCWF, monitoring of the performance of the project is essential and adjustments made as needed. This can involve measuring the production rate, the water cut, and the produced water salinity. If the performance of the project is not meeting expectations, adjustments can be made to the injection rate, the water composition, or other parameters to optimize the process.

Overall, implementing low salinity waterflooding operationally requires careful planning and monitoring to ensure that the project is effective and efficient. While the process is relatively simple and low-cost compared to other 'EOR' techniques, it still requires a significant investment of time and resources. However, DCWF has obvious benefits, including increased oil recovery and reduced environmental impact, making it an attractive option for many operators.

The mechanisms behind DCW waterflooding are yet to gain complete consensus and comprehension, but several theories have been proposed (Nande & Patwardhan, 2022). One theory is that the DCW affects and changes the rock surface wettability, increasing the water-wetness of the rock surface and improving the displacement and mobilization of the remaining oil (Lager et al., 2007; Morrow & Buckley, 2011b; Strand et al., 2006). For carbonates the potential determining ions (PDI) of Calcium, Magnesium and Sulphate are known to alter the crude oil/brine/rock surface interactions, subsequently altering the wettability. The zeta

potential which is, the electro kinetic potential between the particle surface and the bulk phase surrounding the particle surface, charge measured at the surface of the particle slipping plane (Figure 2-1) and it goes to zero as one moves away from the particle and into the solution, is used for wettability determination. The zeta potential is measured by the electrophoretic mobility method (EPM) and streaming potential method (SPM). The preference is for the SPM because it can be performed at the reservoir conditions of temperature, using the core intact and at reservoir brine salinity unlike the EPM which would need the core to be crushed into powder, reduced temperature and salinity (cannot handle reservoir conditions) of experimentation envelope. The low salinity studies in carbonates demonstrate that the primary factors that are responsible for wettability alteration are lowering the salinity of the injected brine, increasing concentration of the PDIs in the injected brine, lowering the ionic potential of the injected brine and or a combination of the aforementioned. It has been shown that injected brine with higher SO_4^{2-} tends to alter the system wettability towards increased water wetness, subsequently improving the recovery of the oil. Additionally, at higher temperatures the replacement of Calcium ions by Magnesium ions results in increased recovery too. This is shown in the Figure 2-2. A key factor that hasn't had detailed research is the weakening of the rock due to the ion substitution.

Another theory is that the low salinity water, being similar to surfactant or alkaline flooding, alters the oil-water interfacial tension in the direction of lowering it, making it easier for the water to displace the oil (Mcguire et al., 2005). This effect is believed to be more pronounced in carbonate reservoirs, where the interfacial tension between the oil and water phases is typically higher than in sandstone reservoirs. The caveat to this theory comes from the fact that a high Acid Number of the oil is a requirement to form surfactants (based on surfactant flood studies) while many DCW floods have shown positive increments in oil recovery with low oil acid number. Additionally, there are core floods of DCW where the changes in IFT were only by 1mN/m (at ambient conditions) while significant incremental recovery were reported (Al-Harrasi et al., 2012; Thomas et al., 2022). This lends uncertainty to the theory that IFT reduction is the main mechanism behind the DCW effects.

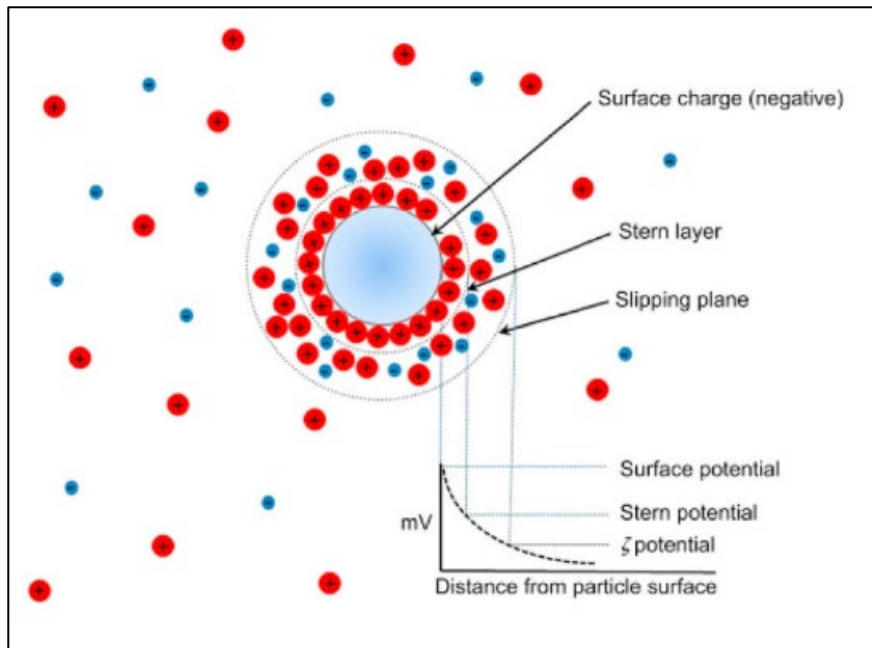


Figure 2-1: Zeta Potential definition in electrical double layer of the particle

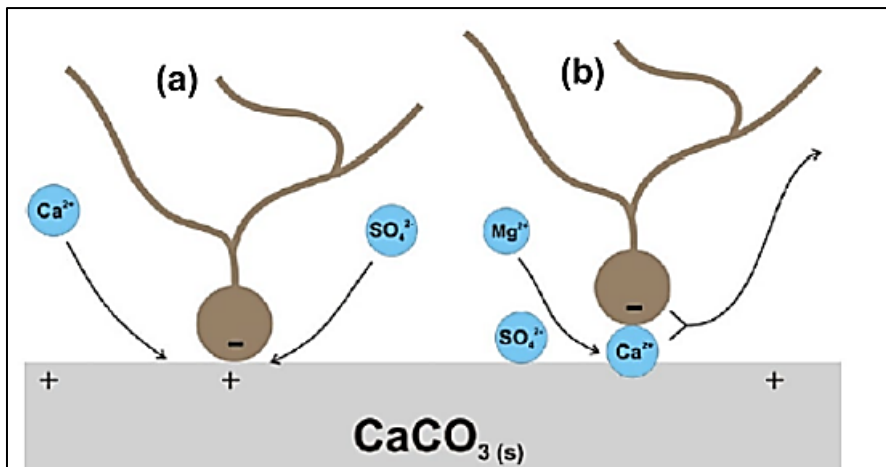


Figure 2-2: Interaction of PDIs (a) Calcium and Sulphate interaction (b) Magnesium and Sulphate at high temperature interaction

Other proposed mechanisms include fines migration, electric double-layer (EDL) expansion, multicomponent-ionic exchange (MIE), saponification, salt in effect, and osmotic effect.

Rock dissolution and fine migration were thought to be primary mechanisms behind increased oil recovery through DCWF but research by Mahani(Mahani et al., 2015) showed that rock

dissolution is not the primary mechanism in carbonates and also the rock mineralogy affects the magnitude DCWF related recovery of oil with dolomites having lesser positive impact from DCWF as compared to limestone. Additionally, the research identifies this mechanism not as the primary but secondary cause towards increased oil recovery. Also, the fine migration on its own isn't the primary mechanism but in combination with dissolution can be a potential mechanism for increased oil. Fines migration involves the movement of fine particles in the reservoir, which can help to mobilize the remaining oil and the release of particles can be triggered by DCWF(G.-Q. Tang & Morrow, 1999; G. Q. Tang & Morrow, 1997). The factors responsible for the fine release/movement are salinity, pH, flowrate, temperature and adsorption of organic matter(Sarkar & Sharma, 1990). The particle release will improve the microscopic sweep efficiency through increasing the water wetness. It also can block pore throats and create a flow diversion of water into the unswept areas of the pore network. Though several experiments are aligned with this paradigm, contradictory results which exhibit incremental oil recovery without permeability reduction and no fines in the effluent stream exist in the literature(Boussour et al., 2009; Cissokho et al., 2010). As shown by other studies the lack of fine production doesn't imply no fine release/movement which can be in part attributed to increase in the delta pressure during flooding experiments and needs further corroboration through pre and post flooding core scans(Fogden et al., 2011).

MIE involves multiple ionic exchanges between the hydrocarbon/water and rock surfaces, leading to changes in the surface charge and wettability. Organic components in crude oil are attracted to surfaces through a mechanism explained by Derjaguin, Landau, Verwy and Overbeek (DLVO) theory of colloid stability. The polar organic species in the oil get attached to charged surfaces by formation of bridges through a number of ionic interactions like ion exchange, ion bridging and others. The mechanism of ion exchange as evidenced for DCWF effectiveness in clastic is through the cation exchange as represented in Figure 2-3, while in carbonate it is through the anion exchange with cation metallic complexation of the organic material(Lager et al., 2007). In sandstones, DCWF breaks hydrocarbon attraction to the rock by exchanging the higher valence cation for a lower valence cation such as sodium (Robbana et al., 2012). DCWF causes the release of the hydrocarbons attached to the rock surface through replacement with the ions present in the injected brine and the system becomes more water-wet. The MIE effect was demonstrated to be valid at the inter-well scale through field experiments in a sandstone reservoir where low salinity water was injected in an injector well and the corresponding produced water and oil were measured in the nearby producers(Lager et

al., 2008). The change in the cation concentration in the produced water and the decrease in the water production to oil production ratio (WOR) at the production well was evidence of the MIE impact and the corresponding improved oil recovery. It was demonstrated that changing salinity alone but keeping the ratio of the divalent to monovalent cations the same, there is increased affinity to adsorb of the divalent cations on the sandstone rock which doesn't lead to an increase in the water wetness but on the contrary, while the reduction in the divalent to monovalent cations in the injected brine does lead to reduced divalent cation adsorption onto the rock surface increasing the water wetness and the low salinity effect comes into play (Bourbiaux, 2020)

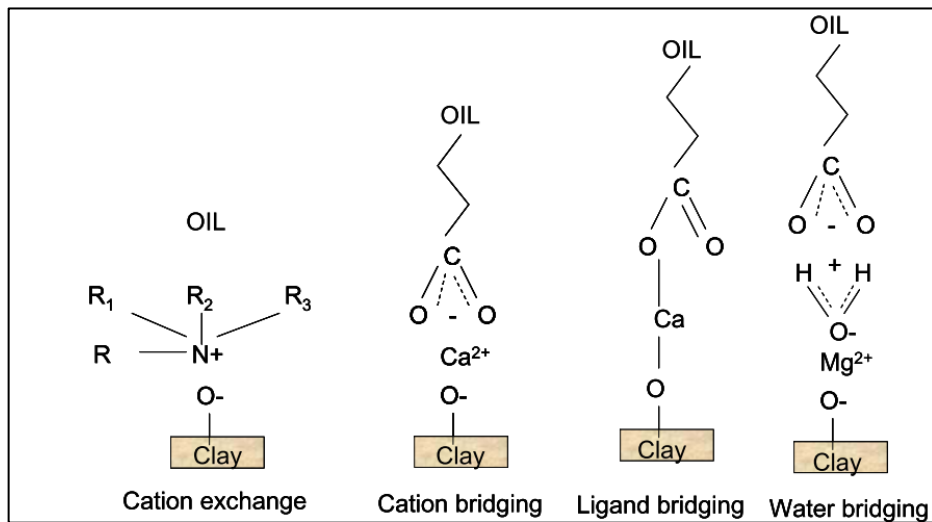


Figure 2-3: Crude to surface attraction involving divalent cations (Lager et al., 2007)

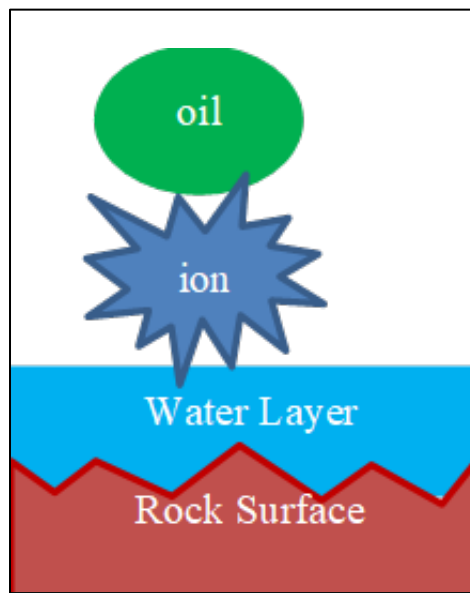


Figure 2-4: Crude oil attachment to the rock surface by ionic assistance.

EDL change involves the electric double layer expansion/contraction around the rock surfaces, leading to alterations of the surface charge and consequently the wettability (Lee et al., 2010). The change in the EDL is due to the ion exchange and interaction between the oil-brine-rock. The EDL changes were further validated through lab experiments with Zeta potential measurement and also wettability identification through contact angle measurements. EDL has been identified as primary mechanism of the DCW effect by researchers (Al-Shalabi et al., 2013; Ligthelm et al., 2009; Nasralla & Nasr-El-Din, 2014). A key observation was that though low salinity brine but with low pH was used it demonstrated that the lower the pH the lower is the zeta potential and hence thinner is the EDL and correspondingly lower is the impact of DCW. This affirmed an expanding EDL as a primary mechanism for a positive DCW effect. Another recently evidenced mechanism for the effectiveness of DCWF has been the fluid-fluid brine and crude oil interplay leading to formation of micro dispersions of the water-in-oil kind. The mechanisms that are considered to effect this increased oil recovery are (1) the removal of the surface active agents from the oil/water interface leading to a change in the wettability (2) the increase in the thickness of the high salinity connate water layer (Mahzari & Sohrabi, 2014).

The key components needed for the formation of the micro dispersions are water with salinity less than 5000 ppm and oil with high percentage of polar compounds. Experiments on micromodels and visualization through Fourier Transform Infra Red (FTIR) spectroscopy

validated that the increase in the micro-dispersions were associated with the oil constituents (asphaltene/resin ratio, aromatics, Sulphur-rich, cyanide and nitrile-base components) , the salinity of the injected brine and temperature (Emadi & Sohrabi, 2012). Saponification involves the reaction of the different composition/salinity water with fatty acids in the oil, creating soap-like compounds that can help to mobilize the remaining oil. This is also related to the reduction in the IFT. Albeit, while a high Acid number and significant change in IFT is required, the DCW effect are seen for oils with low Acid Number and only 1mN/m change in the IFT while producing significant oil recovery.

Salt in effect involves the precipitation of salts in the reservoir, which can help to mobilize the remaining oil. There are two effects the “salting out” and “salting in” effect, where the solubility of the hydrocarbon organic material is drastically decreased and increased respectively through adding salt and removing salt with respect to the solution (Rezaeidoust et al., 2009). It was proposed that an increase of water-wetness of the clay results due to some hydrocarbon organic material that will be desorbed from the clay by “salting in” effect. The underlying premise of this mechanism is that increased recovery is attributed to increased water wettability. However, additional research did not conclusively establish the influence of salt-in effect on DCWF’s ability to recover oil.

Overall, the mechanisms behind low salinity waterflooding are complex and not yet fully understood. Additional research and investigation is required for establishing the most important mechanisms and how they vary depending on the reservoir conditions. However, the positive impact of DCWF has been demonstrated in a wide range of reservoirs, making it a promising ‘EOR’ technique for the future.

Experiments and work at different scales provide understanding related to the mechanisms behind DCWF. Laboratory experiments performed investigate the effect of DCWF on the hydrocarbon displacement and mobilization in core samples. These experiments typically involve core flooding in sequence with high-salinity and low-salinity brine, leading to measurements of oil production and estimating the oil recovery. The results of these experiments have been used to develop numerical models that can simulate the low salinity waterflooding process and predict its effectiveness in different reservoirs.

Experiments have also been conducted at the scale of the pore-network to investigate and identify other parameters that impact the behaviour of a mixed-wet system to DCWF. These experiments typically involve measuring the oil and water phases contact angle configurations on the rock surfaces and the phases' interfacial tension. The results of these experiments have been used to develop models that can predict the positive effect of DCWF in different reservoirs. It has been proposed by various researchers that experiments involving DCWF include X-ray diffraction (XRD), Amott-type spontaneous imbibition test, corefloods, zeta potential and atomic force microscopy measurements. Additionally, there are also tests that evaluate the liquid-liquid interactions through microscopic photographs.

Field tests have also been conducted to evaluate the positive effect of DCWF in real-world reservoirs. These tests typically involve injecting different composition/salinity water and measuring the production rate and water cut over time. The results of these tests have been used to validate the laboratory experiments and numerical models and to optimize the design and implementation of DCWF projects. DCWF projects/field trials/pilots reported in literature cover both sandstones (Abdulla et al., 2013) and carbonates (Yousef, Al-Saleh, et al., 2012; Zahid et al., 2012). Candidate well selection criteria for DCWF was developed (Yousef, Liu, et al., 2012) as shown in Figure 2-5. The respective middle eastern field trials showed reduction of residual saturation of oil by 3 saturation units (s.u.) and 7 saturation units (s.u.) for sandstone and carbonate respectively using Single Well Chemical Tracer (SWCT) tests.

Criteria	Specification
Well Type and Completion	Vertical Producer Active/or newly drilled well Cased Penetrate the test zone above oil/water contact
Reservoir Water Chemistry	Targeted area flooded by field seawater Optimum produced water ionic composition
Well Productivity	Natural Flow or equipped with production means Connected to flow lines
Perforation Intervals	Thickness (<40 ft) Avoid high perm layers Test zone not artificially fractured
Water Cut	Flooded Areas

Figure 2-5: Candidate Well Selection Criteria (Yousef, Liu, et al., 2012)

Overall, experiments and work at different scales have been critical in understanding the mechanisms behind low salinity waterflooding and developing effective 'EOR' techniques. Further research is needed to fully understand the underlying mechanisms and optimize the process parameters, but the results of these experiments and tests have demonstrated positive impact of DCWF as a promising 'EOR' technique for the future.

Different evaluation methods were utilized to ascertain the result of DCWF. Laboratory experiments have been conducted to measure the oil recovery and water cut in core samples flooded with low salinity water. These experiments typically involve sequenced waterflooding the core with high-salinity and low-salinity brine respectively, subsequently estimating oil recovery. The results of these experiments have been used to develop numerical models that can simulate the low salinity waterflooding process and predict its effectiveness in different reservoirs. An example set up of the core flooding (Hadia et al., 2013) is shown in Figure 2-6 where (1) Brine water reservoir, (2) pump (positive displacement), (3) Hassler core holder, (4) core sample, (5) high pressure nitrogen cylinder, (6) differential pressure transmitter, (7) graduated for effluent collection, (8) transmitter by-pass valve and (9) computer.

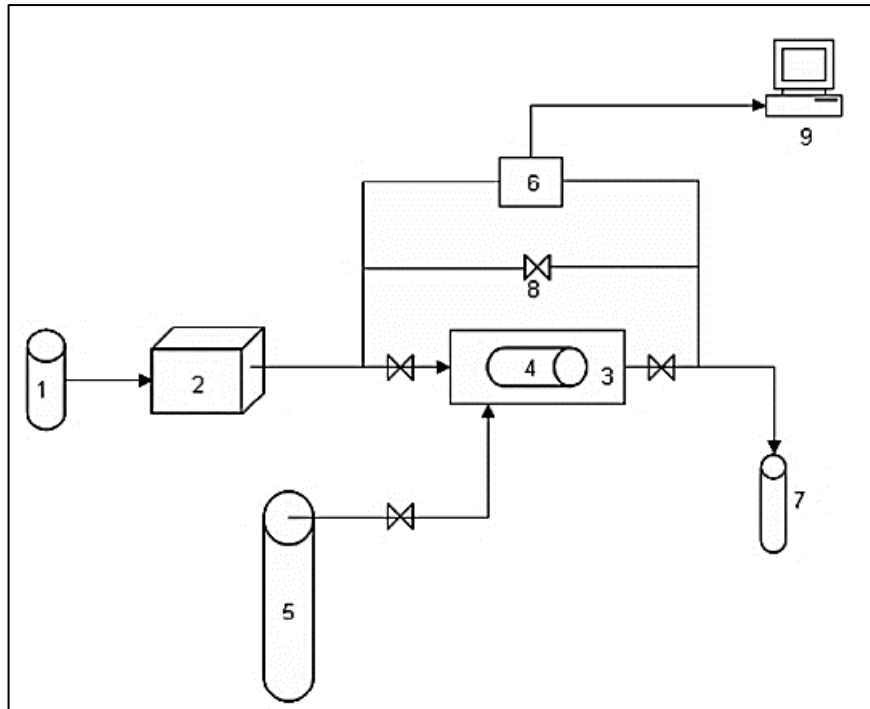


Figure 2-7: Core flooding experimental setup (Hadia et al., 2013)

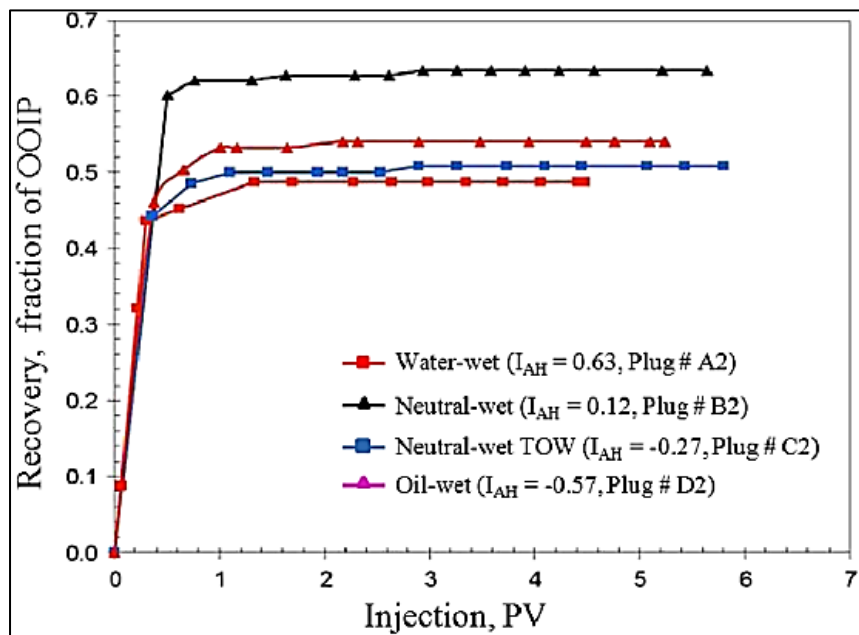


Figure 2-6: Comparison of recovery of oil versus synthetic brine injection (PV) at different wettability conditions (Hadia et al., 2013)

The coreflood experimental results in terms of recovery of oil and the pressure difference between the inlet and outlet as presented by Hadia et al 2013 are shown in figures: Figure 2-7, Figure 2-8, Figure 2-9 & Figure 2-10.

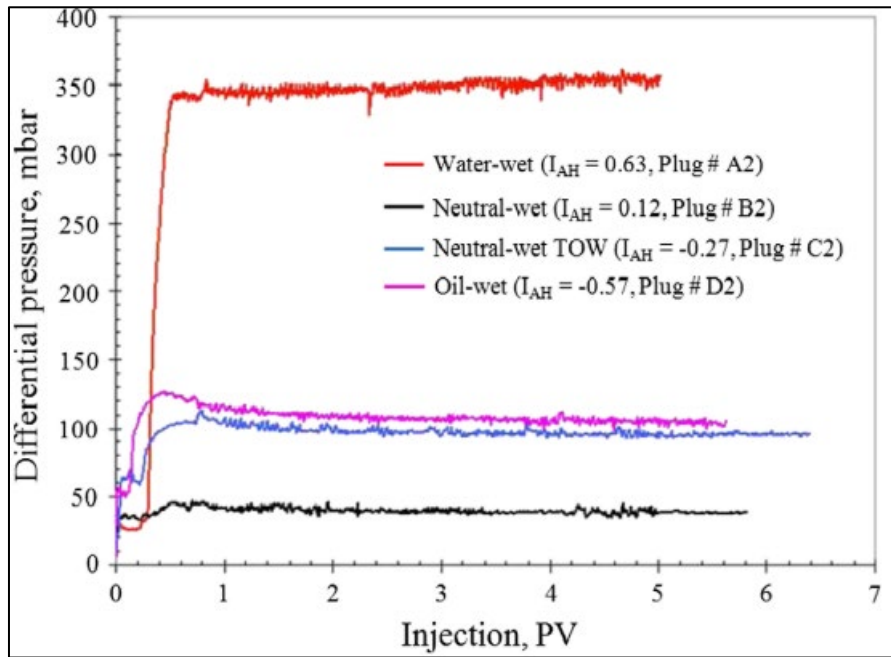


Figure 2-8: Pressure differential transversing the core-plugs for different wettability conditions during synthetic brine injection (Hadia et al., 2013)

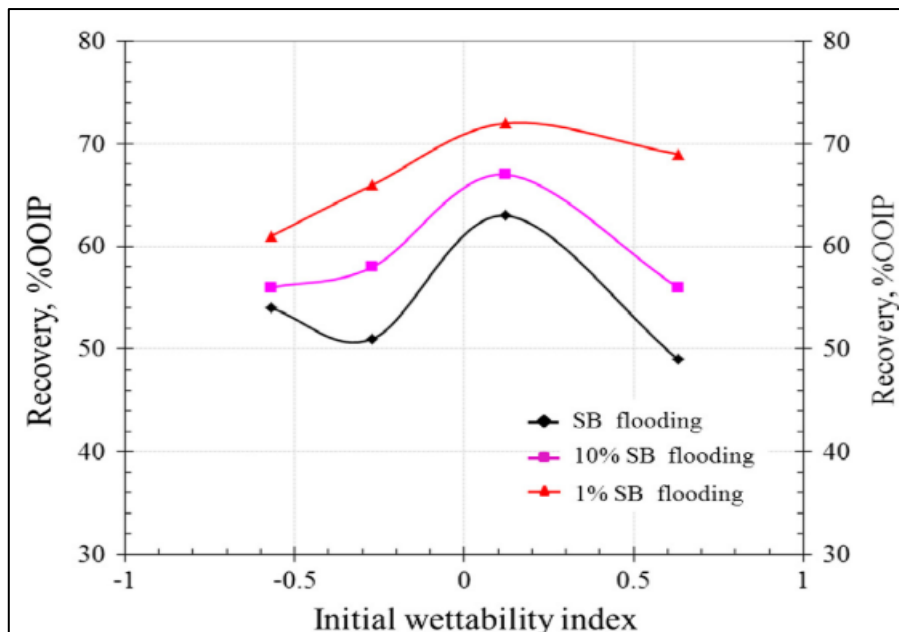


Figure 2-9: Relation between secondary waterflood oil recovery and initial core wettability at high and low salinity brines injection (Hadia et al., 2013)

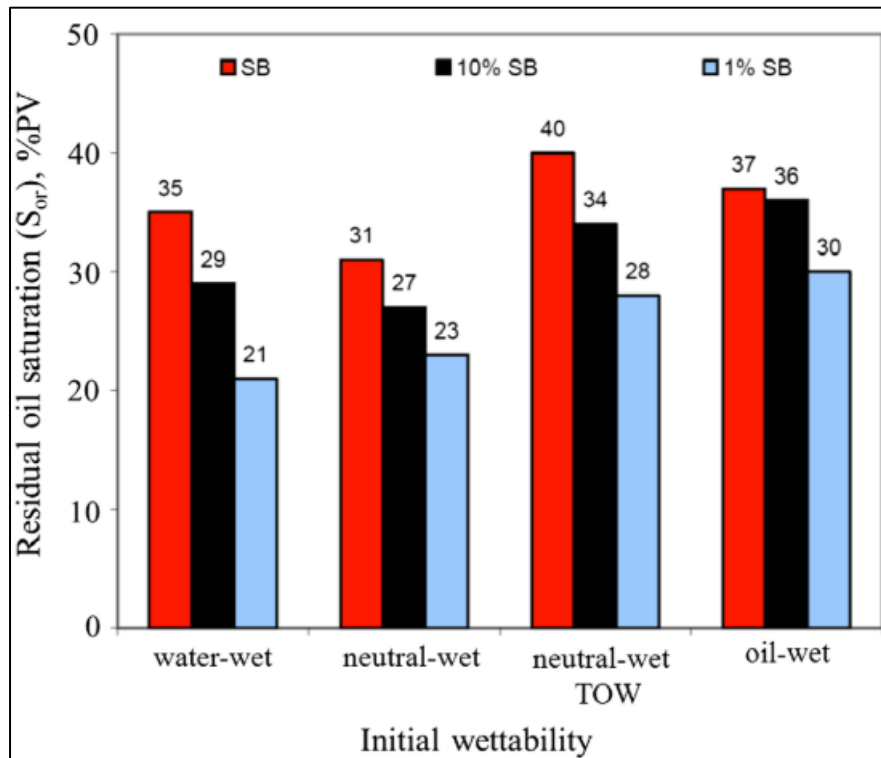


Figure 2-10: Effects of injection brine salinity on saturation of residual oil for varying wettability post secondary waterflooding (Hadia et al., 2013)

Another method for the evaluation of DCWF is the Amott Spontaneous Imbibition (SI) test which is a measurement for wettability determination that is frequently applied and is adept for quick screening because it does not require large amounts of core material, is labour efficient and can be performed simultaneously on large number of samples. The experimental set up consists of placing the crude oil and saline water saturated core in a Amott cell surrounded by similar saline water and then the imbibition process takes place displacing the oil which is measured at the top of the Amott cell and the calculations are performed and represented as a fraction of the oil amount in place in the core, expressed in percentage. The surrounding saline water is then replaced by water that can alter the wettability and the displaced oil is again measured. The experimental schematic (Romanuka et al., 2012) is presented by Figure 2-11

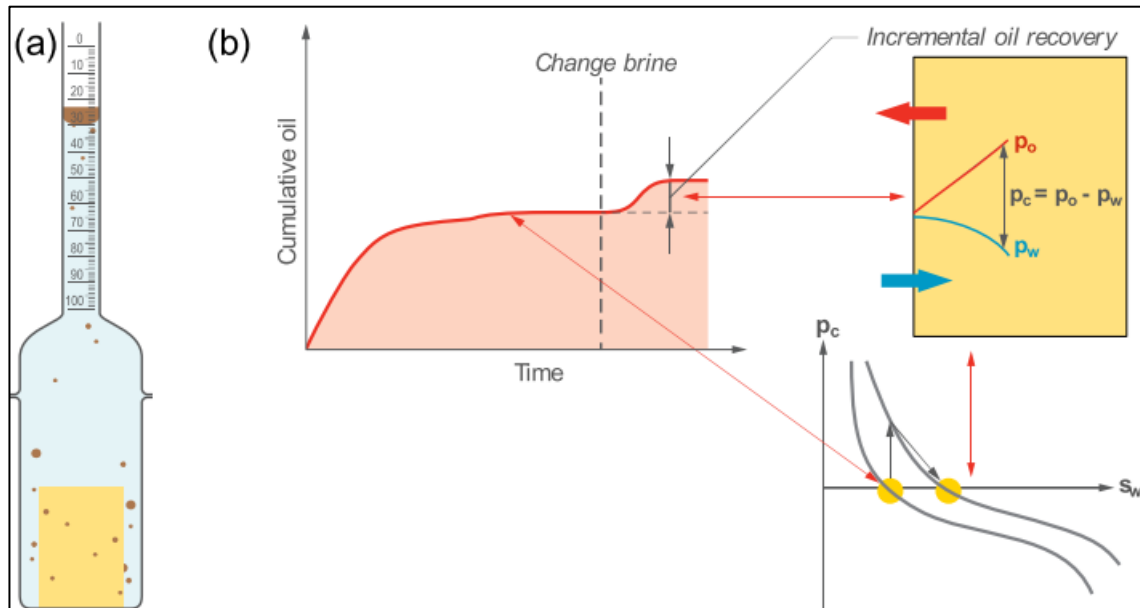


Figure 2-11: (a) Representation of the core plug with oil and connate water saturation in the Amott glass container. Produced oil is collected in the measuring cylinder (b) A schematic representation of the Amott test (Romanuka et al., 2012)

The evaluation of the positive impact of DCWF in real-world reservoirs have been conducted through field tests. These tests typically involve different composition/salinity water injection into the subsurface reservoir and followed by production rate and water cut measurement over time. The results of these tests have been used to validate the laboratory experiments and numerical models and to optimize the design and implementation of low salinity waterflooding projects. The field test begin with using SWCT tests before proceeding with multi-well pilots. The SWCT tests are based on the fact that there is a difference in speed between the tracers that react with the oil, which will be slower, as compared to the tracers that donot mix with the oil and remain in the formation water. The tracers that are injected is an ester which reacts with water to form alcohol during the soak in period after the injection into the well. The well is then flowed back where the alcohol which is only miscible with water returns faster as compared to the parent ester which travels slowly as it is associated with the immobile oil. The different in the return times is used to calculate the Sorw. A schematic of SWCT from Abdulla et al 2013 is presented in Figure 2-12.

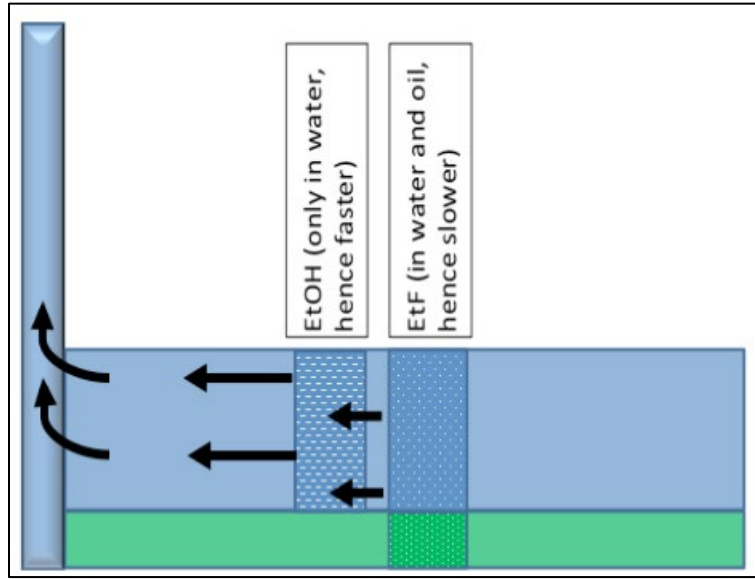


Figure 2-12: EtF (Ethyl Formate) and EtOH (Ethanol) flow (Abdullah et al 2013)

Overall, a combination of laboratory experiments, field tests, and literature reviews have been integrated to analyze the effectiveness of DCWF and subsequently optimize its process parameters for application to different reservoirs. Expansive and in-depth investigation is required for fully understanding the underlying mechanisms and for optimization of the process parameters, current results of these evaluations have demonstrated the positive impact of DCWF as a promising ‘EOR’ technique for the future.

2.3 Modeling of DCWF At Different Scales

Modeling at different scales refers to the use of multiple models at different levels of resolution to describe a system. In the context of low salinity waterflooding, modelling at different scales can be used to simulate the process and predict its effectiveness in different reservoir types and at different levels from the atomic to the reservoir/field level. It has been proposed that the modelling for DCWF would be predictive if it included modelling from the droplet scale to channel scale and finally to the network scale (Suijkerbuijk et al., 2013). This proposed computational model accounts for the physics of the processes at the molecular-scale, core-scale and reservoir-scale. The molecular scale involves the Single droplet scale which considers the physics of the Derjaguin and Landau, Verwey and Overbeek (DLVO) and non-DLVO forces and oil/hydrocarbon, water/brine and mineral/rock interplay are analyzed and resulting

balance of forces will determine the wettability of the surface that will result in different contact angles for different water film thickness and zeta potential based on ionic strength. Next scale is the channel scale model (single pore) where the effect of wettability change on multi-phase flow is quantified in relation to the viscous and capillary forces. The subsequent scale of model is the Network (or Representative Elementary Volume) scale where the incremental oil recovery due to mobilization of trapped oil and changing wettability state of the porous network. In this modelling a dynamic two phase flow model can be coupled with transport of ions and geochemical processes. This modelling workflow connects from the surface scale to core scale and ultimately upscaling to field scale as shown in Figure 2-13 based on the work by Suijkerbuijk et al 2013.

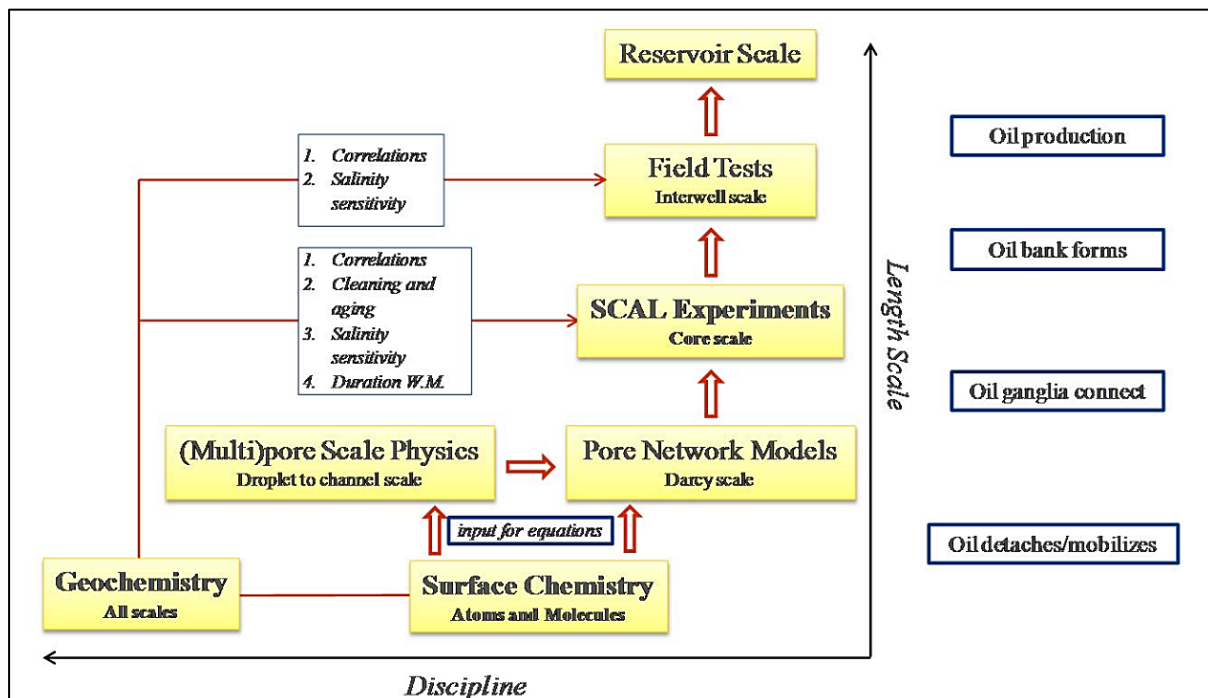


Figure 2-13: Integrated workflow to improve understanding of DCW (Suijkerbuijk et al., 2013)

At the pore-scale level, models can be used for interaction simulation between the different composition/salinity water, hydrocarbon, and the mineral/rock surfaces, subsequently predicting the displacement and mobilization of the remaining oil. These models typically involve the use of computational fluid dynamics (CFD) and pore-network models to simulate the flow of the different composition/salinity water and the oil within pore spaces of the rock. Micromodels enable investigation of the displacement process at the pore level. Through deep reactive ion-etching the different pore throat sizes on the silicon surface which is then

sandwiched between two glass materials by anodic bonding, the micromodels are set up. The fluid is injected in the top left corner of the system while the output is through the bottom right corner. Various photographs are taken of the saturation distribution of the multiphases in the micromodel and different stages of the flooding to understand the fluid distribution, the interactions between the different phases and finally the displacement efficient of the injection scheme. An example of the micromodel experimental set up (Schumi et al., 2020) is shown in Figure 2-14 and its results are shown in terms of the saturation distribution in Figure 2-15. The oil saturation is calculated through image segmentation. In this process, the image is partitioned into multiple segments: oil, water and solid. By counting the pixels of each segment, the oil saturation is calculated.

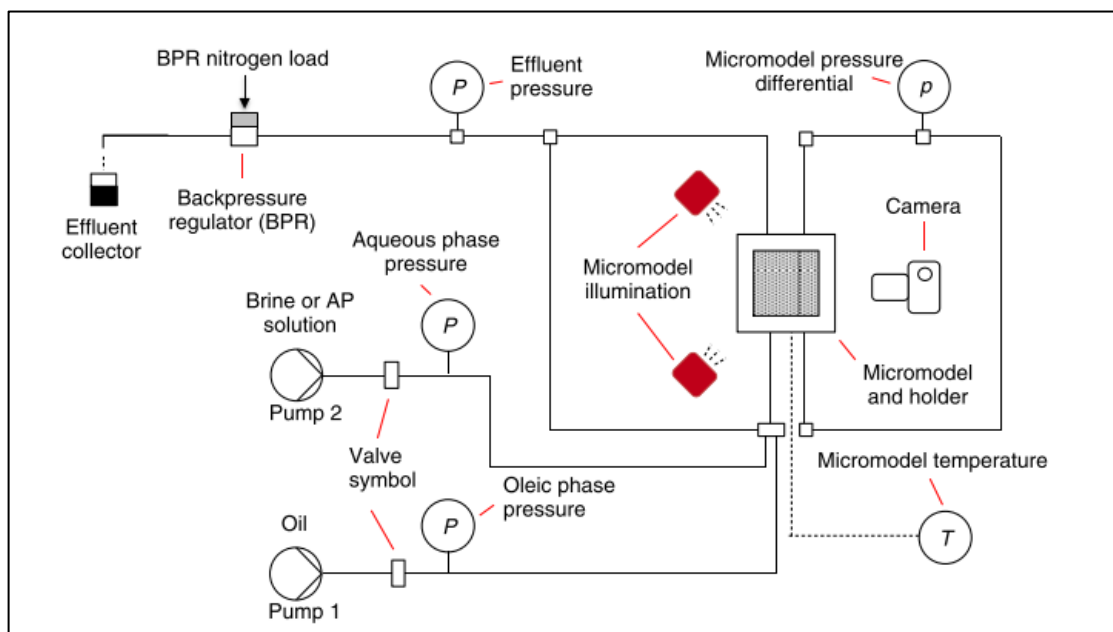


Figure 2-14: Experimental set up of Micromodel investigation (Schumi et al., 2020)

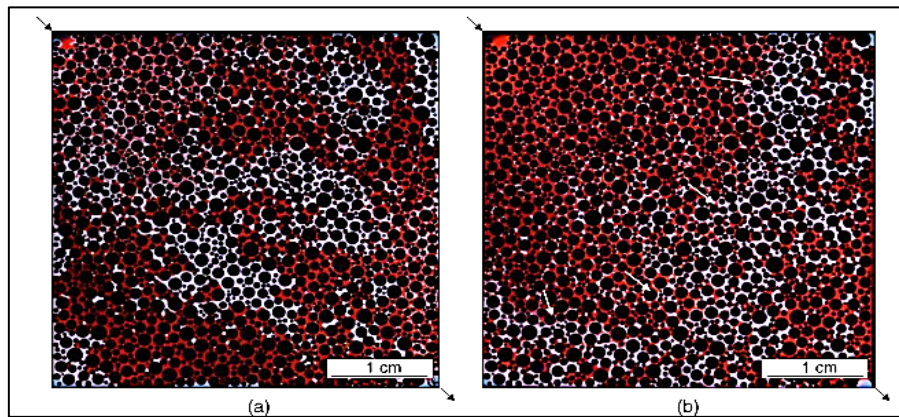


Figure 2-15: a) Oil and Water saturations depicted by the grey and red colours respectively (b) Formation of oil bank depicted by the white arrows (Schumi et al., 2020)

At the core-scale level, models simulate the different composition/salinity waterflooding process in a laboratory setting and predict the oil recovery and water cut. These models typically involve the use of numerical reservoir simulators to simulate the flow of the different composition/salinity water and the oil in the core samples. A typical experimental set up for modelling the DCWF is shown in Figure 2-16 with the results in Figure 2-17. In addition differential pressure across the cores are measured along with the rates and effluent composition. Also the core is scanned through using CT-scans both before and after the coreflooding experiments to determine the change in the saturation along the core and also the change in the core images if any due to mobilization of the fines within the core.

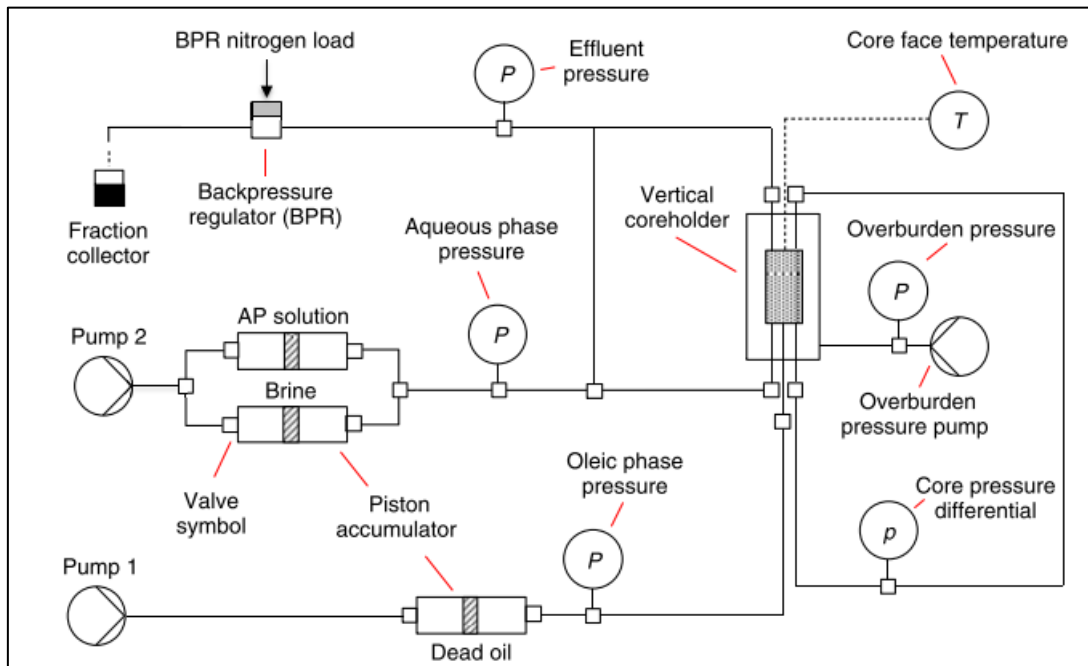


Figure 2-16: Coreflooding experimental set up schematic

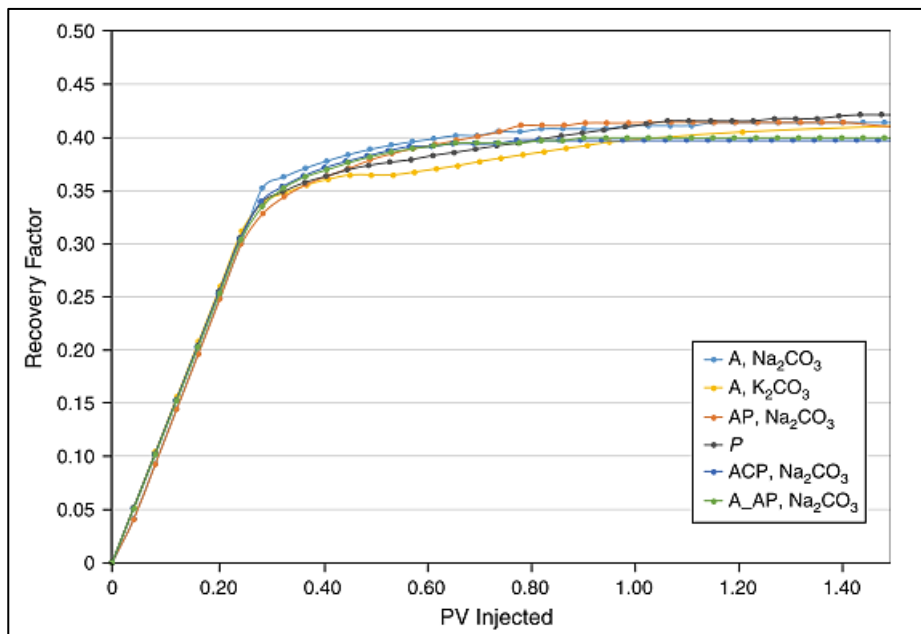


Figure 2-17: RF Vs PV injected for a various coreflood experiments. A refers to Alkali, P to polymer and C to cosolvent

At the reservoir-scale level, models simulate the different composition/salinity waterflooding process in a real-world reservoir and predict the oil recovery and water cut over time. These models typically involve the use of numerical reservoir simulators to simulate the flow of the different composition/salinity water and the oil within reservoir and to optimize the design and implementation of the different composition/salinity waterflooding project. The initial model by Jerauld et al 2008 for predicting DCWF recovery accounted for salt within the aqueous phase as an additional single lumped component and the salinity was the driver which affected the aqueous phase density and aqueous phase viscosity and also impacted the curves of relative permeability and capillary pressure.

Further models started to incorporate geochemical reactions which accounted for rock dissolution and ion exchange along with the flow simulation. A coupling of multiphase/multicomponent flow equation of state compositional simulator with ion exchanges through geochemical processes was demonstrated (Nguyen et al., 2013).

Simulation studies conducted by Shalabi et al and Yousef et al have shown changes in the relative permeability through shifting to the right of the X-axis and lowering of S_{or} (end point saturation of oil) both indicating alteration of wettability to more water wet. Two other modelling techniques were proposed where the contact angle measured was used to alter the relative permeability of oil and the S_{or} while keeping the relative permeability of water constant and the second technique entailed capillary desaturation curve modification through trapping number (Al-Shalabi et al., 2015). The same group of researchers, in 2016, used Gibbs free energy to model different composition/salinity where the S_{or} , end point of relative permeability for oil and Corey's oil exponent were dependent on the Gibbs free energy (Al-Shalabi et al., 2016).

The equation for this model is presented below and its corresponding results are shown. Figure 2-18 shows the linear relationship between S_{or} and Gibbs free energy for the four corefloods.

$$S_{or}(Altered) = \omega \times S_{or}^{LS} + (1 - \omega) \times S_{or}^{HS} \quad \text{Equation 2-17}$$

$$\omega = \frac{G - G^{HS}}{G^{LS} - G^{HS}} \quad \text{Equation 2-18}$$

Where :

S_{or}^{HS} – ROS at high injected-water salinity (sea water)

S_{or}^{LS} – ROS at low injected-water salinity

G – Effective molar Gibbs free energy (J/mol) at in-situ conditions of injected/connate mixed solution

G^{HS} – Effective molar Gibbs free energy (J/mol) at in-situ conditions of sea water/connate mixed solution

G^{LS} – Effective molar Gibbs free energy (J/mol) at in-situ conditions of low-salinity water/connate mixed solution when Sor stops changing.’

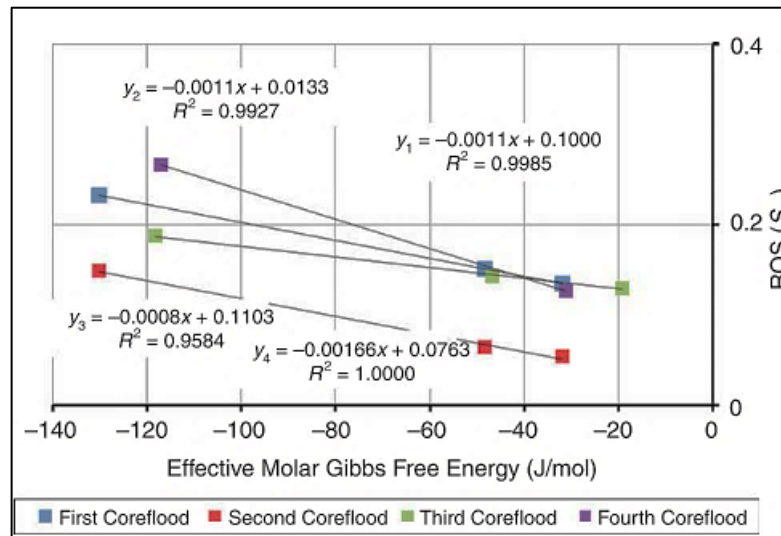


Figure 2-18: Sor vs effective molar Gibbs free energy (Al-Shalabi et al., 2016)

Figure 2-19 shows the linear relationship between the relative permeability endpoint to oil and the effective molar Gibbs free energy where decreasing the salinity of the injected water leads to increase in the effective molar Gibbs free energy and consequently the relative permeability endpoint for oil.

Figure 2-20 shows the direct relationship between Corey’s oil exponent and the effective molar Gibbs free energy’. This implies that decrease in the injection water salinity increases the ‘Gibbs free energy’ and decreases the Corey’s oil exponent. A reasonable match of the experimental coreflood data in terms of the oil cumulative recovery and pressure drop is illustrated in Figure 2-21 and Figure 2-22 respectively.

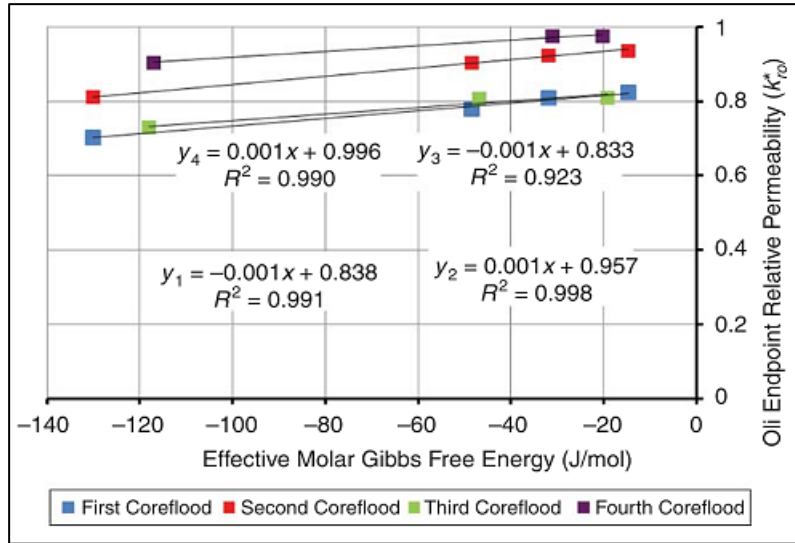


Figure 2-19: Oil end point relperm as a function of effective molar Gibbs free energy (Al-Shalabi et al., 2016)

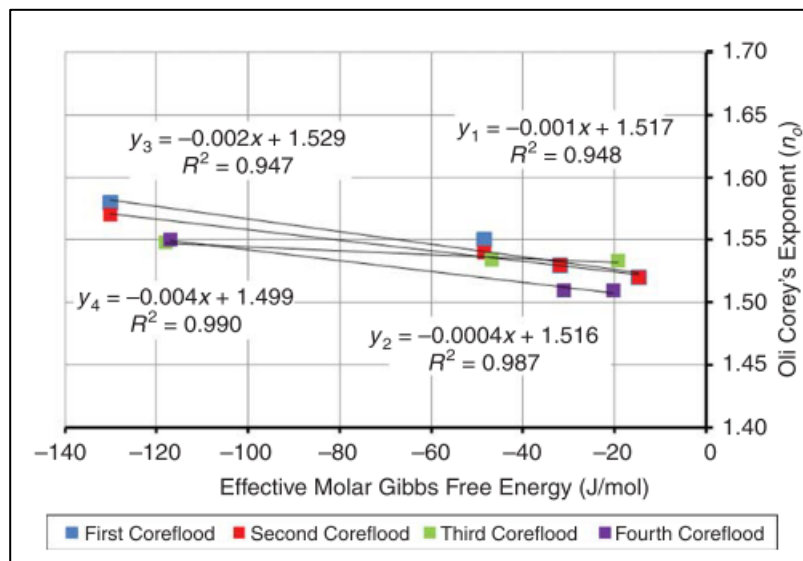


Figure 2-20: Corey's exponent for oil as a function of effective molar Gibbs free energy (Al-Shalabi et al., 2016)

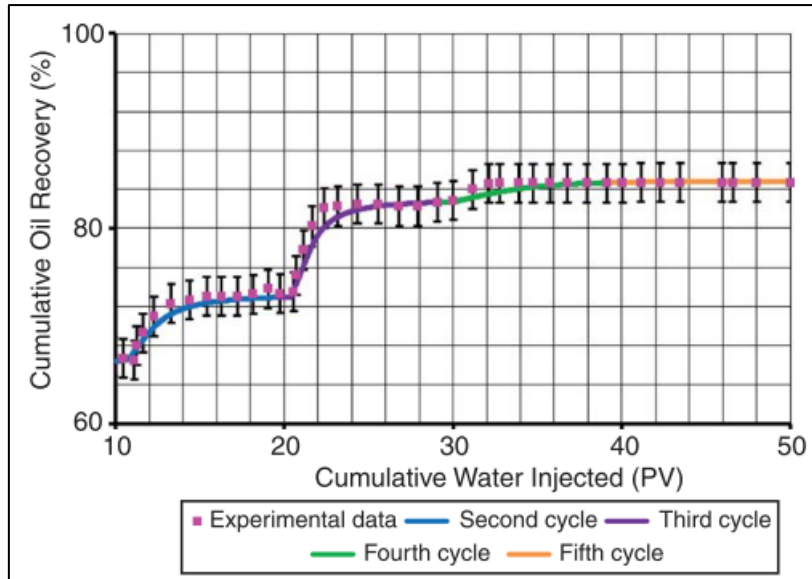


Figure 2-21: Cumulative Oil Recovery history matching (Al-Shalabi et al., 2016)

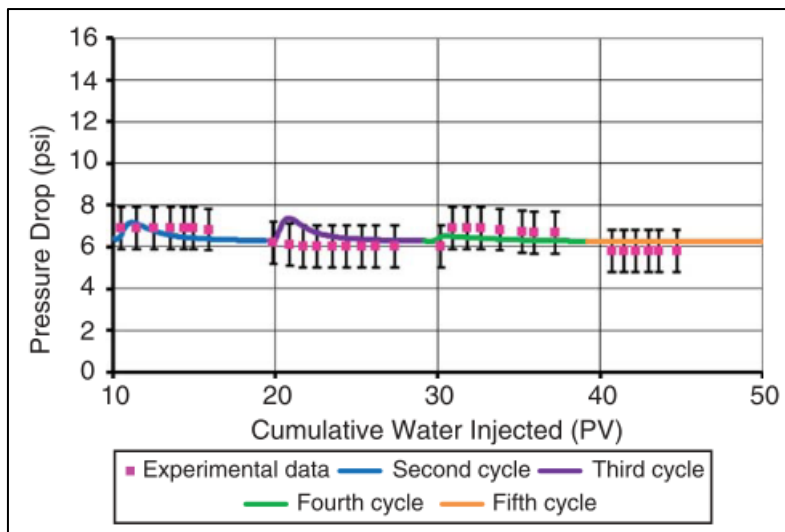


Figure 2-22: Pressure drop history matching (Al-Shalabi et al., 2016)

Artificial Intelligence/Machine Learning (AI/ML) based models are the recent addition to the modelling of DCWF. DCWF is a complex ‘EOR’ process with various parameters involved which are related to the rock, formation brine, injected brine, hydrocarbon and the system conditions. The multi-parameter interaction complexity of DCWF has motivated many researchers to adopt AI/ML tool and techniques to enable accurate, robust and optimum model

creation for DCWF forecasting. Different models of ‘ANN’ (“Artificial Neural Network”), ‘SVM’ (“Support Vector Machine”), ‘DT’ (“Decision Tree”), ‘RF’ (“Random Forest”) and ‘CMIS’ (“Committee Machine Intelligent System”) were used.

The steps leading to the modelling involves preprocessing/preparation of data steps which includes and not limited to removal of data duplication, imputation of data, removal of data outliers, detailed data assessment for collinearity, selection of features from the data, splitting of data and finally usage of statistics to examine the reliability of the models. One of the first steps towards building the AI/ML models is to have sufficient quality data through going through many experiments and published databases on the DCWF. Second step is the data preprocessing which involves removing duplicates and low variance features. This entails removal of those data sets which are identical in both dependent and independent parameters or have same independent parameters but different dependent ones and low variance which is where there is just one value for most samples. Third step involve data imputation which involves treating missing values of important features. The easiest way is to drop the corresponding column or row but this may result in valuable information being not considered. Data imputation involves using the middle values through either modelling or using the mean, median or mode values. Fourth step involves Collinearity assessment where the dependence of independent parameters are analysed and treated. Here the Spearman correlation factor is used along with the Variance Influence Factor (VIF) and the higher the factors the more is the correlation and those parameters can be removed. A heat map of one of the research projects (Shafiei et al., 2022) employing this assessment is shown in Figure 2-23. Fifth step involves removing outliers that would otherwise cause model instability and poor predictions. Sixth step is scaling of data for removal of data offset and acceleration of the optimization speed. Use of the scaled data ensures that all features have the same influence on the model. Seventh step is the substantial performance improvement of the AI models through hyperparameter optimization. Maximum performance of the predictive model developed is ensured through prior determination of the hyperparameters before the start of model training. The final step is the validation of the model through model training and model testing, where the model training is carried out on a specific set of data and then it is used for validation with the testing data set on the accuracy of the forecasts.

Several AI/ML algorithms are available. Some of these are Artificial Neural Network, which is a very fast method and its architecture consists of a 3 layer system which are the ‘input,

hidden and output' layers. Transmission of the processed input data through to the output layer takes place by traversing through the hidden layers, this is facilitated by neurons which provide the interconnections between the layers. ANN implementation requires optimization of its many hyperparameters, mainly number of hidden layers and their neurons.

The next method is SVM which is based on statistical approaches. This is adept for application to problems with high dimensional spaces, through its dimensionality reduction and for situations where the sample number are less than the dimensions number. Out of the many hyperparameters the regularisation parameter (C) and coefficient of the kernel (gamma) are the significant ones.

The next method is a supervised learning method of DT, relatively simple and easy-to-understand, which is utilized in classification and regression cases. The DT predicts by utilization of data features to infer rules.

The next method is RF which improves the model accuracy by applying averaging and alleviates the over-fitting issues related to the DT algorithm.

The next algorithm is CMIS and the underlying concept of this approach is splitting a task into partial operations followed by the results integration. This is a supervised approach.

The model is assessed for accuracy through various statistical parameters of R^2 , statistical parameters of 'RMSE', statistical parameters of Standard Deviation (SD), statistical parameters of 'Mean Relative Deviation' (MRD) and statistical parameters of 'Mean Absolute Relative Deviation' (MARD).

Overall, modelling at different scales is critical in understanding the mechanisms behind different composition/salinity waterflooding and predicting its effectiveness in different reservoirs. Expansive, integrated and in-depth investigation is required to attain full comprehension of the underlying mechanisms and optimize the process parameters, but the results from these modelling approaches have demonstrated the potential of different composition/salinity waterflooding as a promising 'EOR' technique for the future.

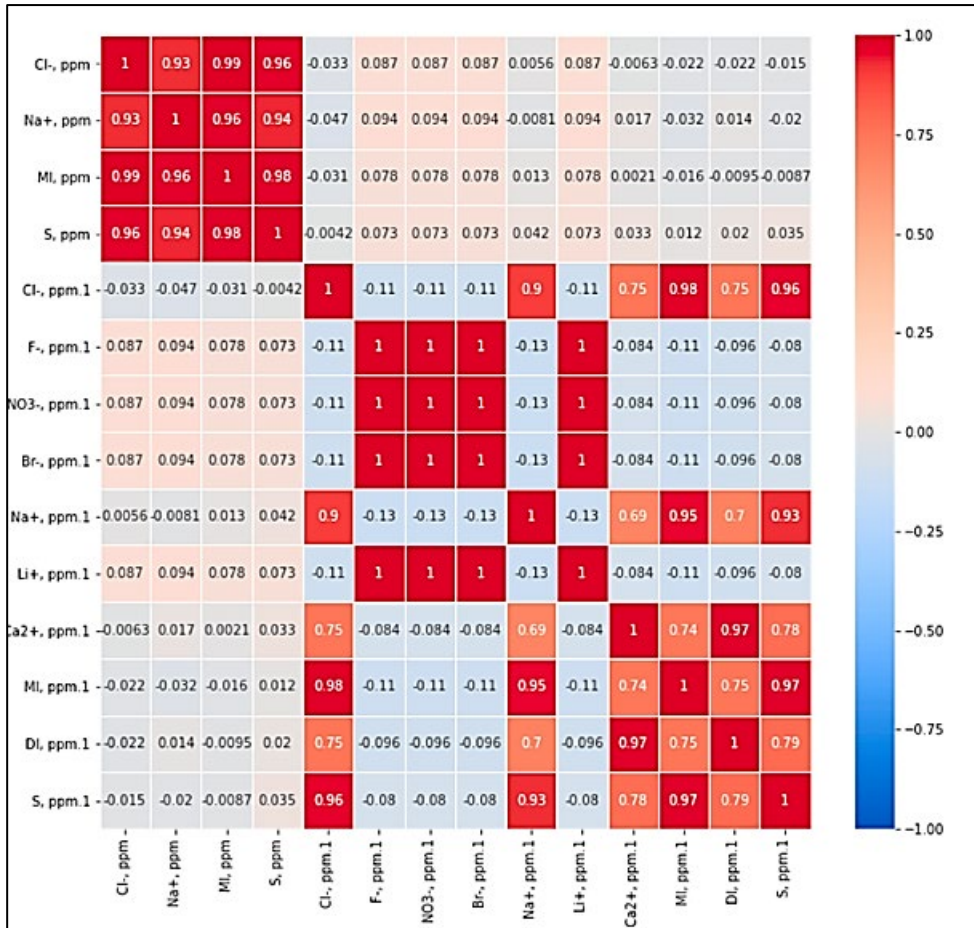


Figure 2-23: Heat Map indicating Collinear features

2.4 Operational Aspects and Monitoring

DCWF is expected to provide additional 6% recovery of the oil in place at initial conditions and expressed in stock tank barrels, apart from that other factors that make it a preferable choice are its reduced potential for reservoir souring, scaling, corrosivity and on the economical aspects its lower capital and operational expenditures as compared to other ‘EOR’ schemes. Further it provides for improved injectivity and synergy with polymer and chemical ‘EOR’ schemes.

A high level DCWF deployment would include:

- The candidate reservoir screening,
- SCAL program to assess the DCWF effect on the core level,
- Subsurface production forecast to determine the prize,

- Facilities and their cost estimates and
- Project economics

Several critical operational aspects need to be scrutinized and accounted for while implementing different composition/salinity waterflooding. These include the following.

Water quality and composition: The quality of the injected water, including its salinity and composition, can significantly impact the effectiveness of different composition/salinity waterflooding. The injection water should be carefully selected and treated to ensure that it meets the desired specifications. It is reported that brine salinity needs to be around 5,000 mg/L or 5000 ppm for the wettability change to come into effect (Sorop et al., 2013).

Injection rate and pressure: The injection rate and pressure should be optimized to ensure that the different composition/salinity water is injected into the reservoir at the desired rate and pressure. This can help to ensure that the water reaches the desired locations in the reservoir/field and maximizes the displacement and mobilization of the remaining insitu oil.

Reservoir heterogeneity: The heterogeneity of the reservoir can significantly affect the effectiveness of DCW. It has been studied with numerical modelling and shown in Figure 2-24 where the effectiveness of the oil recovery in both carbonates and sandstones decreases with increasing heterogeneity (Al-Ibadi et al., 2020). The reservoir should be carefully characterized to identify the locations of remaining oil and to optimize the design and implementation of the different composition/salinity waterflooding project.

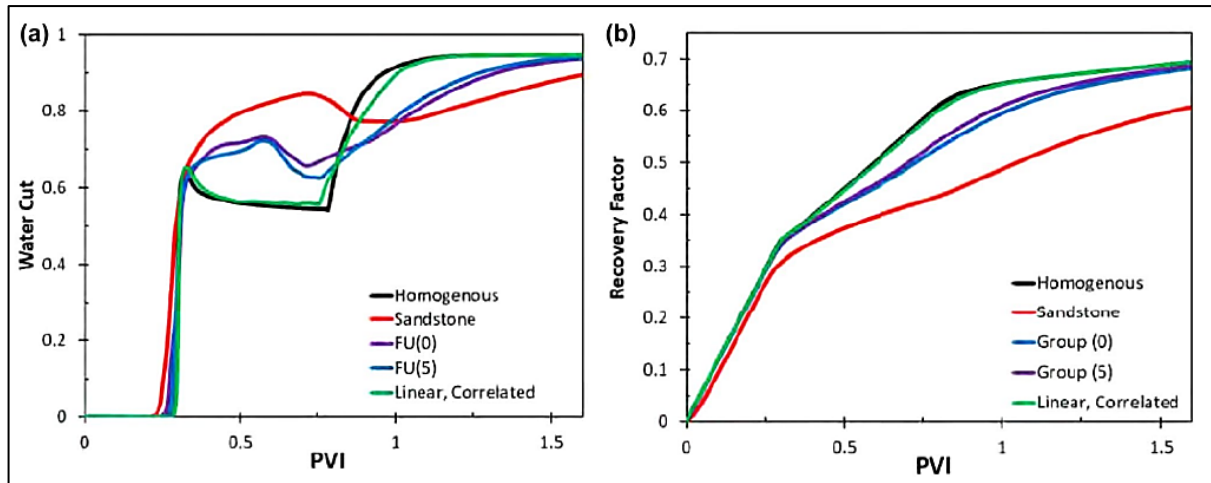


Figure 2-24 Sandstone and Carbonate Models showing evolution of fraction of water to total liquid and hydrocarbon recovery factor with respect to heterogeneity (Al-Ibadi et al., 2020)

Another aspect to be considered for DCWF is the top side facilities for the different composition/salinity water. Various studies considering the desalination studies was conducted by BP, Robbana et al 2012, in which membrane desalination protected upstream by membrane prefiltration (microfiltration, MF or ultra-filtration, UF) to minimize weight and space was identified as the efficient and established methodology for offshore sea water desalination. Ion rejection by reverse osmosis is the mechanism behind membrane desalination. In this process pressure is applied to the sea water feed in order to force water molecule movement through semi-permeable membranes that enable ion rejection, overcoming the osmotic potential of the seawater, and generating reduced salinity permeate and more concentrated retentate (or brine) streams. Membrane filtration offers superior performance in removing high levels of suspended solids, organic matter, and bacteria upstream. These are essential for preventing fouling and ensuring the efficient operation of the desalination process. To keep the filtration membrane efficient, regular and frequent backwash cycles are performed for elimination of the excluded materials. The schematic Figure 2-25 depicts the membrane desalination process and its integration into the topside water system. The desalination through reverse osmosis has challenges associated with its low efficiency (40-50%) and leads to large reject stream of concentrated seawater due to needing 2-2.5 times more source intake like sea. Also, the process is energy intensive requiring additional MWs of power. Another operational consideration is the management of the produced water which will be of higher salinity. This water generally cannot be disposed into the sea and needs to be treated. In many cases they are considered for

produced water re-injection (PWRI) projects. Sorop et al 2013 proposed worst case for the disposal of the reject stream as in Table 2-1

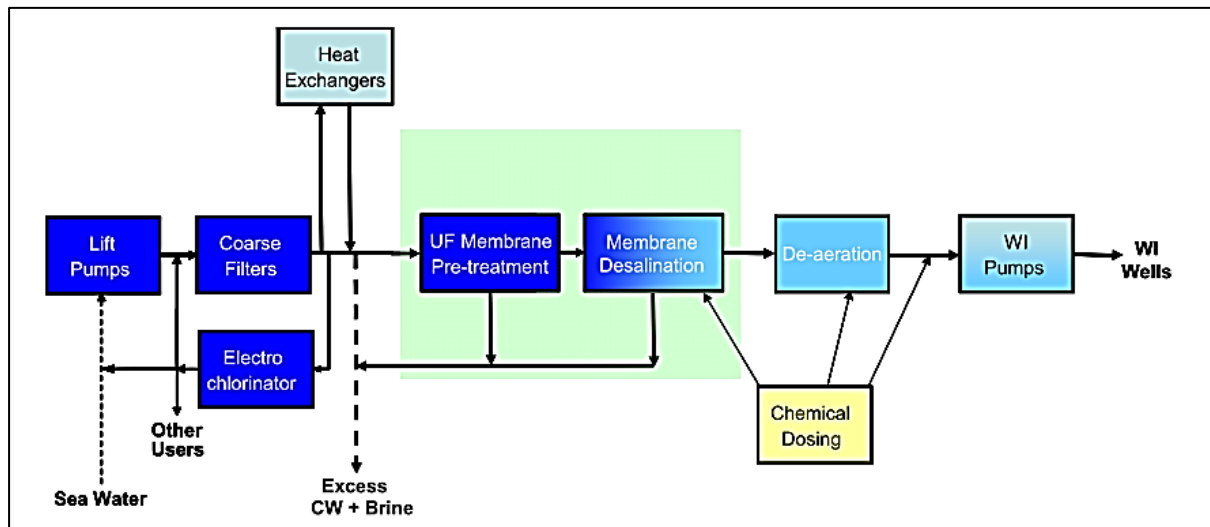


Figure 2-25: Membrane Desalination Integration into waterflood facilities (Robbana et al 2012)

Table 2-1: Reject stream options for onshore project. The choices in red are least favourable (Sorop et al., 2013)

Location for desalination unit	Water source	Reject sink	Produced water sink
coast	sea	sea	sea
field	aquifer	aquifer	aquifer
	surface	oil reservoir	oil reservoir

Monitoring and control: The different composition/salinity waterflooding process should be carefully monitored and controlled to ensure that it is proceeding as planned and to identify any issues or problems that may arise. This can help to optimize the process parameters and ensure that the project is successful. Monitoring considerations for different composition/salinity waterflooding include:

Water quality monitoring: The quality of the injected water should be monitored to ensure that it meets the desired specifications and remains consistent throughout the project.

Injection monitoring: The injection rate and pressure should be monitored to ensure that the different composition/salinity water is being injected into the reservoir/field at the desired rate and pressure.

Reservoir monitoring: The reservoir should be monitored to track the displacement and mobilization of the remaining oil and to identify any changes in reservoir properties or conditions.

Production monitoring: The production rate and water cut should be monitored to track the effectiveness of the different composition/salinity waterflooding project and to identify any issues or problems that may arise.

Environmental monitoring: The environmental impact of the different composition/salinity waterflooding project should be monitored to ensure that it is not causing any harm to the surrounding ecosystem.

Overall, careful consideration of these critical operational and monitoring aspects is essential to ensure the success of DCWF projects.

2.5 Economic Considerations

Economic considerations for different composition/salinity waterflooding involve CAPEX and OPEX analysis and it has to be incremental to ongoing existing development. One of the ways to evaluate the economic attractiveness is to plot the Unit Technical Cost (UTC) versus the incremental recovery. Additionally, the Net Present Value (NPV) and the Value Investment Ratio (VIR) can be calculated for the different ranges of low-mid-high ranges. It additionally also includes taking into consideration:

Cost of implementation: The cost of implementing different composition/salinity waterflooding can vary depending on the size and complexity of the project. This includes the cost of treating and injecting the different composition/salinity water (surface facilities), as well as the cost of monitoring and controlling the process.

Potential increase in oil recovery: Different composition/salinity waterflooding has the probable capacity to increase oil recovery, which can result in increased revenue for oil companies. The economic benefits of different composition/salinity waterflooding will depend on the specific reservoir and the effectiveness of the process.

Cost-benefit analysis: A cost-benefit analysis should be conducted to determine the economic viability of different composition/salinity waterflooding for a specific reservoir. This analysis should consider the costs of implementation, the potential increase in oil recovery, and the overall economic impact of the project.

Regulatory considerations: Regulatory considerations, such as taxes and royalties, should be considered when evaluating the economic feasibility of different composition/salinity waterflooding projects. The disposal cost of the reject water from the water treatment needs to be given due consideration.

Overall, the economic considerations of different composition/salinity waterflooding will depend on the specific reservoir and the effectiveness of the process.

CHAPTER 3

UNDERSTANDING OF THE CRITICAL MECHANISMS FOR DIFFERENT COMPOSITION/SALINITY EOR ASSOCIATED SIMULATION

Modeling and simulation are essential tools for understanding the mechanisms/processes behind different composition/salinity waterflooding and predicting its effectiveness in different reservoirs. The underlying mechanisms/processes of different composition/salinity waterflooding are complex and not yet fully understood, making modelling and simulation critical for optimizing the process parameters and predicting its effectiveness. There are various mechanisms that are associated with different composition/salinity mechanisms which include wettability alteration, surface reactions/MIE, fines migration, Double layer expansion (DLE), Mineral Dissolution, IFT alteration/reduction, Salting-in effect and formation of water-in-oil micro-dispersions.

At different scales, models can be used to simulate the interaction between the different composition/salinity water and the rock surfaces, predict the displacement and mobilization of the remaining oil, and optimize the design and implementation of the different composition/salinity waterflooding project. These models typically involve the use of computational fluid dynamics (CFD), numerical reservoir simulators, and pore-network models to simulate the flow of the different composition/salinity water and the oil in the reservoir. Various researchers, in the last decades, have conducted laboratory corefloods (Egbe et al., 2021; Rivet et al., 2010; Sorbie & Collins, 2010), and several have carried out field tests (Akhmetgareev & Khisamov, 2015; Seccombe et al., 2010; Singh & Sarma, 2021; Vledder et al., 2010) towards finding the underlying mechanisms and also affirming the benefits of DCWF. The mechanisms proposed in the literature and their validity are discussed in detail in various studies (Al-saedi & Flori, 2020; Al-Shalabi et al., 2014; Alshakhs et al., 2020; Emadi & Sohrabi, 2013; Mahzari & Sohrabi, 2014; Sheng, 2014; Skauge, 2013).

DCWF research started with focus on understanding the underlying mechanisms through lab (core based & micromodels) and then to a larger scale of single well, multi-well and reservoir level pilots and trials. The research next progressed to modelling of DCWF through using flow functions of relative permeability and capillary pressure as a function of the salinity and

subsequently incorporation of geochemical interactions into flow simulations (Al-Shalabi et al., 2016; Dang et al., 2015; Farajzadeh et al., 2011; Okabe, 2005)

3.1 Mechanisms of Different Composition/Salinity EOR

The dominant mechanisms of DCWF and the key parameters that need to be understood and their value ranges quantified to better model and understand different composition/salinity effectiveness required careful study of various experiments from lab corefloods to field trials evaluating the various critical parameters of initial reservoir conditions, wettability, compositions of the rock and fluids (crude oil, formation water and injected water) and their interactions Figure 3-1. There are different parameters that are critical to the understanding of the DCWF mechanisms and these are detailed next. The initial conditions of the set up or reservoir with respect to wettability, pH, temperature and saturation of water; the properties of the rock which include the permeability heterogeneity, mineral composition, presence of clay or not, Cation Exchange Capacity (CEC) of the rock; the connate brine properties: brine ionic composition and concentration, salinity compared to the injection water salinity; oil properties: Saturates Aromatics Resins and Asphaltene (SARA) composition, Total Acid Number (TAN), Total Base Number (TBN); injected brine properties: ionic composition, salinity as compared to the connate water. The critical mechanisms are depicted in Table 3-1

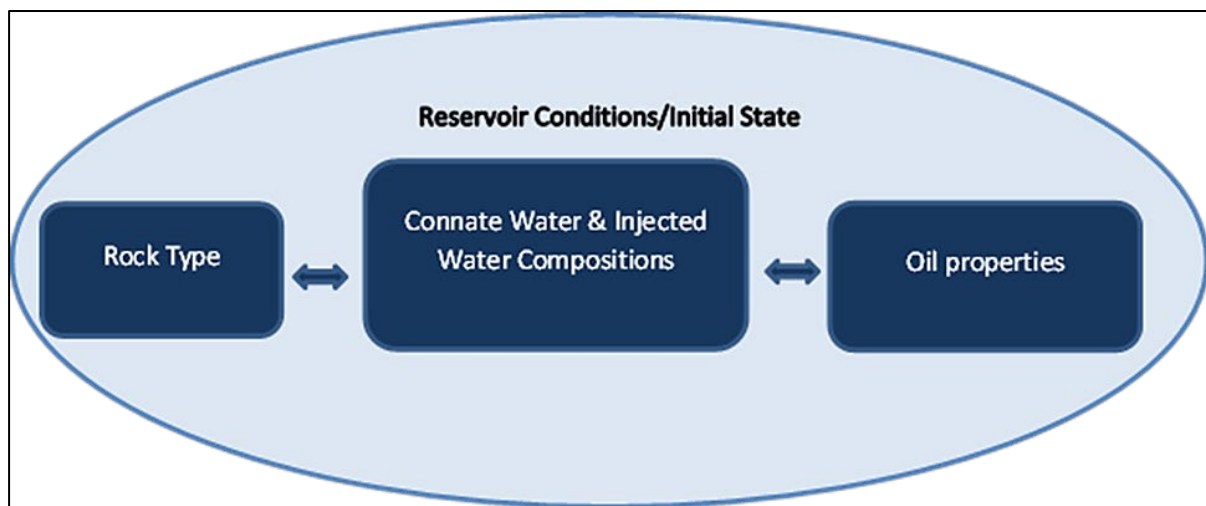


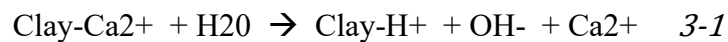
Figure 3-1: Elements and their interactions which impact the recovery of oil in DCW

Table 3-1: Summary of the critical DCWF mechanisms

Mechanisms	Pre-requisite Parameters	Rock-Fluid Interaction	Fluid-Fluid Interaction	Effect
pH change	<ul style="list-style-type: none"> Initial wetting state to be moderately to low water wet. Acid Number of the oil. Monovalent cations in the injected water. 	-	Creation of natural surfactants in the oil	<ul style="list-style-type: none"> IFT reduction pH increase Increase in Water wetness Divalent cations in the effluent stream
Fine particle release/movement	<ul style="list-style-type: none"> Initial wetting state to be moderately to low water wet. Clay presence 	Transportation of fines at the oil-water interface	-	<ul style="list-style-type: none"> Fine production in the effluent Increase in Water wetness
Ion Exchange/ EDL	<ul style="list-style-type: none"> Multivalent ions in formation water. Monovalent ions in injection water. Initial wetting moderately to low water wet 	Ion exchange at the rock surface and double layer expansion	Ion exchange between the injected and connate water	<ul style="list-style-type: none"> Increase in Water wetness Divalent cations in the effluent stream
Salt-in Effect	<ul style="list-style-type: none"> Initial wetting state to be moderately to low water wet. Low salt concentration in the injected water compared to connate water 	-	Dissolution of the organic component of the oil in the water.	<ul style="list-style-type: none"> IFT reduction Increase in Water wetness
Micro dispersions	<ul style="list-style-type: none"> Initial wetting state to be moderately to low water wet. Surface active materials 	-	Micro dispersion with water core and oil surrounding	<ul style="list-style-type: none"> Microdispersion formation Increase in Water wetness

Analysis of the work done by researchers highlight that certain conditions are necessary for the oil recovery to be effective through DCWF and these conditions were presence of clay/mineral composition, connate water, crude-oil, composition of the cations/anions in the injected water, the wettability of the system and the temperature of the system (Awolayo et al., 2014; Strand et al., 2006; Yousef, Al-Saleh, et al., 2012). The main interaction mechanisms are detailed as follows.

Changes in pH has been indicated as one of the outcome of DCW. The pH increase value ranges from 7-8 pH to 9-10 pH. This has been shown in Figure 3-2. The injection of DCW results in non-equilibrium of the cations attached to the clays and its replacement by the protons which leads to an increase in the hydroxyl ions and hence increase in the pH of the system (Austad et al., 2010)



The released hydroxyl ions then react with the acid and base components of the crude oil attached to the rock surface facilitating the release of the oil from the rock surface and hence leads to the surface being less oil wet.



The nature of the above reactions are impacted by the kind of clay and its CEC (Cation Exchange Capacity)

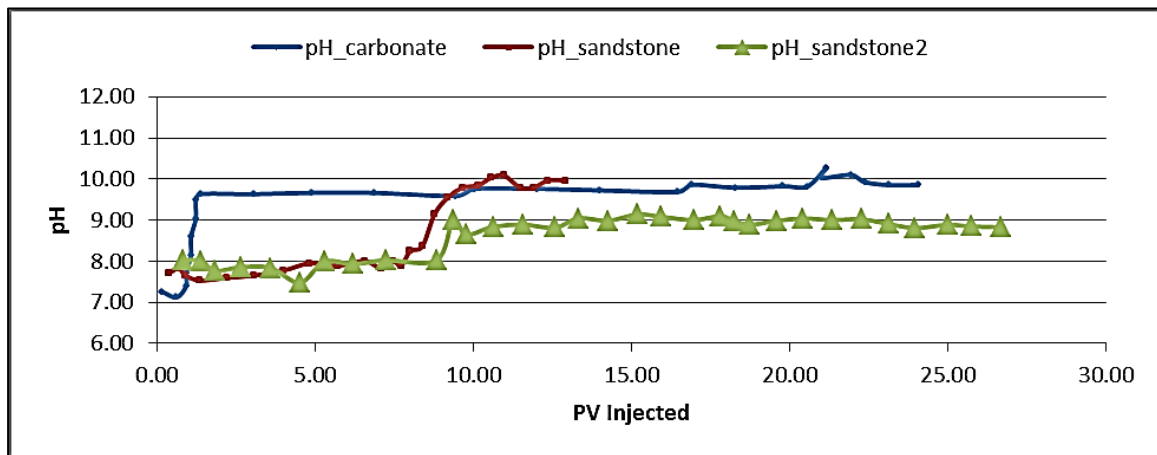


Figure 3-2: pH changes Vs Pore Volume Injected

Fine particle release and its movement was investigated where it was purported that DCW could trigger the release of the particles of clay through factors such as pH, flowrate, temperature and adsorption of organic matter. The release of the fine particles leads to increasing the water wettability of the rock/mineral surface and through blocking existing pore spaces it leads to water diversion into unswept areas. The critical analysis carried out in this research highlights that though there is no permeability reduction, or fines present in the effluent stream, research needs to include pre and post flood core scans and close monitoring of the pressure changes to effectively conclude on the fine migration.

The mechanism of MIE in clastic is through cation exchange, while in carbonates it's through anion exchange with the cation metallic complexation of the organic material. This mechanism is effectively demonstrated at the inter-well scale where the hydrocarbon and brine production were measured at the nearby producers with respect to the amount of injected water in the injector well. The change in the ion concentration in the produced water and the decrease in the water-oil ratio at the producer was evidence of the MIE impact and the corresponding improved oil recovery. It is very evident that salinity reduction along with composition change in the ions is required for effectiveness of the DCWF.

The EDL between the oil-brine-rock due to ion exchange and interaction leads to its expansion resulting in the change in the wettability of the rock surface. The further analysis of the EDL expansion is done through the zeta potential measurements. But we need to understand that Zeta potential measurements are done on crushed samples and at different conditions to the core or reservoir conditions.

Surfactant generation is also considered as a mechanism where the DCW interaction/interplay amidst the brine/water, oil/hydrocarbon and rock/mineral leads to alteration of the IFT and subsequently formation of surfactants. This is inline with the micro-dispersion of water in oil that were visually evidenced. But many changes in the IFT are in the order of 1mN/m at experimental conditions akin to ambient conditions even through significant incremental recovery was reported.

The integrated analysis carried out in this research identifies the key parameters that enable better understanding of the DCW effectiveness as the initial conditions of the reservoir (wettability and temperature) along with the pH change of the system and its change. The initial water saturation at the start of the DCW. The rock properties which include permeability heterogeneity, mineral composition, presence of clay and 'Cation Exchange Capacity' (CEC). The brine properties of the brine ionic composition and concentration (both connate and injected water), salinity comparison between the connate and injected water. The oil properties in terms of 'Saturates Aromatics Resins and Asphaltene' (SARA), 'Total Acid Number' (TAN) and 'Total Base Number' (TBN).

The meta- analysis of the various experiments leads to the conclusion that all the critical mechanisms can be based on two main interactions/interplay between the 'rock/mineral-fluid' and the 'fluid/hydrocarbon-fluid/brine' which leads to changes in the wettability, IFT or both. The prominent mechanisms are the EDL expansion, MIE and microemulsion formation which are the main causes the rest like 'pH changes', 'fines migration' are more the effects. Initial wettability and temperature should be considered as driving factors impacting the magnitude of the DCW impact Figure 3-3. The incremental recovery range evidenced for DCW is in the range of 2-17%.

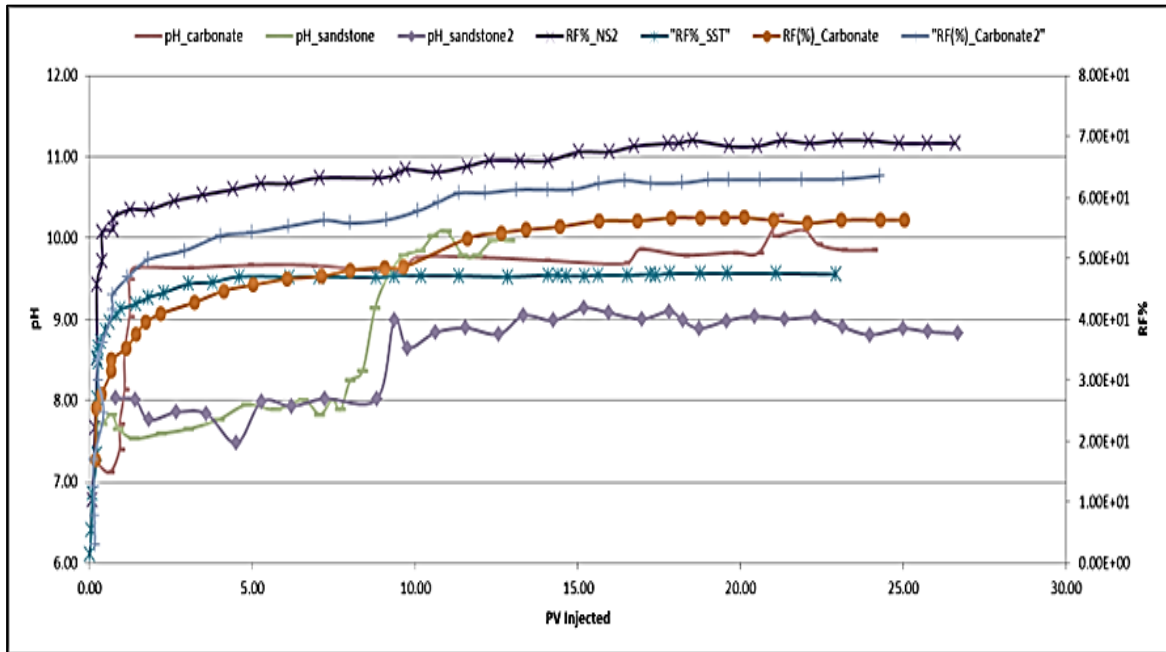


Figure 3-3: Analysis of DCW Recovery for sandstones and carbonates

3.2 Modeling and Simulation of Different Composition/Salinity (Eclipse)

The ‘BRINE’ model in ‘Eclipse 100’ (Eclipse 100 is a licensed SLB product) activates the option of an extra phase of the salt phase to the existing phases. This aids in exploring and assessing the impact of brine/water composition and its injection into subsurface reservoirs. The mass conservation equation (Eclipse Reference Manual) is resolved, on a grid block basis, for the salt phase as per the following equation and also the assumption for the salt existence is only in the water phase.

$$\frac{d}{dt} \left(\frac{VS_w C_s}{B_w} \right) = \sum \left[\frac{T k_{rw}}{B_w \mu_{s\,eff}} (\delta P_w - \rho_w g D_z) \right] C_s + Q_w C_s \quad 3-4$$

Where V denotes ‘the volume of the block pore’, S_w denotes ‘the saturation of water’, C_s denotes ‘the salt concentration present in aqueous phase’, \sum denotes the summation over neighbouring cells, T denotes transmissibility, k_{rw} denotes the ‘relative permeability of water’, B_w denotes ‘formation volume factor for water’, $\mu_{s\,eff}$ denotes ‘salt effective viscosity’, P_w denotes ‘pressure of water phase’, ρ_w denotes ‘water density’, D_z denotes ‘cell center depth’, g denotes ‘acceleration due to gravity’ and Q_w denotes ‘the production rate of water’.

The ‘LOWSALT’ keyword available and input in the ‘RUNSPEC’ section of the simulation model data deck allows the activation of the ‘BRINE’ option and introduction of salinity dependent sets of saturation, relative permeability and capillary pressure curves. In addition, the ‘LSALTFNC’ keyword in the ‘PROPS’ section allows for interpolation between these salinity dependent curves through weighting factors (F_1 and F_2) which controls and calculates the saturation end points, water and oil relative permeabilities and water-oil capillary pressure. The following equations demonstrate the interpolation of the aforementioned.

$$k_{rw} = F_1 k_{rw}^L + (1 - F_1) k_{rw}^H \quad 3-5$$

$$k_{ro} = F_1 k_{ro}^L + (1 - F_1) k_{ro}^H \quad 3-6$$

$$P_{cow} = F_2 P_{cow}^L + (1 - F_2) P_{cow}^H \quad 3-7$$

Where,

‘ F_1, F_2 : Functions of the salt concentration

k_{rw} : water relative permeability

k_{ro} : oil relative permeability

P_{cow} : oil-water capillary pressure

The superscripts of H and L stand for the high salinity and different composition/salinity curves respectively.'

The end point saturations are calculated by the following set of equations:

$$S_{wco} = F_1 S_{wco}^L + (1 - F_1) S_{wco}^H \quad 3-8$$

$$S_{wcr} = F_1 S_{wcr}^L + (1 - F_1) S_{wcr}^H \quad 3-9$$

$$S_{wmax} = F_1 S_{wmax}^L + (1 - F_1) S_{wmax}^H \quad 3-10$$

$$S_{owcr} = F_1 S_{owcr}^L + (1 - F_1) S_{owcr}^H \quad 3-11$$

Where:

' S_{wco} : saturation of connate water

S_{wcr} : saturation of critical water

S_{wmax} : maximum saturation of water

S_{owcr} : critical saturation of oil in water presence

F_1 : function of the concentration of salt'

The superscripts of H and L stand for the high salinity and different composition ('low salinity') curves respectively. In the 'REGIONS' section through the 'SATNUM' and 'LWSLTNUM' the different areas of the model are assigned the appropriate saturation functions. The different composition/salinity water 'PVT' properties are assigned through the 'PROPS' section of the simulation modelling data deck by adding the keyword 'PVTWSALT' which includes one table for the reference pressure and salt concentration and a second table for salt concentration, water formation volume factor, water compressibility, water viscosity and water viscosibility. The connate water salt concentration is set through 'SALTVD' or 'SALT' added in the 'SOLUTION' section. 'SALTVD' comprise a table of salt concentration vs depth. The 'SALT'

however specifies the concentration of salt at initial conditions for each grid. The salinity of injection brine is set through 'WSALT' keyword added in the 'SCHEDULE' section of the simulation modelling data deck which assigns the salt concentration in the brines of the injection wells.

A numerical simulation model with dimensions of 15x15x3 was set up to generate responses to different composition/salinity flooding as illustrated in Figure 3-4

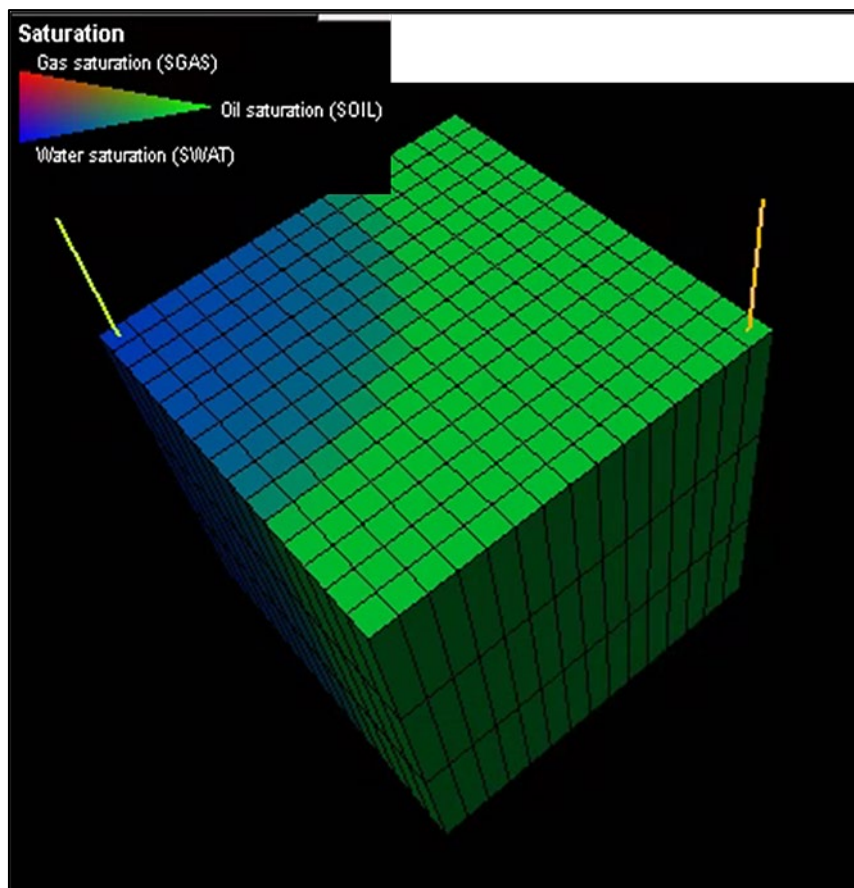


Figure 3-4: Dynamic Simulation model set up

The model had constant properties of porosity 25% , Perm_x and Perm_y equal to 200 mD, Perm_z equal to 20 mD and initial water saturation (S_{wi}) equal to 20%. The Corey model is used to set up the saturation functions in the model which also enables uncertainty and sensitivity evaluation on the same. The Corey model for an oil-water system is represented by the following equations.

$$k_{rw} = S_*^{N_w} E_w \quad 3-12$$

$$k_{ro} = (1 - S_*)^{N_o} E_o \quad 3-13$$

$$E_w = k_{rw}(S_{or}) \quad 3-14$$

$$E_o = k_{ro}(S_{wi}) \quad 3-15$$

$$S_* = \frac{S_w - S_{wi}}{1 - S_{wi} - S_{or}} \quad 3-16$$

Where:

' k_{rw} : water relative permeability

k_{ro} : oil relative permeability

S_* : normalised saturation of water

E_w : is the end point relative permeability of water

E_o : is the end point relative permeability of oil

N_w : corey's water exponent'

N_o : corey's oil exponent'

Different sensitivity analyses were performed which included the salinity variation of the connate and injection brine, the timing of the start of the injection, the weighting factors, the end points for the hydrocarbon and brine relative permeabilities, the corey's exponents and the residual oil to water saturation. This is shown in the mentioned figures of Figure 3-5, Figure 3-6, Figure 3-7 and Figure 3-8 along with the results from the simulation runs in terms of the cumulative oil production.

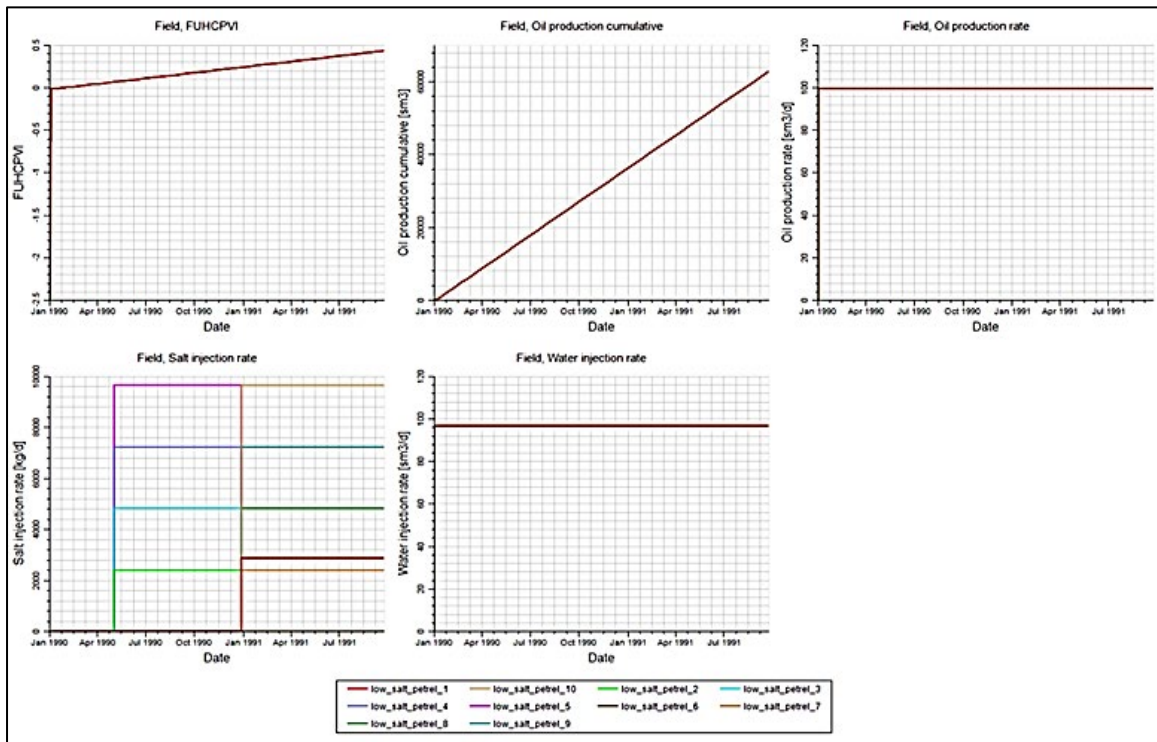


Figure 3-5: Simulation sensitivity for different salt injection

Table parameters

Phases: Gas Oil Water

Relative permeability

Use correlation

Table entries: 11

Sgr:	0.05	Sorw:	\$\$SORW	Swmin:	0.2
Corey gas:	6	Sorg:	0.2	Swcr:	0.22
Krg@Swmin:	0.9	Corey O/W:	\$NO	Corey water:	\$NW
Krg@Sorg:	0.8	Corey O/G:	3	Krw@Sorw:	\$EW
		Kro@Somax:	\$EO	Krw@S=1:	1

Figure 3-6: Corey Parameters Uncertainty Input

	Type	Pr	Int	Name	Base value	Distribution	Arguments					
1	Control		<input type="checkbox"/>	SSALT1	1		Min	1	Max	100	Start	2
2	Control		<input type="checkbox"/>	SSALT2	30		Min	1	Max	100	Start	2
3	Control		<input checked="" type="checkbox"/>	SYEAR	1990		Min	1990	Max	1999	Start	1991
4	Uncertain		<input type="checkbox"/>	SF1HS	0.1	Uniform	Min	0	Max	0.3		
5	Uncertain		<input type="checkbox"/>	SF1LS	0.5	Uniform	Min	0.4	Max	1		
6	Control		<input type="checkbox"/>	SEO	0.5		Min	0.5	Max	0.8	Start	0.79
7	Control		<input type="checkbox"/>	SEW	0.6		Min	0.6	Max	0.8	Start	0.61
8	Control		<input type="checkbox"/>	SNO	3		Min	2	Max	3	Start	2.1
9	Control		<input type="checkbox"/>	SNW	3		Min	2	Max	3	Start	2.9
10	Control		<input type="checkbox"/>	SSORW	0.2		Min	0.1	Max	0.3	Start	0.2

Figure 3-7: Uncertainty and Sensitivity Parameters

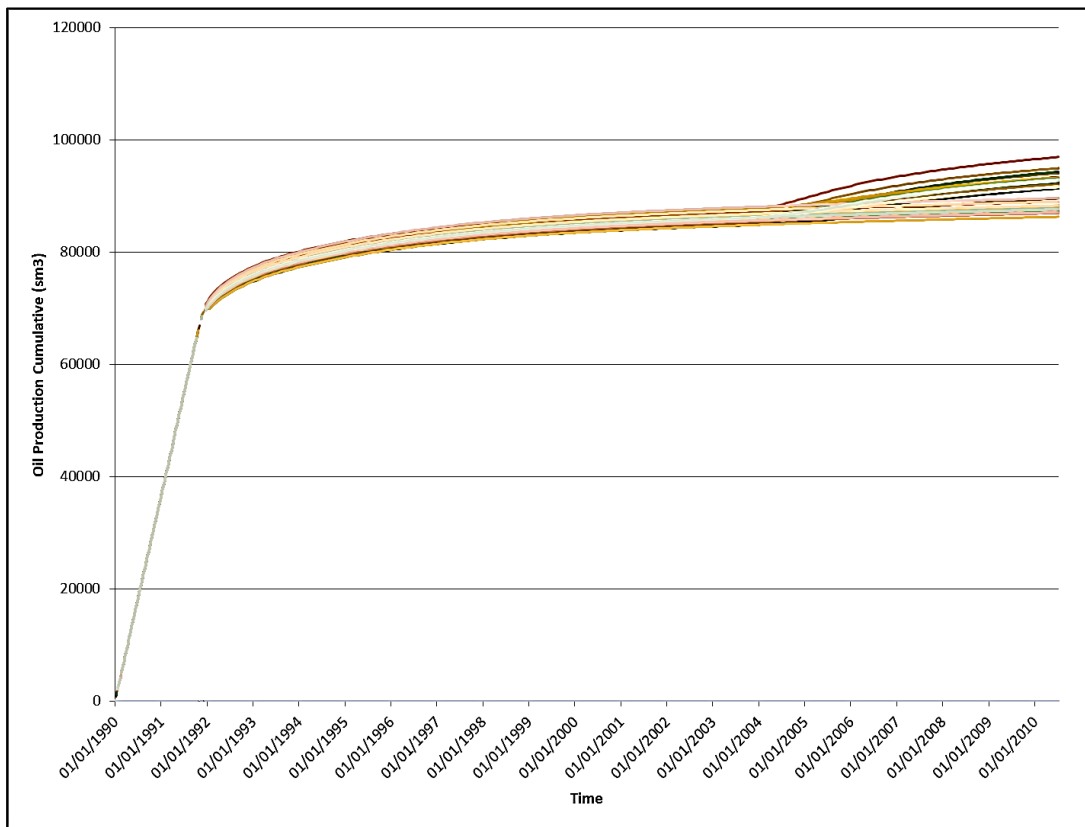


Figure 3-8: Cumulative Oil Production Vs Time for the various sensitivities

CHAPTER 4

ARTIFICIAL INTELLIGENCE METHODS APPLIED IN EOR

Screening of reservoir candidates for ‘EOR’ based on the setting depth of the subsurface reservoir, temperature of the subsurface zone, permeability of the reservoir, saturation of oil, viscosity of oil, oil °API and composition was first done Taber et al (Taber et al., 1997) and the work was further extended by Goodlett et al. The various work with regards to screening/selection of the reservoir candidates for a particular ‘EOR’ involved data analysis using tables and graphs, lab work and AI. A procedure for the data collection for ‘EOR’ was presented by Kang et al (Kang et al., 2014) which is presented in Figure 4-1

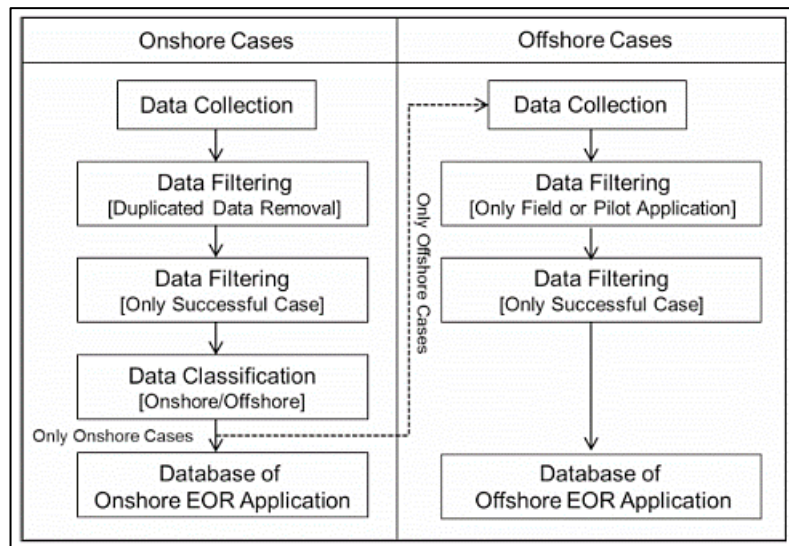


Figure 4-1: Illustration of Data Collection Procedure and Workflow (Kang et al., 2014)

One of the initial AI screenings for ‘EOR’ was published by Guerillot, subsequent works were done towards improvement of the quality and accuracy in relation to the models. The variety of AI models used are fuzzy-logic (FL) AI model, expert system AI model, ‘artificial neural network’ (‘ANN’) AI model, ‘least square support vector machine’ (‘LSSVM’) AI model and ‘combination of FL and neuro-fuzzy (NF)’. The AI models start with data gathering of the different ‘EOR’ and their reservoir properties (Ramos, 2017) as shown in Figure 4-2 where in addition to the successful ‘EOR’ projects the Block T from Angola is compared. The utilization of plots like scatter plots, box plots and histograms offer a rapid and effective method for

analysing and determining the significance of the data. Further analysis of the data with respect to their uncertainty will be carried out through the AI models.

The data set in the AI/ML process goes through a ‘training, validation, and testing’ process. The data is randomly split by 80% for training purpose and the remaining 20% for validation and various model fit parameters like Root Mean Square Error (RMSE), standard deviation, etc. were utilized in fine tuning of the models to the data. Then the validated model is used in the testing phase to predict the values and compared to observed data. The selected ‘EOR’ methods were then further screened by lab and field experiments. An overview of the different kinds of models needed to interact with each other to attain the required objective is shown in Figure 4-3.

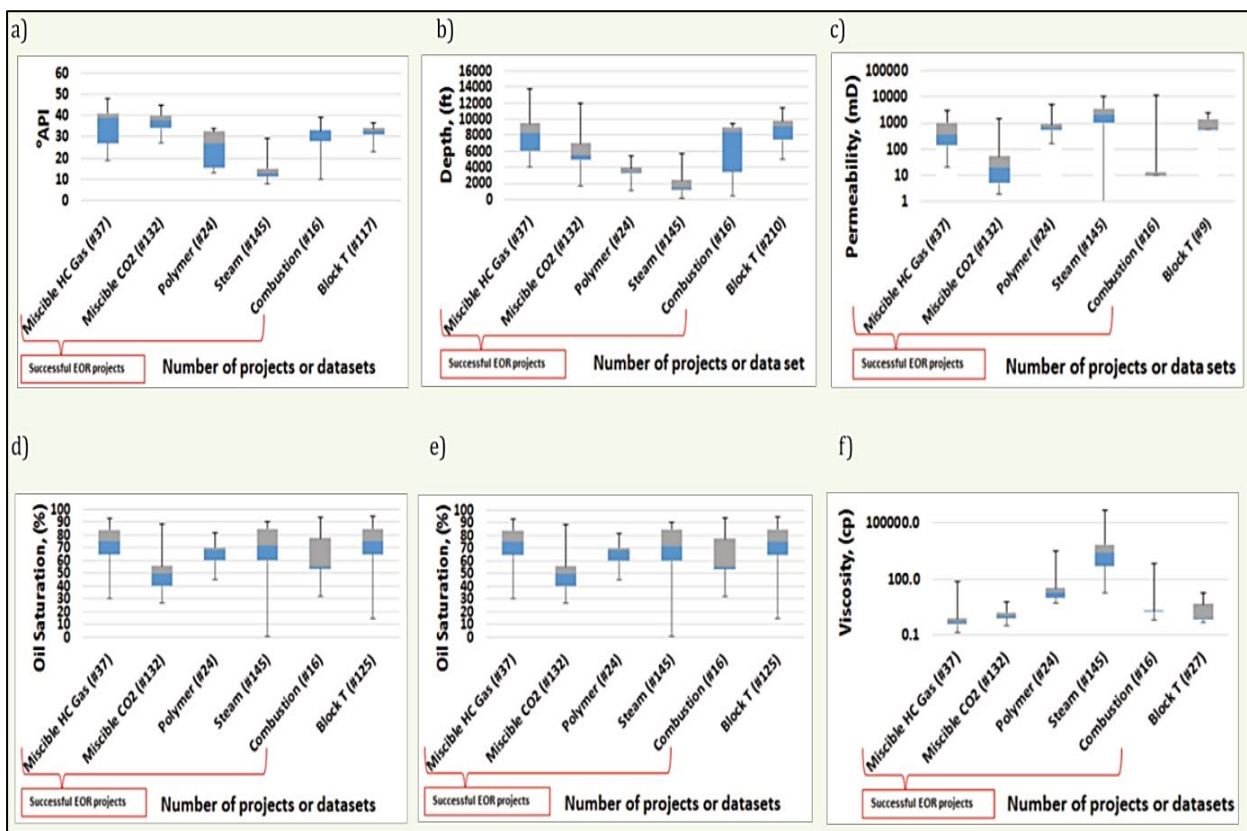


Figure 4-2: Box Plots of Reservoir Properties Vs EOR methods (Ramos, 2017)

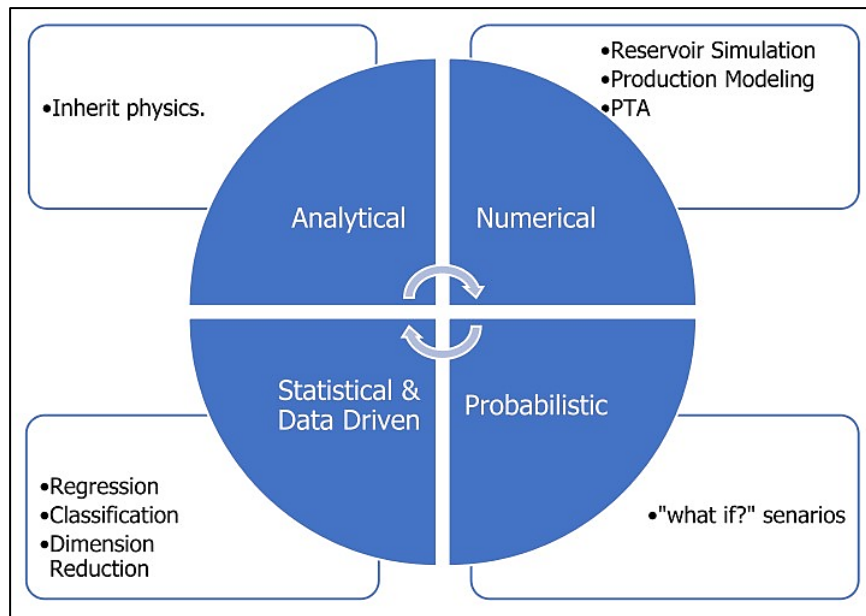


Figure 4-3: Interaction between the different models

4.1 Overview Of Various Artificial Intelligence Methods And Algorithms

ML/AIT are employed, both as a classifier and regressor, in different facets of the hydrocarbon extraction industry in areas of subsurface hydrocarbon reservoir exploration, subsurface hydrocarbon reservoir management, subsurface hydrocarbon reservoir development and predictive maintenance (Tariq et al., 2021). Another researcher has demonstrated the application of ANN to polymer projects (Sun & Ertekin, 2018). For prediction purposes, ANN based on 10 parameters involving the rock and fluid properties was utilized and prior to that it involved prediction of the recovery factor for a waterflood (Mahmoud et al., 2019). The common approach involved AI/ML tools utilization, including Random Forest AI/ML tools, Decision Trees AI/ML tools and Gradient Boosting AI/ML tools coupled with numerical simulation and optimization algorithms (El-M Shokir et al., 2002; Javadi et al., 2021; Ng et al., 2021; Syed et al., 2021).

The artificial intelligence/ machine learning methods begins with the utilization of linear regression and logistic regression. The utilization of linear regression is for regression analysis while the utilization of logistic regression is for classification problems.

The relationship and interaction between two or more variables are analysed through the utilization of linear regression. This is based on the assumption that the interactions amongst the variables can be modeled effectively using a linear equation or an equation of line. The variable that is used in prediction is the ‘independent variable’ and the ‘predicted variable’ is termed as the ‘dependent variable’. An example is given as

$$y = w_0 + w_1x \quad 4-1$$

where w_0 is the intercept on y-axis, w_1 is slope of the line, x is the ‘independent variable’ and y is the ‘dependent variable’.

There are three types of evaluation metrics frequently used for the linear regression model evaluation and assessment :

The metrics of R² measure, the metrics of Mean Absolute Error (MAE) and Root Mean Square Error (RMSE) metrics.

A sigmoid mathematical function is utilized in the logistic regression, this maps to a probability between 1 and 0 for any real number. Figure 4-4 illustrates the sigmoid function, which is an S-shaped graph, which means as x approaches infinity, the probability becomes 1 and as x approaches negative infinity, the probability becomes 0. The performance measures in logistic regression includes the following where it starts with a confusion matrix which maps the True Positive (TP), False Positive (FP), False Negative (FN) AND True Negative (TN) and shown in Figure 4-5. From the confusion matrix different measures like Accuracy, Precision, Recall and F1 scores are derived. Accuracy represents the number of data occurrences that are correctly classified (TN+TP) divided by the total number of data occurrences (TN+TP+FN+FP).

$$Accuracy = \frac{TN+TP}{TN+FN+TP+FP} \quad 4-2$$

Recall can be used as a measure in cases where the spotting of the real positives are more important.

$$Recall = \frac{TP}{FN+TP} \quad 4-3$$

A good evaluation metric to be used when the cost of a false positive is very high and the cost of a false negative is low is called Precision.

$$Precision = \frac{TP}{FP+TP} \quad 4-4$$

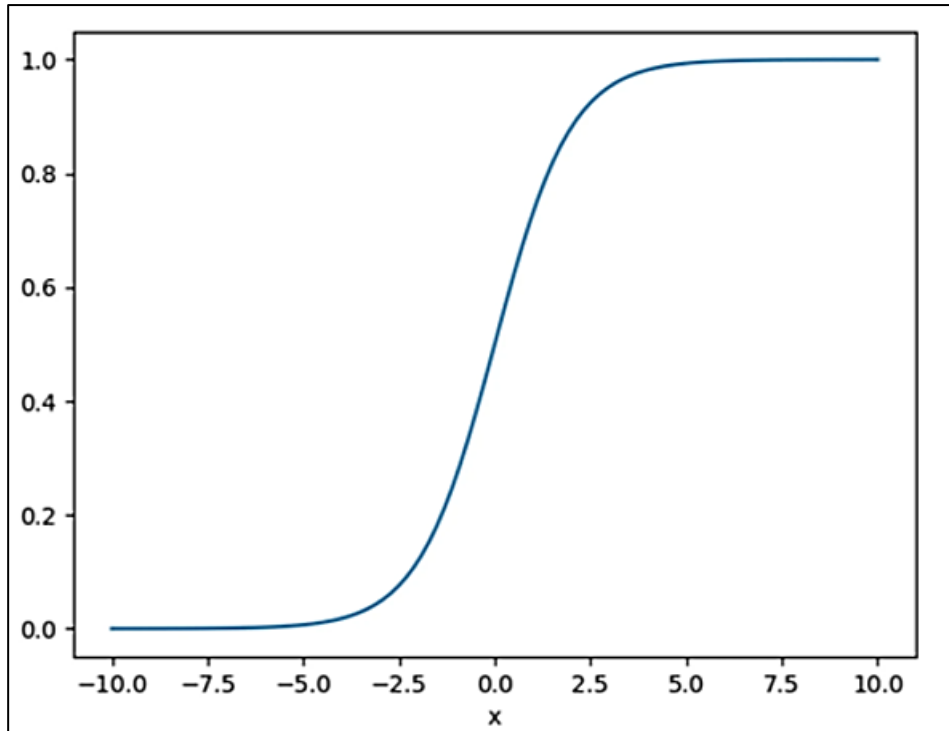


Figure 4-4: Sigmoid function

The F1 metrics score uses a combination of the Precision metrics and the Recall metrics and is used for measurement of the correctness of the model where we don't want to miss any correct predictions.

$$F1 \text{ Score} = 2x \frac{\text{Precision} \times \text{Recall}}{\text{Precision} + \text{Recall}} \quad 4-5$$

		Actual	
		0	1
Predicted	0	TN	FN
	1	FP	TP

Figure 4-5: Confusion Matrix

For classification problems at various threshold levels, the receiver operating characteristic (ROC)- Area Under Curve (AUC) curve is a performance metric. The degree or measure of separability is represented by the AUC, while the ROC is a probability curve. The reliability of the model to distinguish between classes is indicated by this curve. The greater the AUC, the better the model predicts 0 classes as 0 and 1 classes as 1. As illustrated in Figure 4-6 the ROC curve is displayed with 'True Positive Rate' (TPR) versus 'False Positive Rate' (FPR), with TPR on the y-axis and FPR on the x-axis.

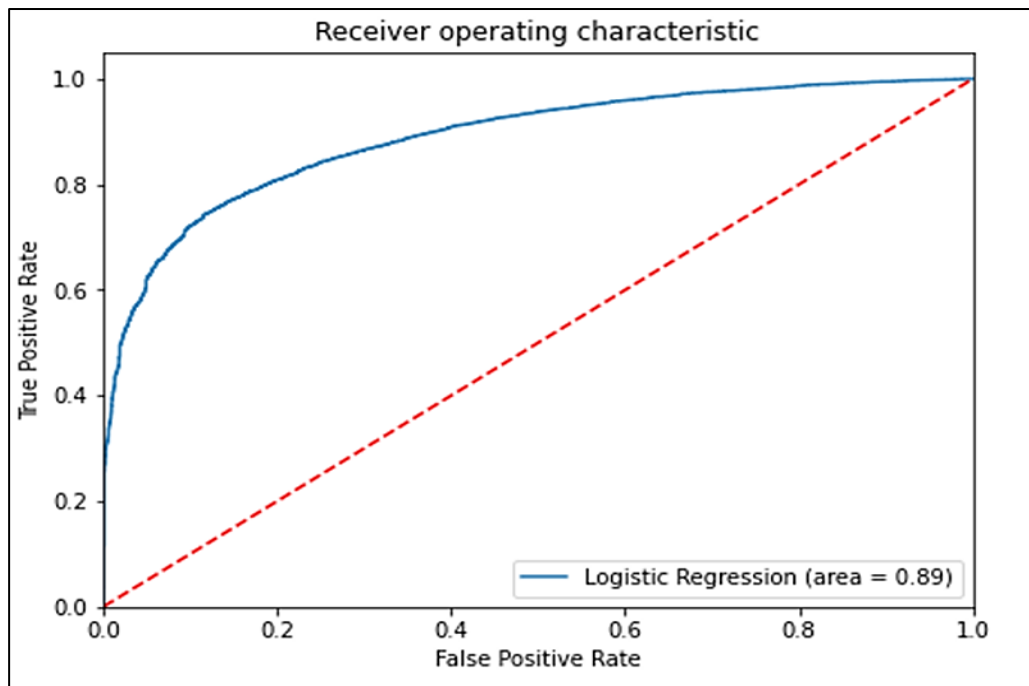


Figure 4-6: ROC- AUC curve

As illustrated in Figure 4-7 a non-parametric 'supervised learning' method used for classification and regression is the Decision Trees (DTs). A listing of common terms utilized in Decision tree models are as follows :

'Root Node': This encompasses the complete sample set which are separated into multiple branches or sub-tress of homogeneous sample sets.

'Parent Node' and 'Child Node': The parent node is the node which gets divided into sub-nodes and consequently the child node is the sub-node of a particular parent node.

‘Branch/ Sub-Tree’: The entire tree is split into a subsection which is known as the ‘Branch/Sub-Tree’.

‘Decision Node’: A sub-node that further splits into further sub-nodes based on a criterion is known as a ‘Decision Node’.

‘Leaf/Terminal Node’: The end nodes that do not get further divided are known as ‘Leaf/Terminal Node’.

‘Splitting’: The process of utilizing a splitting criterion (eg: Gini-Index and/or Information Gain) to divide a node into two or more sub-nodes is known as splitting.

‘Pruning’: The methodology of tuning a tree remove decision bias through removal of the sub-nodes of a decision node is called Pruning. This process is the opposite of the splitting process.

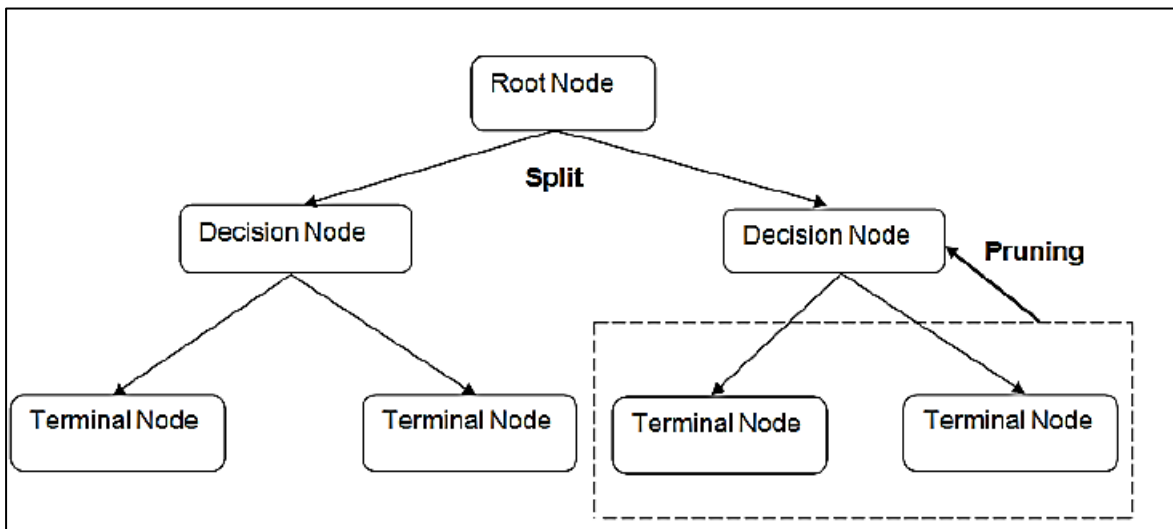


Figure 4-7: Illustration of an example Decision Tree

The impurity measures in DTs are shown in Figure 4-8. The advantages of the DTs are their ease of comprehension and interpretation; the DTs find wide application in exploration of data as it enables splitting based on the significance of the variables; Not influenced by the outlier/Null values and hence requires less data cleaning. Require less time and effort during data pre-processing than other algorithms; Can handle both continuous and categorical variables; Does not require any underlying assumptions in data. Works with both linearly and nonlinearly related variables. The disadvantages of DTs are minute incremental changes in the

data set results in significant alterations with regards to the structure of the DT resulting in model instabilities; large trees can be difficult to interpret; tends to overfit.

	GINI INDEX	ENTROPY	INFORMATION GAIN	VARIANCE
When to use	Classification	Classification	Classification	Regression
Formula	$1 - \sum p_i^2$	$-\sum p_i \log(p_i)$	$E(Y) - E(Y X)$	$\Sigma(x - \bar{x})^2/N$
Range	0 to 0.5 0=most pure 0.5=most impure	0 to 1 0=most pure 1 = most impure	0 to 1 0=less gain 1 = more gain	≥ 0
Characteristics	Easy to compute, Non-additive	Computationally intensive, Additive	Computationally intensive	The most common measure of spread

Figure 4-8: Impurity Measures in DTs

‘Random Forest’ (‘RF’) AI/ML models are also utilized for both classification and regression-based cases. RFs are comprised of DTs. The increase in the number of DTs within the RF model is directly proportional to its increase in complexity. A selection process is performed by the RF whereby the best results out of the votes that are pooled by the trees is chosen, thus making it a robust AI/ML algorithm. ‘Random Forest’ (RF) creates several subsets from a given data set, this technique is known as the Bagging technique. The segregation and training are performed on these datasets separately. In RF even the features are divided and used to grow the trees separately in a process called feature bagging. Unlike a DT, where, based on a given data the rules are generated, a RF classifier averages the results obtained from several decision trees which are built based on randomly selected features. The process of utilizing several random subsets of data and providing them as inputs to various decision trees fixes the problem of overfitting. The Bagging technique used here utilizes several predictors independently contrary to the Boosting technique which utilizes predictors sequentially.

Gradient Boosting (GB) is focused on the gradient optimization and utilizes the boosting type of ensemble technique. This technique is used both for regression and classification problems. In GB the accuracy is increased through reduction in the Loss Function (which is the error/difference between the actual value and the predicted value) and the next iteration takes this Loss Function into account. In GB the gradient is calculated for the Loss Function in relation to the values of the prediction. The algorithm in GB considers the mistakes/errors of several weaker models to develop a stronger learner model (predictive model). An initial model is created utilizing the training data and subsequently another model is created utilizing the initial one through reduction of the errors from the initial model. Sequential addition of models is performed, each an improvement in error over its preceding model, this continues until either the prediction of the training data is perfect or the addition of the maximum number of models have reached. If the loss is defined as ‘mean squared error’ (‘MSE’) then it is formulated as:

$$Loss = MSE = \sum (y_i - y_i^p)^2 \quad 4-6$$

Where, y_i is the i th target value, y_i^p is the i th prediction, the loss function is represented by $L(y_i, y_i^p)$.

The predictions should be such as to minimize the loss function (MSE).

ANN is inspired by how the neurons in the brain work and replicates the human way of learning, Figure 4-9. The most common ANN consists of a three layers of network structure: The first layer is an ‘input layer’; A ‘hidden layer’ (this is the most important layer where feature extraction takes place, and adjustments are made to train faster and function better); A third ‘output layer’. ‘Deep learning’ algorithms like CNN, RNN, GAN, etc. utilize neural networks. With neural networks there are hyperparameters which are parameters with values assigned prior to the start of the learning process. The training and structure of the network (number of hidden units, rate of learning, epochs) is determined by the hyperparameters.

The main challenge with using AI/ML models is that they need a lot of data for calibration which needs to be done repeatedly. This involves watching out for the challenges of overfitting, excessive training, coincidence, bias and lack of interpretability. A summary of the challenges to be aware of is presented in Table 4-1 (Thomas, Sharma, & Gupta, 2023a)

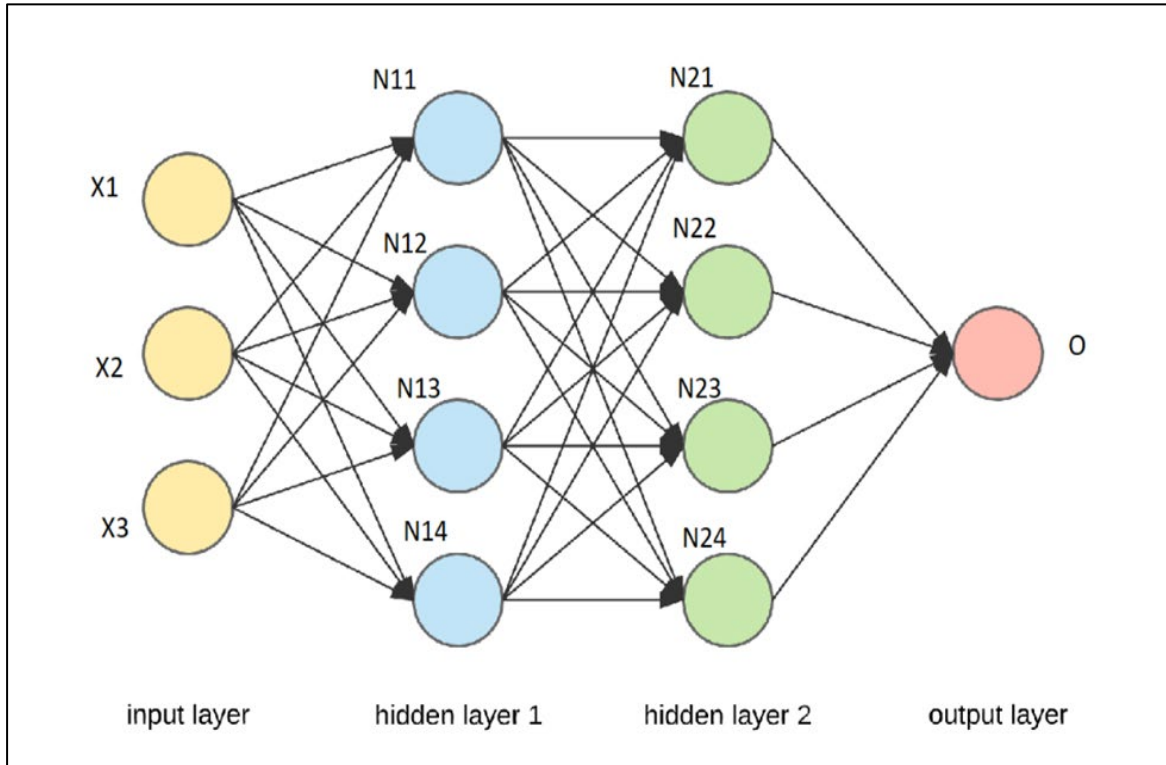


Figure 4-9: Schematic representation of ANN

Table 4-1: Summary of AI/ML Challenges

Challenge	Cause	Remedy
Overfitting	Training missing sufficient data	Ratio of input data points to the total number of network weights used by the connections (ρ) to be used.
Coincidence	Coincidence of Good match	Discriminant Analysis
Overtraining	Updating the model structure keeps decreasing the error and the model gets more complex than necessary	Applying Early Stopping and Reinforcement learning with supervision.
Data Availability	Limited Data	Pre-training of the AI model with another similar data set.
Interpretability	Entire model connections combined affect results and not a single connection	Explanations from local models. Use of generalized models
Generalization	Failure of the model in circumstances different from the original while building the model	More resources to be utilized.
Bias	Naturally prone to bias	Utilize perturbations independent of the model

4.2 Selection Of Approach For Different Composition/Salinity EOR

The application of AI/ML in DCWF involved choosing the prediction output variable as tertiary recovery factor that ranges from 0 to 16.2% , while the model training included 80% of the data and the model testing included 20% of the data (Tatar et al., 2021). The models were then optimized for reliability which involved hyperplanes being optimized for maximum distance amongst data points in SVM, 1 to 100 being the number of trees in RF and hidden layers between 1-2 with 1 to 12 being the number of neurons used for ANN. Five subsets were used to group the input variables which panned specific interactions/interplays. Some researchers chose the rate of different composition/salinity brine injection, reservoir/system temperature, oil/hydrocarbon viscosity, rock permeability, porosity and brine salinity as input parameters that impact the recovery of oil. The models are evaluated for reliability based on relative error, MSE, ‘mean average percentage error’ (‘MAPE’) and R^2 . The final recovery factor is generally used as the output and several preprocessing (removal of low variance features, imputation of data, assessment of collinearity of data, removal of outliers and duplicates, feature importance, splitting data, and scaling data) were applied to increase the model accuracy and model reliability. In most of the research work in DCWF five general categories of the input are identified as rock ‘features/parameters’ (Aladasani et al., 2014), oil ‘features/parameters’, brine ‘features/parameters’, connate water ‘features/parameters’ and operational or system features. Table 4-2 shows the general input features with the slashes shown for removal of the low variance features.

Table 4-2: 'Input features with removal of features of low variance'
(Aladasani et al., 2014)

	Operational Parameters	Rock Properties	Oil Properties	Brine Properties	Connate Water Properties
1	T , °C	l , cm	ρ , g/cm ³	HCO_3^- , ppm	HCO_3^- , ppm
2	Q , mL/min	d , cm	μ, cP	Cl^- , ppm	Cl^- , ppm
3	t , h	ϕ , %	TAN , mg KOH/g	BO_2^-, ppm	BO_2^-, ppm
4	RF_i , % OOIP	K_b , mD	TBN , mg KOH/g	F^-, ppm	F^-, ppm
5	Flooding Stage	S_{wi} , %	$Saturate$, %	NO_3^-, ppm	NO_3^-, ppm
6		C_{Clay} , %wt	$Aromatic$, %	Br^-, ppm	Br^-, ppm
7		C_Q , %wt	$Resin$, %	N_3^-, ppm	N_3^-, ppm
8		C_{Mic}, %wt	$Asphaltene$, %	Na^+ , ppm	Na^+ , ppm
9		C_{Calc}, %wt		K^+, ppm	K^+, ppm
10		C_{Dol}, %wt		Li^+, ppm	Li^+, ppm
11		C_{Car}, %wt		SO_4^{2-} , ppm	SO_4^{2-} , ppm
12		C_A , %wt		Mg^{2+}, ppm	Mg^{2+}, ppm
13		C_F , %wt		Ca^{2+} , ppm	Ca^{2+} , ppm
14				Ba^{2+}, ppm	Ba^{2+}, ppm
15				Sr^{2+}, ppm	Sr^{2+}, ppm
16				CO_3^{2-} , ppm	CO_3^{2-} , ppm
17				Fe^{2+} , ppm	Fe^{2+} , ppm
18				$S_2O_4^{2-}$, ppm	$S_2O_4^{2-}$, ppm
19				Fe^{3+}, ppm	Fe^{3+}, ppm
20				MI , ppm	MI , ppm
21				DI, ppm	DI, ppm
22				S , ppm	S , ppm

Data preprocessing is a very important step where the elimination of duplicates and low variance features/parameters are carried out. This is followed by data imputation where missing data is filled in using the mean, mode or median and modelling algorithm. Next collinearity assessment of the features is done as these features/parameters lead to amplifying the complexity of the model without adding a positive contribution. The Spearman correlation factor (R) is used to assess the collinearity of the parameters. The variance inflation factor (VIF) is utilized as a condition of multicollinearity and the features/parameters with low VIF can be kept while the high VIF discarded. Figure 4-10 depicts a heat map of the collinearity assessment of parameters.

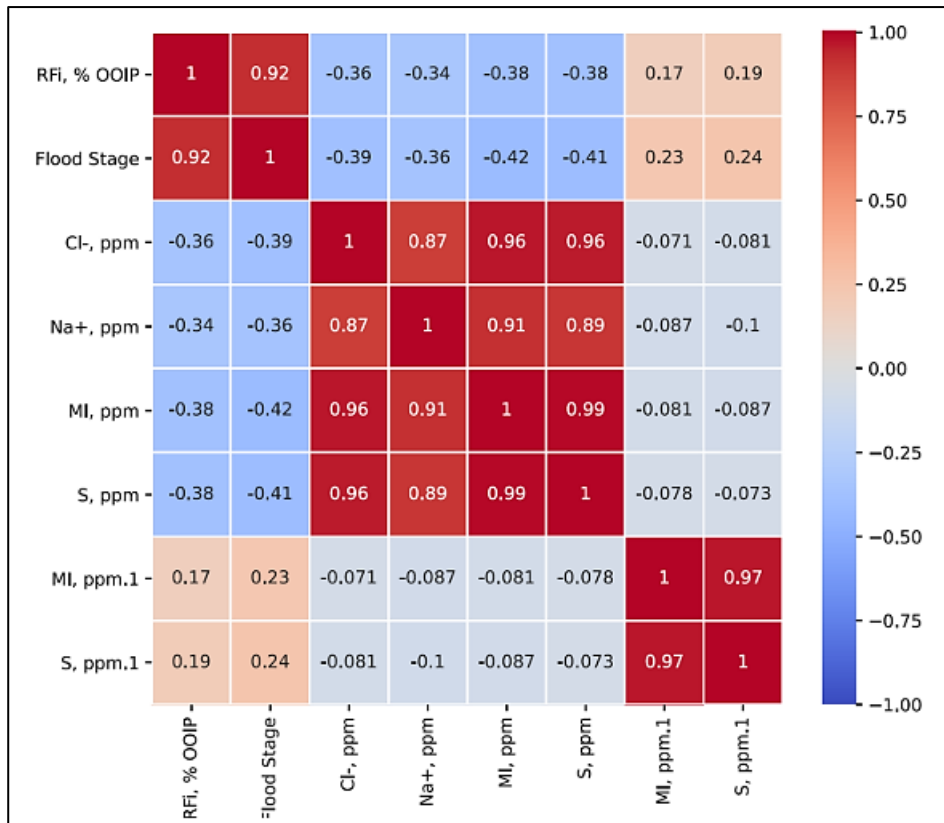


Figure 4-10: Collinear features with Pearsons correlation

Further preprocessing involves data characteristics of distribution, outlier removal and data scaling which accelerates the optimization speed. Finally, the hyperparameter optimization of the models is carried out, using either Grid search, random search (RS) or annealing (AL), prior to the process of training and this impacts the performance of the model and ensures best performance of the models.

The next step is in the model building which uses the standard training-testing (80:20) approach. The data set for training is utilized to determine the model parameters and the key is to avoid overfitting. The model which is developed is then assessed for accuracy through comparison with the testing data set. Then the models are compared for the optimum model selection.

An example approach is where the linear regression (LR) AI/ML model, ‘multilayer perceptron neural network’ AI/ML model, ‘support vector machine’ AI/ML model, and ‘committee

machine intelligent system' ('CMIS') AI/ML model are developed and compared. The comparison of the model is done through various statistical based error functions and graphical based approaches. The statistical error functions include the 'coefficient of determination' (R^2) error function, 'root mean squared error' ('RMSE') error function, 'standard deviation' ('SD') error function, 'mean relative deviation' ('MRD') error function and 'mean absolute relative deviation' ('MARD') error function. The equations of the error functions are formulated as follows

$$D_i = X_{Pred}^i - X_{Exp}^i \quad 4-7$$

$$RD_i = \frac{D_i}{|X_{Pred}^i| - |X_{Exp}^i|} \times 100 \quad 4-8$$

$$MRD = \frac{1}{N} \sum_{i=1}^N RD_i \quad 4-9$$

$$ARD_i = |RD_i| \quad 4-10$$

$$MARD = \frac{1}{N} \sum_{i=1}^N \frac{D_i}{|X_{Pred}^i| - |X_{Exp}^i|} \quad 4-11$$

$$R^2 = 1 - \frac{\sum_{i=1}^N D_i^2}{\sum_{i=1}^N (X_{Pred}^i - \overline{X_{Exp}})^2} \quad 4-12$$

$$\overline{X_{Exp}} = \frac{1}{N} \sum_{i=1}^N X_{Exp}^i \quad 4-13$$

$$RMSE = \sqrt{\frac{1}{N} \sum_{i=1}^N (D_i)^2} \quad 4-14$$

$$SD = \sqrt{\frac{1}{N-1} \sum_{i=1}^N (D_i - \overline{D_i})^2} \quad 4-15$$

The graphical error analysis comprises of evaluating the RD_i for the different models and understanding their symmetry Figure 4-11. The model with the best symmetry is chosen. Positive values indicate overprediction and vice versa.

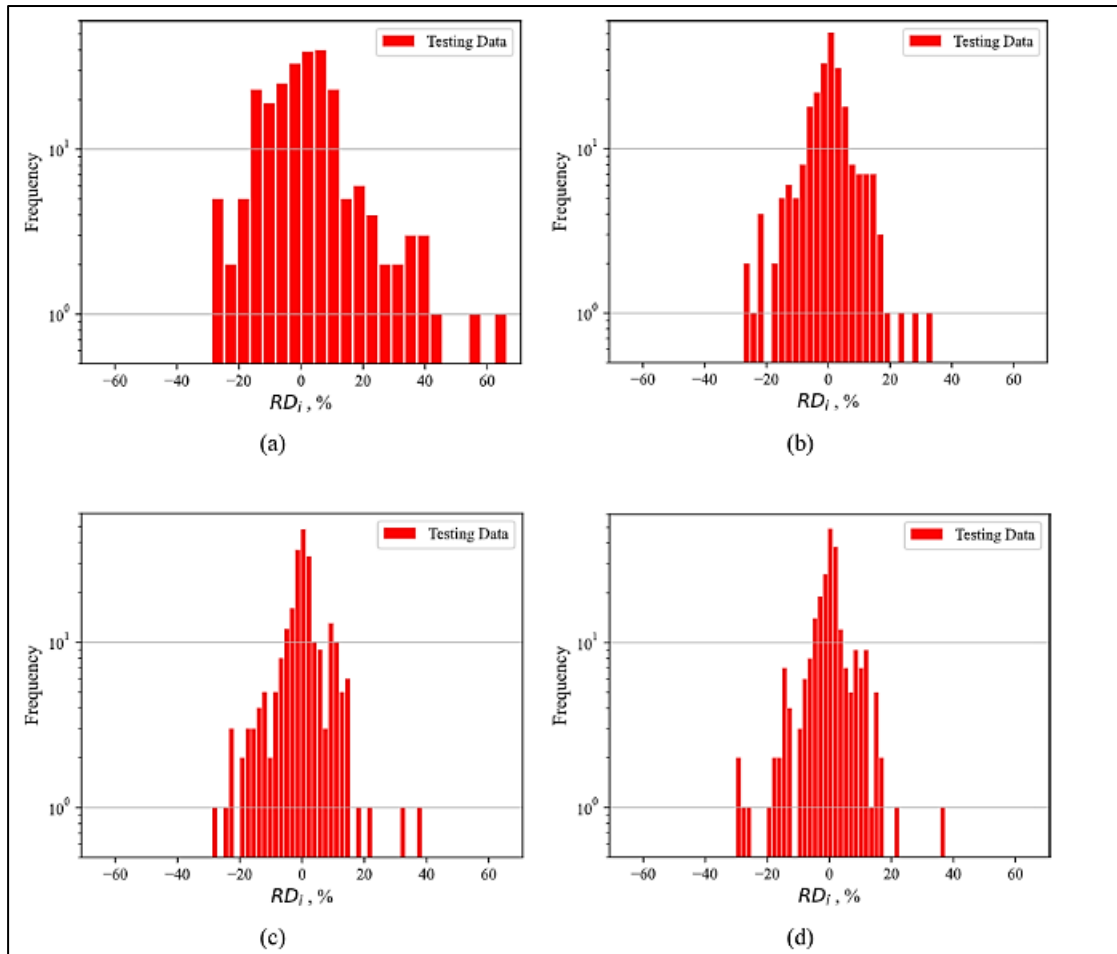


Figure 4-11: Relative Deviation (RD_i) distribution for (a) Linear Regression (b) Multilayer Perceptron (c) Support Vector Machine (d) CMIS. The CMIS distribution is closer to normality compared with the other AI/ML models

Fine tuning of the model also involves the feature selection and elimination of the least important features can avoid overfitting. As shown in Figure 4-12 and Figure 4-13 the reduction in the features from 35 to 11 doesn't change the RMSE and enables for better model without overfitting. The final step is to compare the model accuracy and this is done through a combination of plots as show in Figure 4-14 which shows the majority of the data surrounding the bisector line for both the 'training data' and 'testing data' and indicates the quality of the performance of the model. Another plot is Figure 4-15 where the plotting of data points close to the zero line indicates the model accuracy. The Figure 4-17 shows the simultaneous representation of the experimental recovery factor and predicted final recovery factor with respect to the data point index, the purple diamonds are the experimental data and the blue solid lines are the predicted values and it indicates the accuracy of the model forecasting. A plot Figure 4-16 for comparison between the different models is the cumulative frequency vs

ARDi(%) where the % of data set with less than a particular ARDi is compared. In this case the different models of CMIS, SVM, MLP and LR have 93%, 91%, 90% and 63% of the dataset with ARDi values of $\leq 10\%$ respectively.

Providing such detailed and robust workflows for applications of AI/ML models and their implementation enables reliable and accurate models that translates to better performance of production prediction, process design and optimization of DCWF and furthers the understanding of the major parameters/features and mechanisms that influence DCWF results from meta-data analysis.

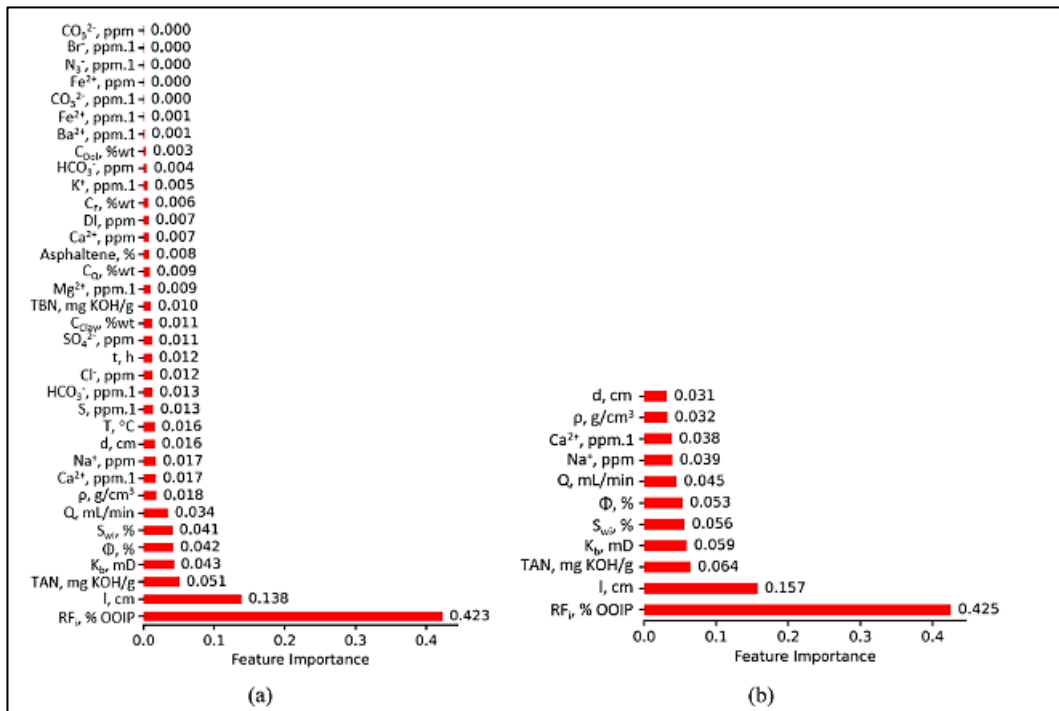


Figure 4-12: Feature importance of DT model with (a) 35 number of independent features/parameters (b) 11 number of independent features.

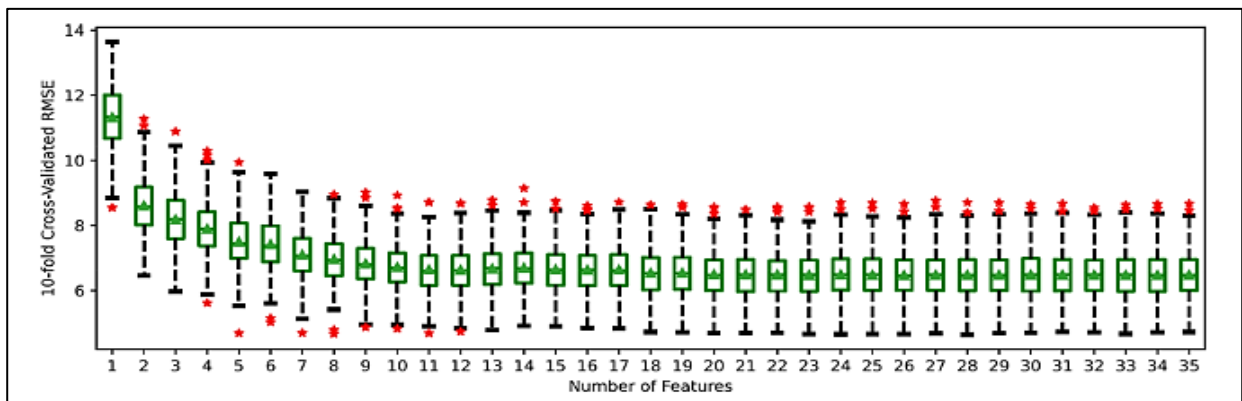


Figure 4-13: RMSE variation for models built using varying number of parameters/features

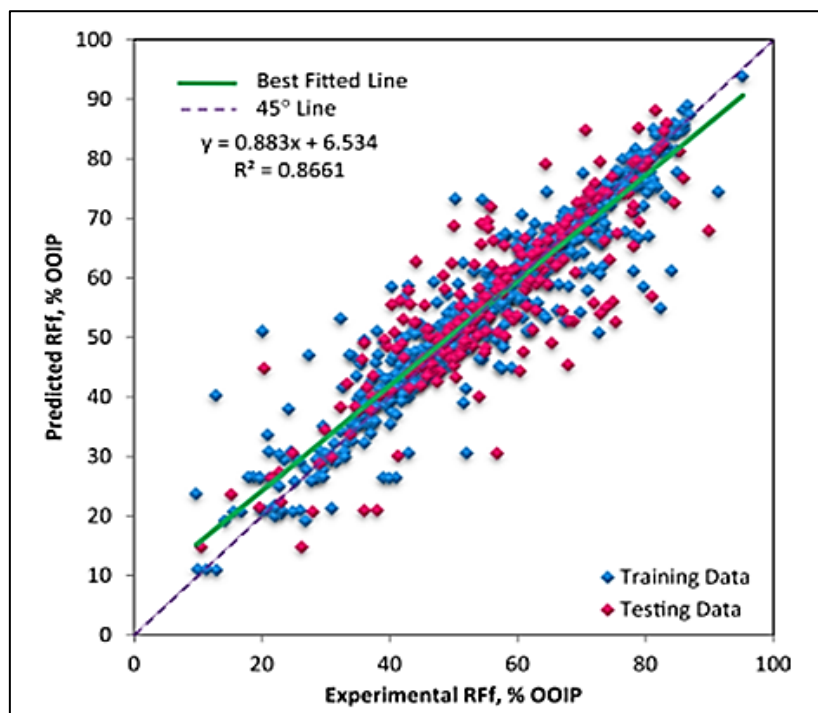


Figure 4-14: Predicted vs experimental final recovery factor

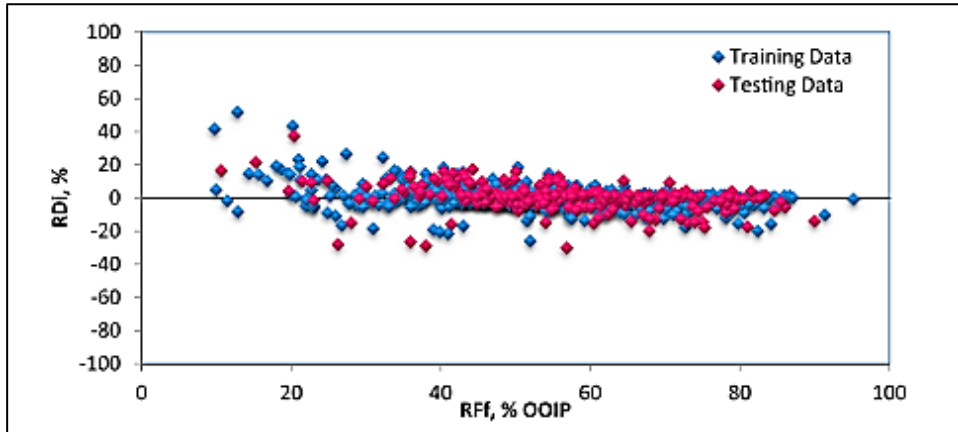


Figure 4-15: Training data and Testing data relative deviation.

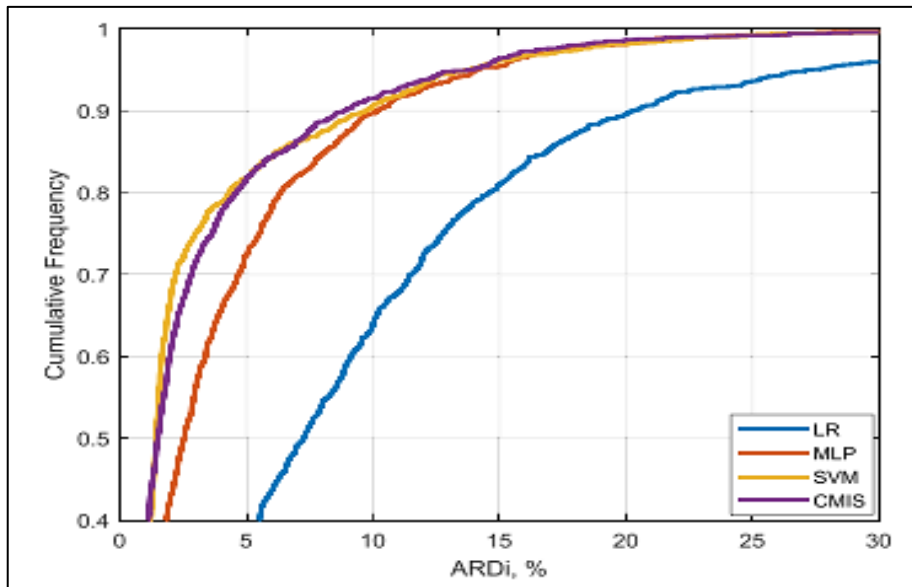


Figure 4-16: Error comparison between the models.

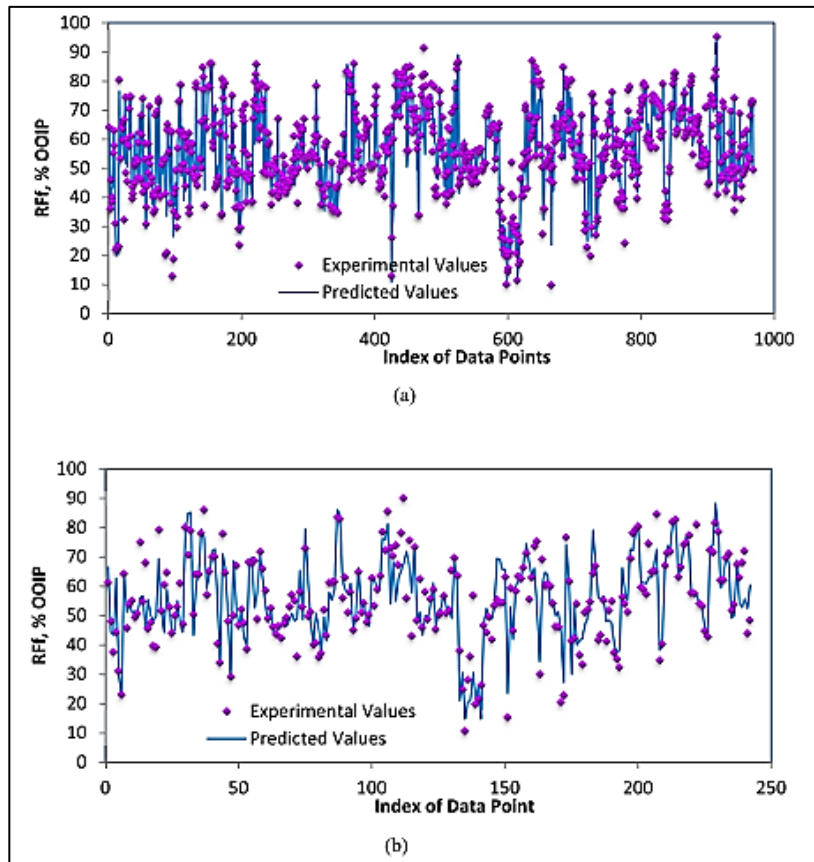


Figure 4-17: Illustration of predicted values and experimental values (a) training (b) testing data

CHAPTER 5

EOR SCREENING METHODOLOGY AND MODELING APPLYING ARTIFICIAL INTELLIGENCE

Meta-analysis of the interaction mechanisms and their parameters highlights that modelling and screening of DCW is a complex process that is resource, expertise and time intensive. This warranted an expert system tool that can assist in speeding up the process of screening for DCW before proceeding to modelling. The application of the expert system or any other artificial intelligence system can be employed to determine complex parameters like recovery factors from multitude of reservoir parameters (Mahmoud et al., 2019). The expert system workflow illustrated enables screening of the different parameters and incorporates the findings from the analysis towards understanding the technical viability of the process before proceeding with more time and resource intensive activities like coreflood and modelling. The high-level workflow is illustrated in Figure 5-1



Figure 5-1: Application of Expert System in DCW

5.1 Screening Matrix

The detailed workflow for screening is presented in Figure 5-2 . The workflow starts with the first step which includes the collection of all the necessary information regarding the initial conditions of the reservoir setting which is the reservoir temperature, the initial water saturation, the porosity, permeability, the wettability. It is important to collect information about the formation brine at this point: its compositions and salinity, the rock composition and the presence of the clay and clay types to be determined where applicable. It is also important at this step to have an idea on what kind of injection water is available in terms of its salinity and ionic composition.

In the second step the initial wettability is checked from the various sources available which is usually from the lab data to understand whether it is water wet. If it is strongly water wet then the chances of success with DCW decreases strongly and there is probably a careful test to be done with imbibition experiment before proceeding.

The third step will involve comparing the brine composition and salinity between the formation or connate water and the injected brine. If the formation or connate brine has higher salinity and higher ionic composition compared to the injected brine then the risks are high for proceeding with DCW. If the injected brine composition and salinity are lower compared to the formation brine then proceed to the next step.

The fourth step involves analyzing the oil composition in terms of SARA and the presence of surface active agents. If the surface active agents are not present then the chances of DCW risk of failure is high. Otherwise, move to the next step.

The fifth step involves identification of the rock composition and depending on whether it is sandstone or carbonate the prominent reservoir systems the use of DCW is recommended. This expert system was further tested with different cases and the results were compared to the outcomes from experiments which is presented in Table 5-1

Table 5-1: Expert system results with different cases

Case	Expert System	Lab
Sandstone	Proceed with DCW	Incremental Recovery 10%
Carbonate	Proceed with DCW	Incremental Recovery 16%
Sandstone	Proceed with DCW	Incremental Recovery 6%

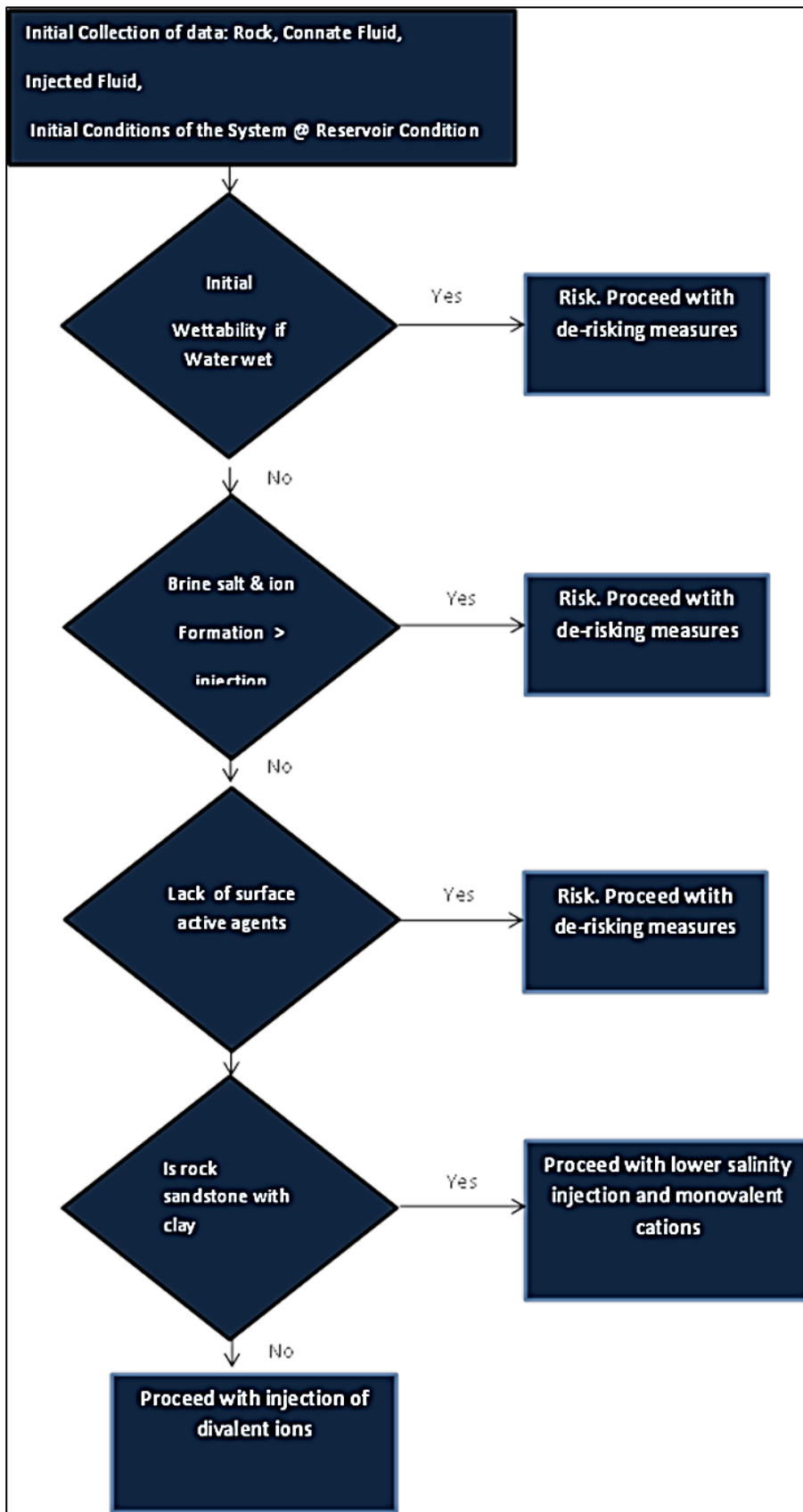


Figure 5-2: Expert System Workflow based on the meta-analysis

5.2 Screening Methodology (AI/ ML)

Sustainable application of the ML/AIT approach would hence involve first the collection of data from different sources either from lab/experiments and/or couple with data from physics based models and then using the data for training, validation and testing phase using different ML/AIT algorithms. This method has been used to develop a sustainable approach to understanding and screening for the DCW EOR. The major challenge in the usage of ML and AIT is that they cannot be generalized as they are specific to a data set to which they are calibrated, and this also requires that they are supplied with large amounts of data for repeated calibration. Additionally, the challenges of overfitting, excessive training, coincidence, bias and lack of interpretability are prevalent in these cases. Physics based numerical simulations with different uncertainties on the operations of the flooding mechanisms were carried out to determine the responses for the cumulative oil production. The numerical simulation set up is shown in Figure 3-4 of Chapter 3 with an injector at one end and the producer at the other end. This was followed by the creation of the multiple experiments for the different salinity injection. The data snapshot followed by the statistical summary of the data are shown in Table 5-2 and Table 5-3 respectively. The correlation matrix of the parameters as illustrated in Figure 5-3 provides understanding of the collinearity between the parameters and enhancing the understanding of the pertinent parameters. This is followed by application of the different ML models where multi-variate linear regression training and testing scores are presented in Table 5-4 and Table 5-5 respectively. The high R-squared values of the training and testing provide confidence in the model.

Table 5-6: Prediction Results and the Error % from multi-variate linear regression shows the model predictability with respect to the cumulative oil production and the error % is between -0.7% to 1.2% which demonstrates the high predictability of the multi-variate linear regression model.

Table 5-2: Key input and output parameters for DCW physics based model

Serial Number	Oil Cumulative	Oil Rate	Salt Injection Rate	Water Injection Rate	Salt Production Rate
0	92,639.8203	20.131918	1573.96987	96.71246	1487.757223
1	92,874.6328	23.188352	1633.21025	96.72685	1433.805503
2	91,,315.3125	22.906847	1628.47469	96.72571	1434.469796
3	92,644.1094	22.964913	1628.47503	96.72572	1436.759638
4	94,064.1563	23.714615	1637.91078	96.72912	1427.805137
5	88,271.8594	22.727471	1633.21126	96.72697	1432.184682
6	92,489.625	22.963549	1628.47472	96.72571	1436.31514
7	89,551.1484	23.208965	1633.21095	96.72809	1425.309749
8	92,139.4141	22.915001	1628.4748	96.72572	1436.540591
9	93,325.0078	23.243745	1633.21017	96.72684	1433.721528

Table 5-3: Statistics of the parameters for DCW EOR physics based model

Statistics	Oil Cumulative	Oil Rate	Salt Injection Rate	Water Injection Rate	Salt Production Rate
count	66	66	66	66	66
mean	90,204.8248	22.893558	2266.77132	96.726845	1821.712399
std	27,50.77324	0.522679	645.710367	0.002144	393.397018
min	86,274.9297	20.131918	1573.96987	96.71246	1425.032223
25%	87,591.1074	22.577548	1633.21018	96.72582	1433.809963
50%	89,254.0859	22.964231	2137.17665	96.72696	1741.492088
75%	92,824.1426	23.185488	2890.3578	96.727998	2203.411014
max	96,922.7344	23.890052	3568.35387	96.72925	2618.744446

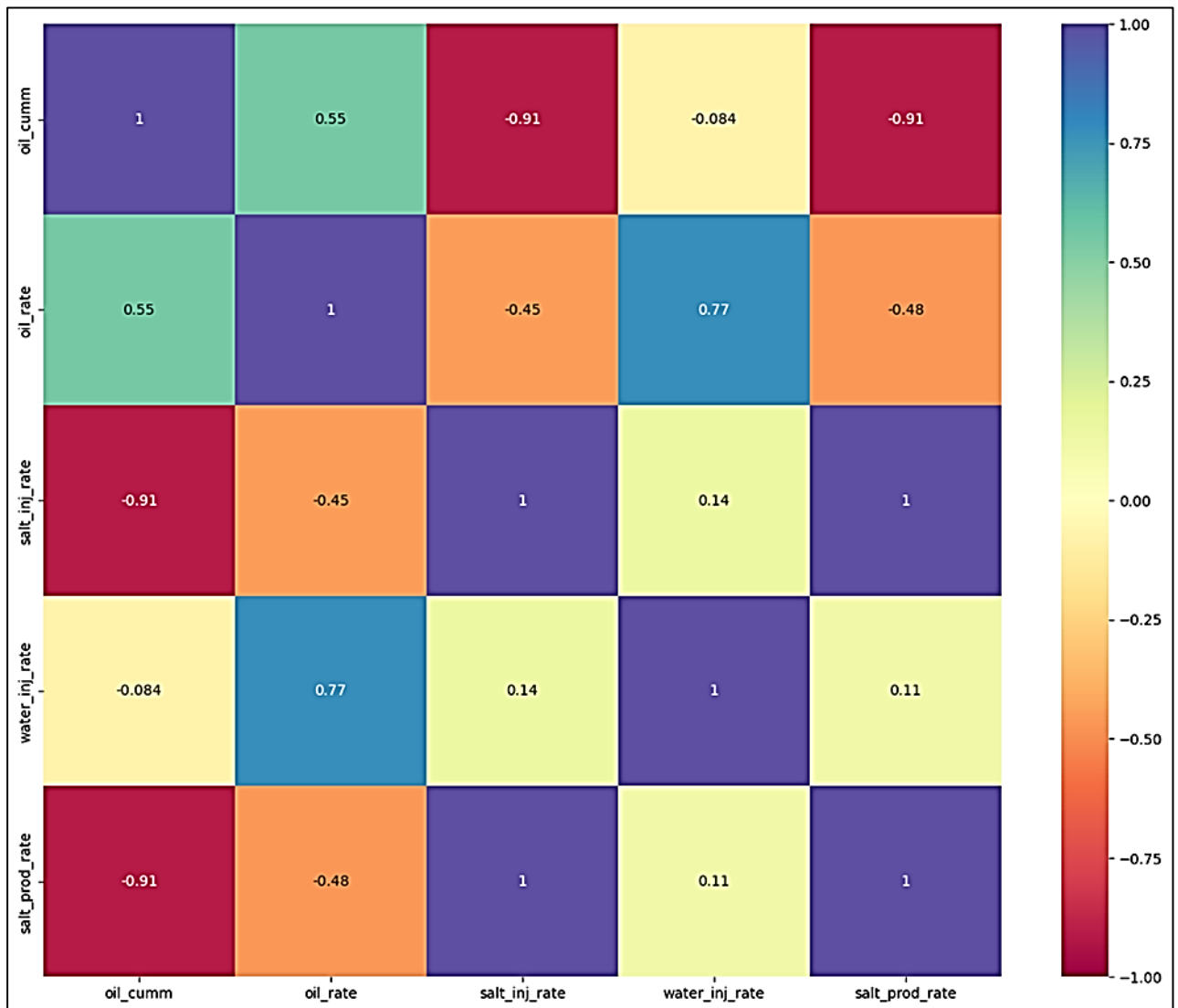


Figure 5-3: Correlation Matrix of the parameters for the 3D Physics based model

Table 5-4: Training performance scores from multi-variate linear regression

Training Performance	RMSE	MAE	R-Squared	Adj. R-Squared	SMAPE
0	466.007248	326.026657	0.972258	0.970524	0.359848

Table 5-5: Testing performance scores from multi-variate linear regression

Test Performance	RMSE	MAE	R-Squared	Adj. R-Squared	SMAPE
0	607.824835	467.198228	0.884826	0.850273	0.521664

Table 5-6: Prediction Results and the Error % from multi-variate linear regression

Experiment	Actual Oil_Cumulative	Predicted Oil_Cumulative	Error percent
46	91,706.5	92,845.49211	1.241997
57	89,577.67969	90,569.364	1.107066
47	87,611.79688	87,471.97086	-0.159597
2	91,315.3125	92,377.58595	1.163303
38	87,687.17969	87,836.18783	0.169931
55	88,272.46094	87,618.89959	-0.740391
21	92,742.54688	92,837.8847	0.102798
26	87,190.76563	88,095.1093	1.037201
53	87,771.74219	87,677.05167	-0.107883
41	87,223.54688	87,320.80931	0.111509
48	87,581.03906	87,800.08334	0.250105
40	88,082.32813	87,538.30888	-0.617626
43	87,544.52344	87,278.03825	-0.3044
33	87,587.80469	87,403.55803	-0.210357

The integrated analysis performed on the varied and diverse experiments (corefloods, single well , multi well, sector and field) assisted in identifying the key parameters and also highlighting which of those key parameters are not being measured and reported in Figure 5-4, where the of 1 and 36 on the left side of figure depicts the number of experiments while the numbers of 8 and 32 on the right side of the figure depicts the number of parameters reported in each of the experiments. The capturing and reporting of these critical parameters are essential to build a comprehensive data set that enables understanding of the success of the DCWF. The

statistical summary of the parameters is reported in Table 5-7. Data analysis through a correlation matrix was carried out to understand the correlation between various parameters listed in the different experiments as shown in Figure 5-5. In the figure the blue colours show the positive correlations while the orange colours show the negative correlations. Strong correlations are seen with respect to the fluid properties of Oil API and cation concentrations to incremental recovery.

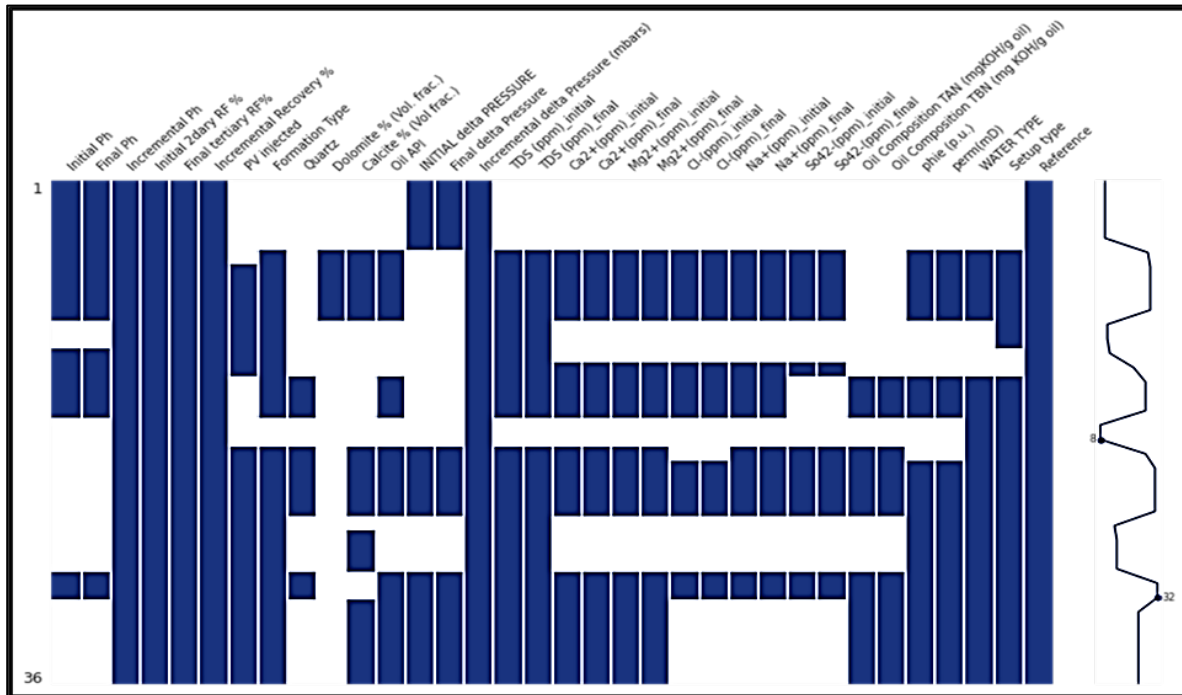


Figure 5-4: Matrix illustration of parameters in experiments reported and missing

Table 5-7: Statistical Summary of the Various Input Parameters from DCW Experiments

	Count	Mean	Std	Min	25%	50%	75%	Max
Initial Ph	400	7.345	0.645769	6	7	7	8	9
Final Ph	400	7.9225	1.053217	6	7	8	9	10
Incremental Ph	400	0.413025	0.725292	-0.6	-0.1725	0.285	0.93	2.42
Initial 2dary RF %	400	55.78925	17.915644	21.1	40.7	57.9	71.2	84.6
Final tertiary RF%	400	62.3985	14.501375	33.6	50.8	63.35	75.375	85.4
Incremental Recovery %	400	7.25325	4.743611	0.5	3.6	6.25	10.5	19.5
PV injected	400	9.738029	5.959649	2.0176	4.883825	8.61605	13.650375	32.292
Calcite % (Vol frac.)	400	79.100822	13.262753	18.317211	71.408474	81.740385	89.387394	96.973293
Oil API	400	38.161622	2.814191	32.17528	36.042618	38.14266	40.247431	45.901551
INITIAL delta PRESSURE	400	1850.5525	1405.91191	38	659.75	1551	2932.5	5721
Final delta Pressure	400	1511.85007	1146.82214	45.437148	524.058782	1240.58035	2308.95522	4599.31634
Incremental delta Pressure (mbars)	400	-274.2325	692.205366	-3438	-660.25	-124.5	260.75	599
TDS (ppm)_initial	400	103138.78	60508.9967	356.686492	56538.5582	98518.3141	146442.64	251562.568
TDS (ppm)_final	400	25921.7213	18062.5151	218.107931	11397.6902	22468.4393	36697.1033	90599.6645
Ca ²⁺ (ppm)_initial	400	15772.2792	9990.0498	47.271032	7233.59186	15165.7159	23731.3163	35719.1144
Ca ²⁺ (ppm)_final	400	3300.4944	2452.14977	7.002135	1306.36644	2836.29868	4797.66486	13399.1734
Mg ²⁺ (ppm)_initial	400	6645.61677	4490.62125	78.394785	2805.63705	6040.21025	9829.99925	16963.18
Mg ²⁺ (ppm)_final	400	1986.18929	1492.30691	4.931813	820.920485	1671.39675	2878.697	7756.01576
Cl ⁻ (ppm)_initial	400	69601.4136	34150.7379	2082.16468	43464.9675	67684.0769	93635.0201	159308.712
Cl ⁻ (ppm)_final	400	9998.65875	6049.26692	197.113809	5237.78223	9161.02435	13651.6003	26839.5109
Na ⁺ (ppm)_initial	400	27442.6826	14167.119	1075.4852	16439.5947	25960.7544	37865.4821	78307.6518
Na ⁺ (ppm)_final	400	4668.7699	2851.4983	125.072798	2325.6318	4298.11026	6612.70635	12181.6632
So ₄ ²⁻ (ppm)_initial	400	1518.925	1054.06688	6	629.75	1389	2241	4147
So ₄ ²⁻ (ppm)_final	400	987.084518	724.766487	13.753987	454.212929	860.997331	1348.04794	3578.42331
perm (mD)	400	132.299676	93.602232	2.562917	54.007955	121.621899	194.152594	419.508137

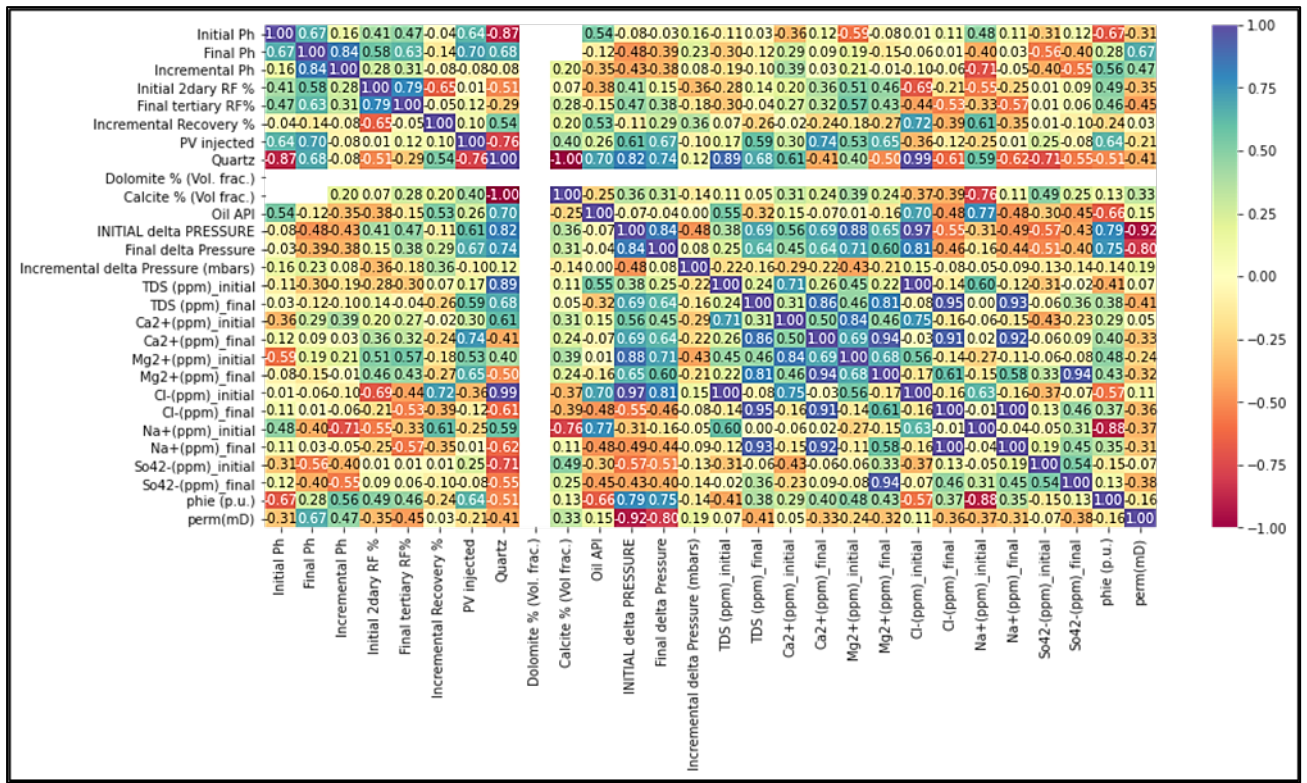


Figure 5-5: Matrix Illustration of Positive and Negative Parameter Correlations

The detailed analysis from the correlation matrix of Figure 5-5 provides evidence that the incremental and final recovery are influenced by the initial pH, final pH, the fluid ion composition, the rock composition, rock porosity and permeability, delta pressure of the flooding experiment and the initial recovery factor attained before the start of DCWF.

Based on this research work a sustainable and efficient workflow for the application of AI/ML is illustrated in Figure 5-6. The process starts with data collation from various experiments, this is followed by data screening, data analysis, followed by application and finally evaluation of AI/ML algorithms. Bivariate data analysis is illustrated in Figure 5-7 which enables understanding of the relationship and correlation between the multi-parameters.



Figure 5-6: Sustainable Workflow for AI/ML Application in DCWF

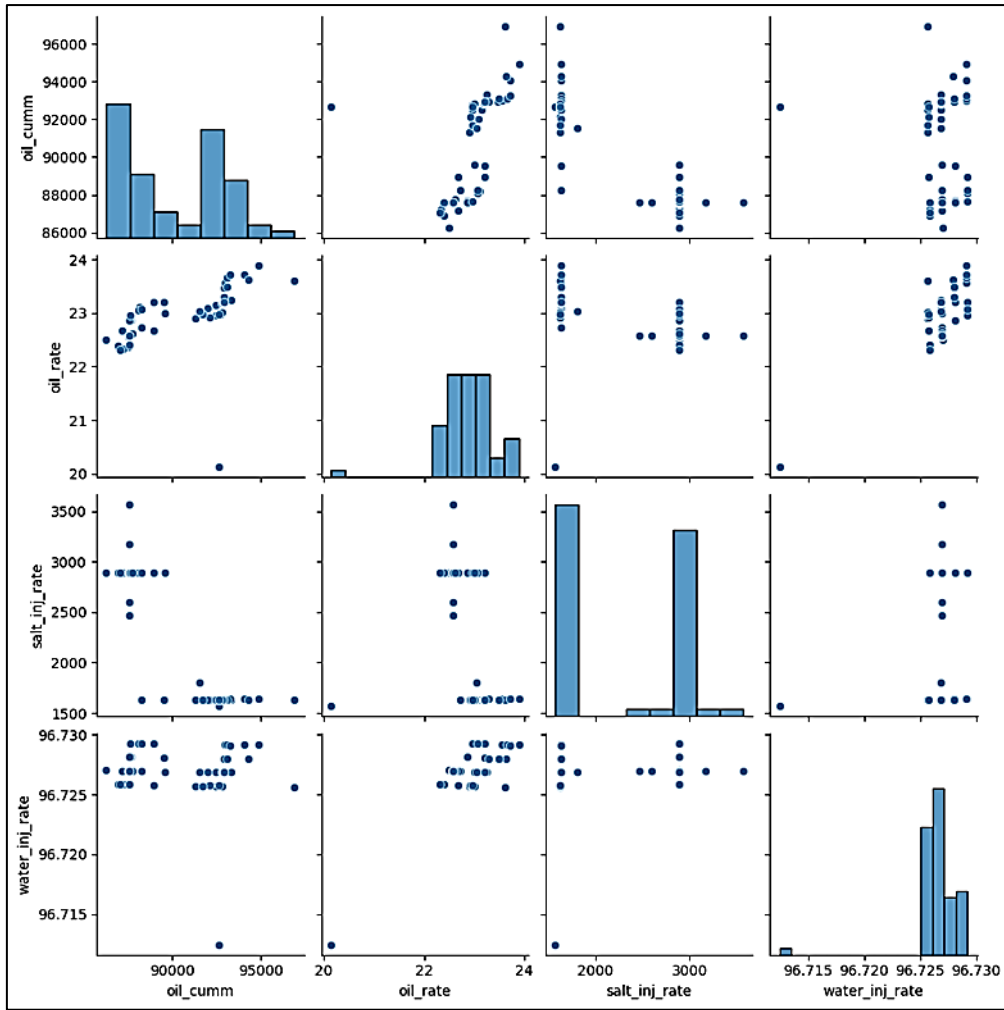


Figure 5-7: Pair Grid Analysis of the different parameters from the physics based model.

Random Forest AI/ML algorithm was used and its corresponding training and testing statistics are presented in Table 5-8 and Table 5-9 respectively. The hyperparameters used in the RF are max_depth in the range from 4 to 10, max_features of sqrt and log; n_estimators in the range of 80 to 120 which were optimized based on the grid search.

Table 5-8: Random Forest Training performance scores

Training Performance	RMSE	MAE	R-Squared	Adj. R-Squared	SMAPE
0	327.933212	188.713807	0.986262	0.985403	0.206424

Table 5-9: Random Forest Testing performance scores

Testing Performance	RMSE	MAE	R-Squared	Adj. R-Squared	SMAPE
0	397.490904	272.626693	0.950745	0.935968	0.303536

The model predictability with respect to the cumulative oil production is shown in Table 5-10 where the error % is between -0.4% to 1.07% which demonstrates the high predictability of the Random Forest model.

Table 5-10: Random Forest Prediction Results and Error%

Experiment Number	Actual Oil_Cumulative	Predicted Oil_Cumulative	Error Percent
46	91,706.5	92,691.87184	1.074484
57	89,577.67969	89,138.82447	-0.489916
47	87,611.79688	87,586.11232	-0.029316
2	91,315.3125	91,933.3289	0.676794
38	87,687.17969	87,636.05965	-0.058298
55	88,272.46094	88,474.28232	0.228635
21	92,742.54688	92,644.77877	-0.105419
26	87,190.76563	87,830.34617	0.733542
53	87,771.74219	87,586.11232	-0.211492
41	87,223.54688	87,334.95017	0.127722
48	87,581.03906	87,573.81931	-0.008244
40	88,082.32813	88,474.28232	0.444986
43	87,544.52344	87,601.87695	0.065514
33	87,587.80469	87,582.80968	-0.005703

AdaBoost is applied next, a supervised ML model used for classification and regression problems, which provides strong predictions through sequentially learning from a combination of series of weak models. AdaBoost training and testing results are presented in Table 5-11 and Table 5-12

Table 5-11: AdaBoost Training performance

Training Performance	RMSE	MAE	R-Squared	Adj. R-Squared	SMAPE
0	368.878285	303.819095	0.982617	0.981531	0.332918

Table 5-12: AdaBoost Testing performance

Testing Performance	RMSE	MAE	R-Squared	Adj. R-Squared	SMAPE
0	415.037139	295.10578	0.9463	0.93019	0.328256

The hyperparameters used in AdaBoost are learning rate from 0.01 to 1; n_estimators in the range of 10 to 100 which are optimized based on the grid search. The AdaBoost model predictability with respect to the cumulative oil production along with its error % is shown in Table 5-13. The increased model predictive capability of the AdaBoost model is shown through its error % which is in the range of -0.7% to 0.99%

Table 5-13: AdaBoost Prediction and Error%

Experiment Number	Actual Oil_Cumulative	Predicted Oil_Cumulative	Error Percent
46	91706.5	92297.1338	0.644048
57	89577.6797	88950.4137	-0.700248
47	87611.7969	87612.0938	0.000339
2	91315.3125	92224.3879	0.995534
38	87687.1797	87916.7227	0.261775
55	88272.4609	88168.5313	-0.117737
21	92742.5469	92297.1338	-0.480268
26	87190.7656	87916.7227	0.832608
53	87771.7422	87728.0063	-0.049829
41	87223.5469	87383.9336	0.18388
48	87581.0391	87463.8581	-0.133797
40	88082.3281	88168.5313	0.097867
43	87544.5234	87612.0938	0.077184
33	87587.8047	87612.0938	0.0277

The performance metrics comparison between the multiple AI/ML models of multi-variate linear regression, Random Forest and AdaBoost are presented in Table 5-14 (Thomas, Sharma, & Gupta, 2023b).

Table 5-14: Performance metrics comparison between various AIT/ML models

Test Performance Comparison	Linear Regression	Random Forest Tuned	Adaboost Tuned
RMSE	607.824835	397.490904	415.037139
MAE	467.198228	272.626693	295.10578
R-squared	0.884826	0.950745	0.9463
Adj. R-squared	0.850273	0.935968	0.93019
SMAPE	0.521664	0.303536	0.328256

CHAPTER 6

DATA SELECTION FOR DIFFERENT COMPOSITION/SALINITY FLOODING AND COMPARISON BETWEEN DIFFERENT METHODS

The testing and evaluation of DCW occurs at different scales of cores through corefloods and spontaneous imbibition experiments, then they are carried out at the well level followed by inter-well scale of application, then at the field level and finally using sector models 2D and 3D to be able to predict the performance at core, well and field scale.

6.1 Corefloods

The first set of experiments related to DCW started with the laboratory corefloods. They were initially done for Berea sandstones (G.-Q. Tang & Morrow, 1999; Webb et al., 2005; Yildiz & Morrow, 1996). After years of research it was identified that the kind of ions and the concentration of active ions (SO_4^{2-} , Ca^{2+} and Mg^{2+}) in the injected water changes the carbonate surface charge and correspondingly increases the wetness of water (Austad et al., 2012; Strand et al., 2006; P. Zhang & Austad, 2005; T. Zhang et al., 2020).

Experimental evidences demonstrate that the wettability in carbonates are altered by increasing the concentrations of the surface-interacting ions (phosphate, borate, sulphate) and reduction of the salinity/ionic strength of the brine/water (brine dilution, cation concentration reduction, removal of non-active ions, ie. Sodium and Chloride). For the contact angle measurements, the surface roughness can lead to hysteresis which significantly impacts this measurement, so the plates of the rock are polished with sand paper to reduce the hysteresis effect. For atleast a two hour duration, the polished rock plates are then placed under vacuum and subsequently aged in the base brine/water (FB) for another 24 hours, after which they are aged in reservoir hydrocarbon/oil at reservoir temperature of 230 degF for atleast 1.5 months. A drop of hydrocarbon/oil is placed onto the plate and digital photographs are taken to monitor the wettability changes over time. The coreflood is conducted usually with an apparatus that consists of various parts like the hassler type core-holder, transducers for measurement of pressure differential, module for overburden pressure, regulator for backpressure, displacement pumps, oven and fluid accumulators as shown in Figure 6-1.

The Soxhlet extraction process is used to clean the core plug which is subsequently dried, and weighted. Post routine analysis of the core, plugs of the core are saturated for 3 days with formation brine/water and under vacuum to establish the ionic equilibrium with the brine. The core is then flooded with subsurface reservoir oil/hydrocarbon until it reaches irreducible saturation of water identified by cessation of water production. The permeability is then again measured which is now the permeability to oil and then the ageing in reservoir oil is carried out for the core plug at 230 degF and 2000 psi for atleast 6 weeks. For the coreflood water flooding the core samples are placed inside the rubber sleeve and then mounted on a coreholder which is connected at both ends to the end plugs which in turn are connected to the piping for the fluid inlet and fluid outlet. Subsurface reservoir hydrocarbon/oil and water/brines were injected from the piston accumulators by operation of high pressure displacement pumps. Injection of hydraulic oil into the annulus between the rubber sleeve and inner surface of the core-holder simulated the application of overburden pressure upon the core. A backpressure regulator (BPR) located at the outlet was used to maintain the pore pressure which in turn utilizes differential pressure transducers to be measured. Pressure drop across the core was measured through measurement and difference between the absolute pressure at both ends of the core.

Commencement of each waterflood test was with stable injection rate of base brine at 1 ft/day. Cessation of the oil production led to sequential injection of smart brines. The effluent production was sampled for quantification of the recovery of hydrocarbon/oil and to conduct effluent brine analysis for active ions (Ca^{2+} , Mg^{2+} and SO_4^{2-}) and non-active ions (Na^+ and Cl^-). Ion chromatography is carried out on selected samples of brine/water and at specific brine/water injected pore volumes for analysis. The final stages of the coreflood include cleaning of the core plugs utilizing Dean-Stark extraction and validation of the results through material balance application and analysis.

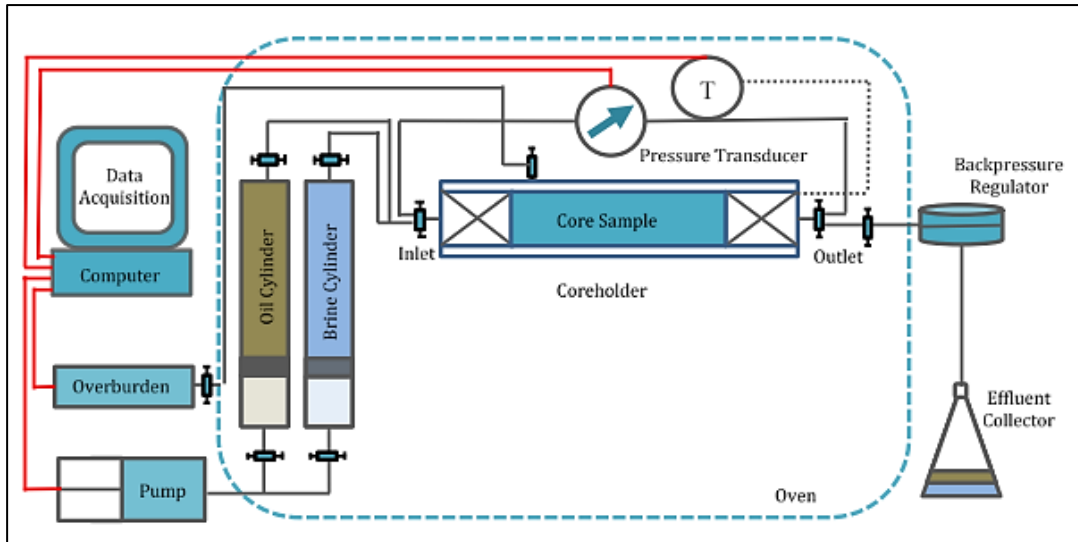


Figure 6-1: Coreflood Setup

This level of detail is scrutinized and applied in selection of the coreflood data that were utilized within AI/ML research work applied to DCW modeling and prediction. Graphical results from the coreflood experiments are shown in Figure 6-2 and Figure 6-3 as an example from the work done by Awolayo (Awolayo et al., 2014). The end point data from these experiments and others (Boussour et al., 2009) Figure 6-4 where the effect of temperature is depicted, modeling of coreflood 1-D and performing model match of the historical observed oil recovery and observed pressure drop (Egbe et al., 2021) are collated for use in further research and modeling.

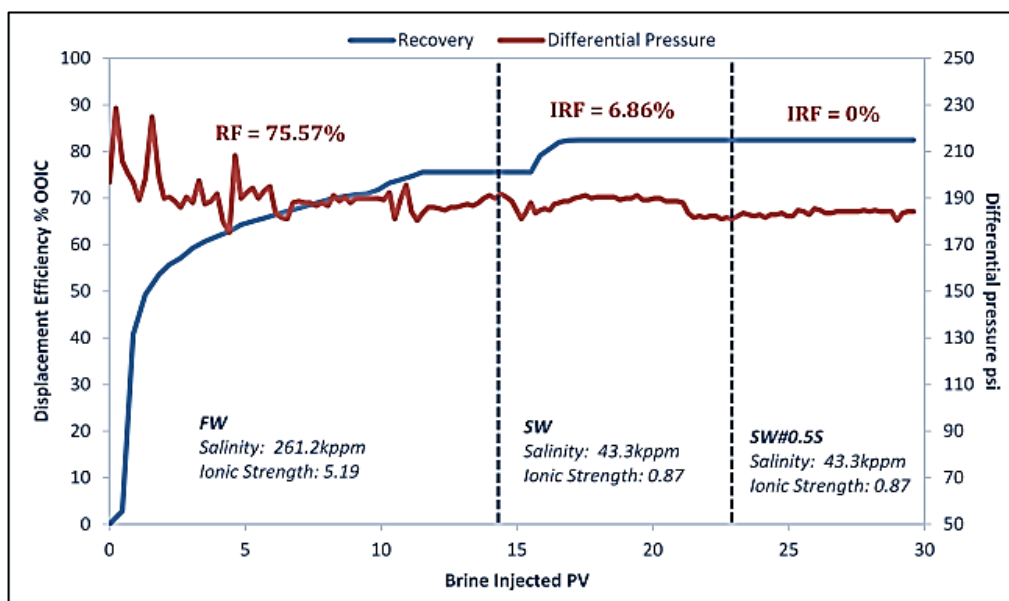


Figure 6-2: Plot of Displacement Efficiency on primary y-axis and Differential Pressure on secondary y-axis vs Pore Volume of Brine/Water Injection (Awolayo et al., 2014)

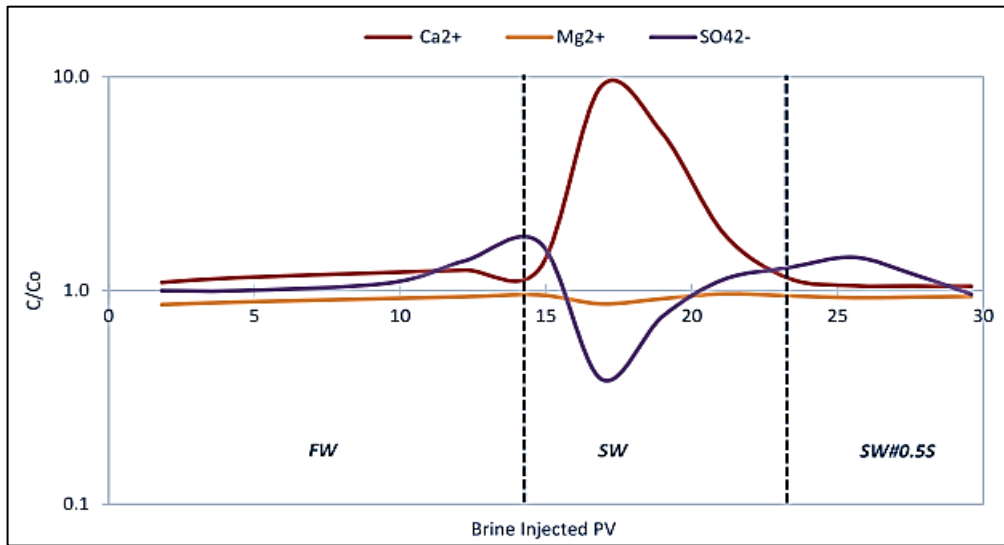


Figure 6-3: Plot of Effluent active ions at normalized concentrations (Awolayo et al., 2014)

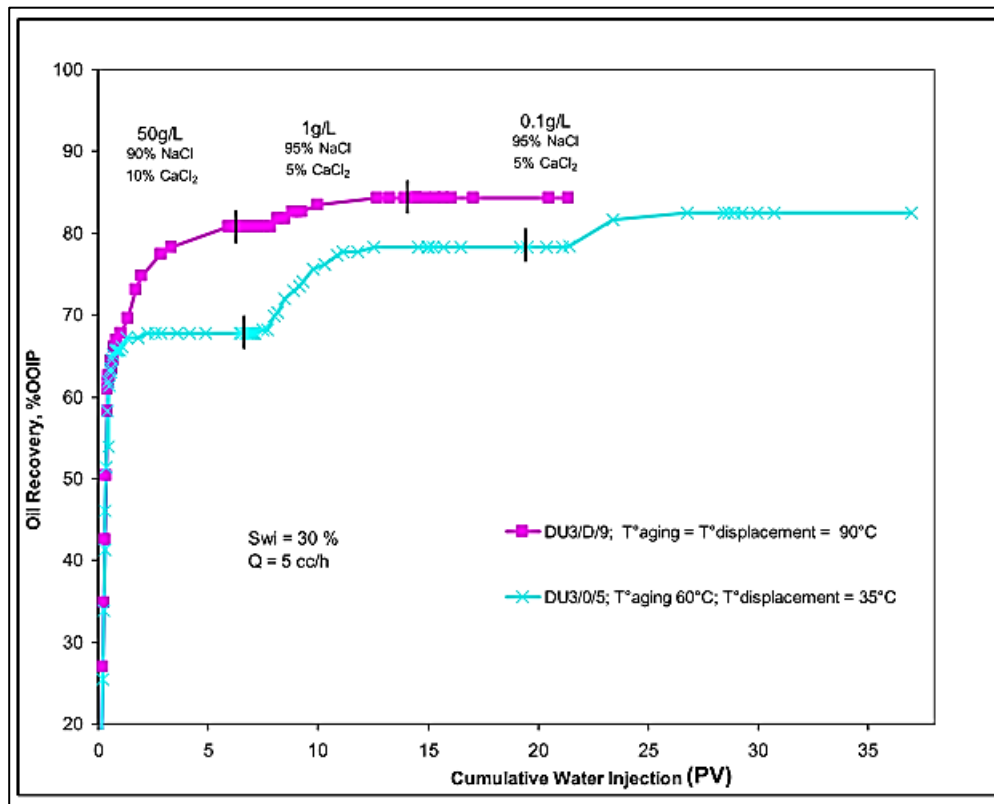


Figure 6-4: Oil Recovery at different dilutions and temperature (Boussour et al., 2009)

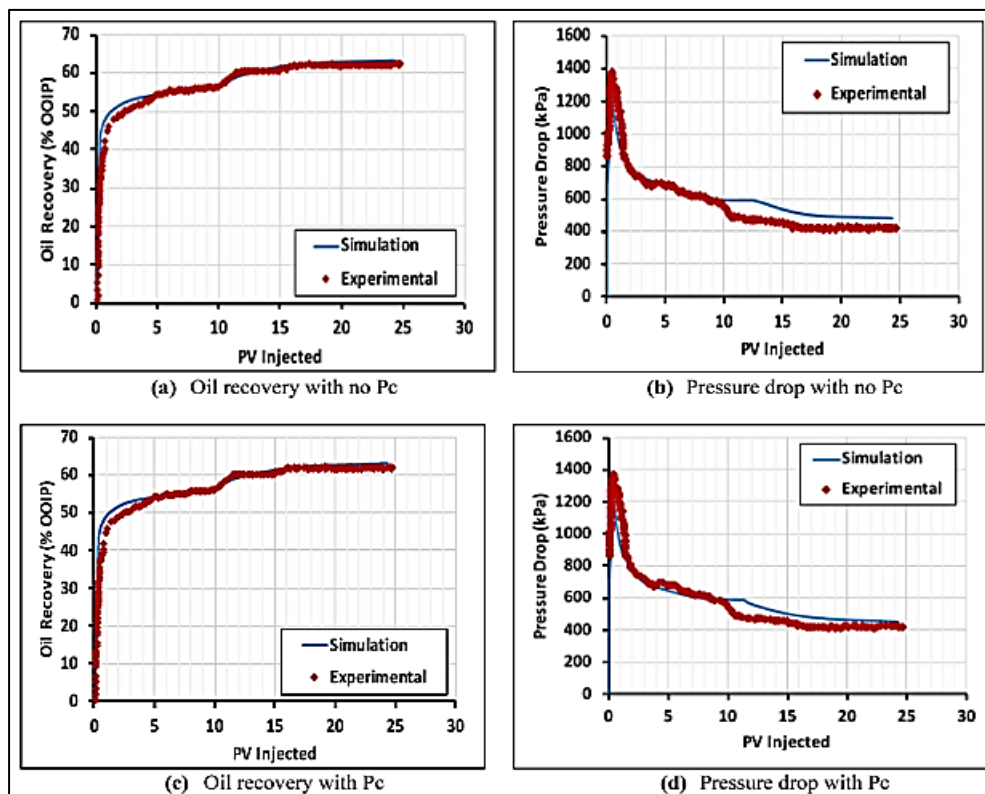


Figure 6-5: Matching of historical observation points of oil recovery and observed difference in pressure

6.2 Single Well Data

Single well data takes the form of SWCTT which is one of the predominant methods employed for field evaluation Figure 6-6. The SWCTT assists in confirming the changes to the saturation of the residual oil/hydrocarbon around the wellbore regions due to DCWF (Skrettingland et al., 2011). The SWCTT is based on the injection of a reactive partitioning tracer known as ethyl acetate (EtAc), where part of the EtAc dissolves in the remaining oil and water. The well is then shut in and the part of the EtAc in the water phase gets hydrolysed into the product tracer of ethanol (EtOH). The next step involves producing the well where the product tracer production follows the water production and the unreacted tracer gets produced after a delay. The production delay timing of the tracer is dependent on the remaining saturation of oil and this saturation of oil is determined through theoretical computations involving saturation variations to obtain a fit of the tracer concentrations during back production. The injection volumes of the tracers determine the average radius of investigation for the remaining oil

saturation and in cases can be in the order of 10 meters. The SWCTT tracer production curves are shown in Figure 6-7. The SWCTT modelling needs to take into account of temperature effects and accuracy in the volumes measured.

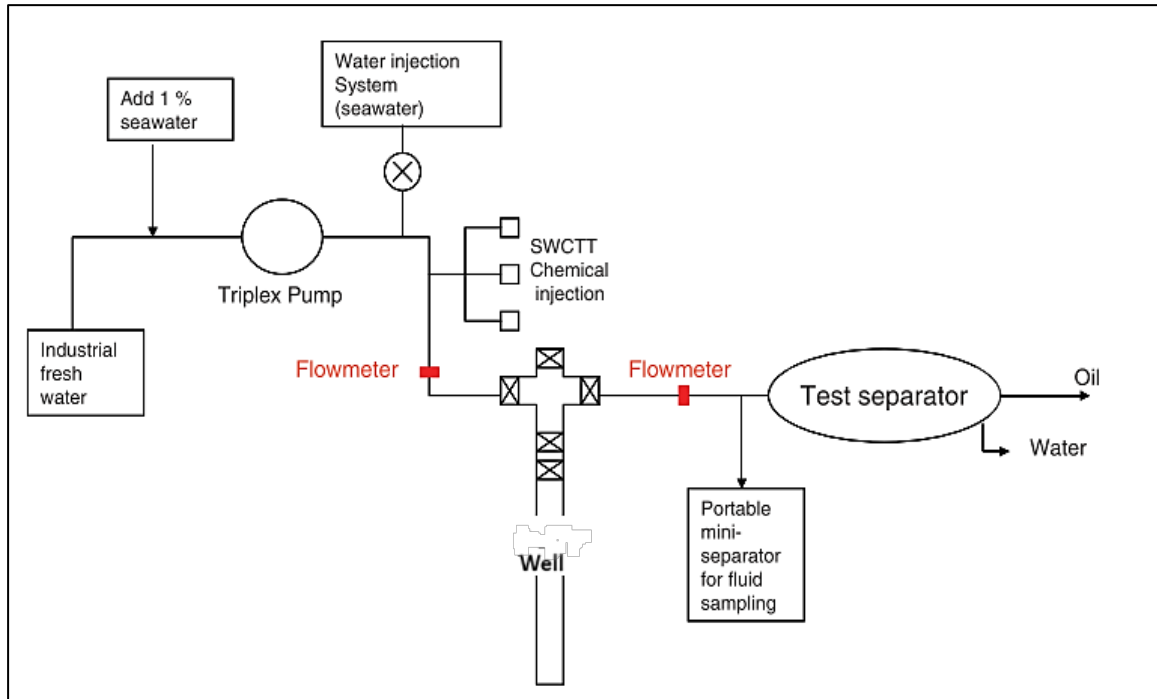


Figure 6-6: SWCTT Surface Layout (Skrettingland et al., 2011)

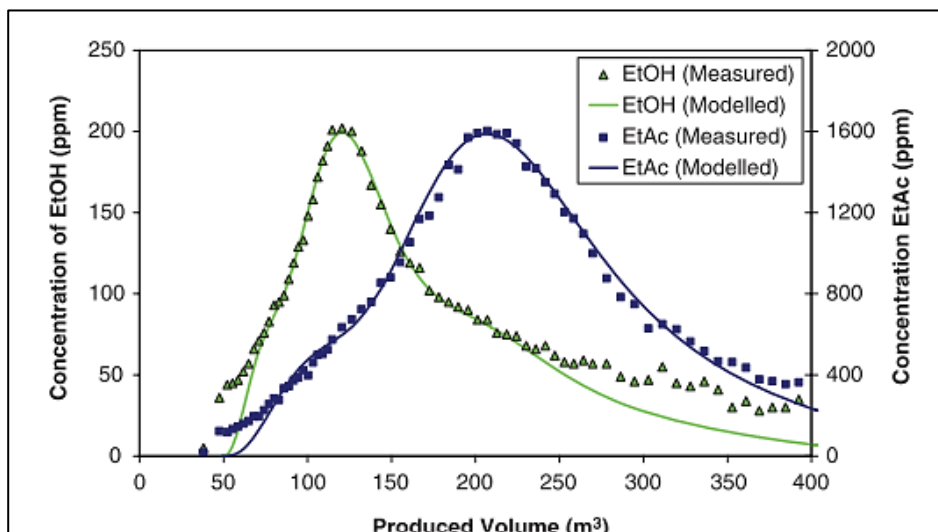


Figure 6-7: Measured tracer concentrations and profiles modeled (Skrettingland et al., 2011)

6.3 Sector Models 2D and 3D

The sector models for 2D and 3D are modeled using reservoir simulators, most of the modelling approach is in terms of having the two phase relative permeability functions and capillary pressure functions dependent/related to salinity, contact angle or ion concentration to account for the alteration of wettability from oil wet to water wet. An example case (Mahani et al., 2011) where 2D models were constructed and the match on the producer water cut was obtained is shown in Figure 6-8. In this case 2D models were constructed for ease of comparison and understanding with 1D results.

The 3D model is detailed in Chapter 3 section 3.2. The main summary of parameters are presented by Table 6-1

Table 6-1: Parametric Summary through physics based modeling

Statistics	Oil Cumulative	Oil_Rate	Salt Injection Rates	Water Injection Rates	Salt Production Rates
Count	66	66	66	66	66
Mean	90,204.83	22.89	2266.77	96.73	1821.71
std	27,50.77	0.52	645.71	0.002	393.39
min	86,274.93	20.13	1573.97	96.71	1425.03
25%	87,591.11	22.58	1633.21	96.72	1433.81
50%	89,254.09	22.96	2137.18	96.73	1741.49
75%	92,824.14	23.19	2890.36	96.73	2203.41
max	96,922.73	23.89	3568.35	96.73	2618.75

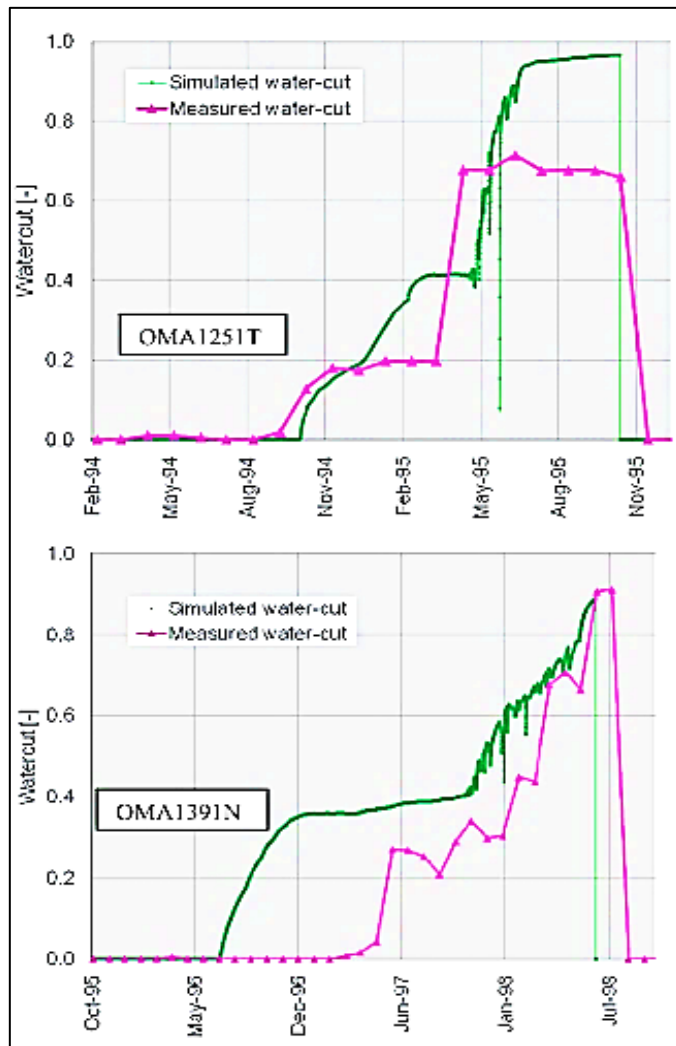


Figure 6-8: Comparison of observed (in maroon colour) and simulated (in green colour) water cut for two wells (Mahani et al., 2011)

6.4 Validation and Application of Optimum Model

The summary of the collation of the various data is mentioned in the Figure 6-9

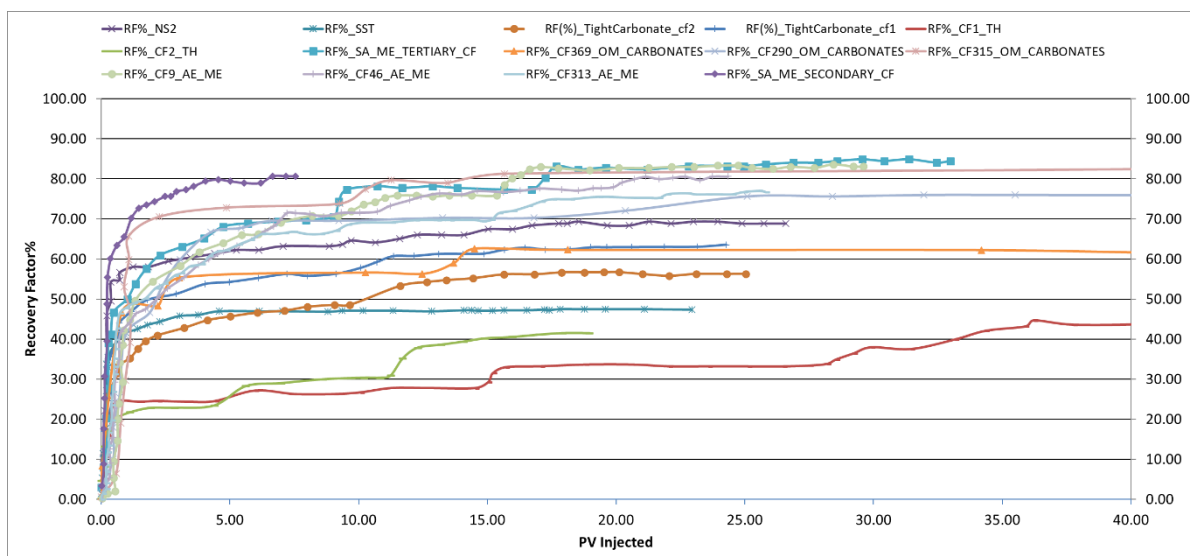


Figure 6-9: Recovery Factor Vs Pore Volume Injected from different cases around the world

The data matrix for the different experimental data sets are presented in Table 6-2. The collection and curation of the data required analysis of the different experiments understanding their various assumptions and the conditions at which the experiments were carried out. The pertinent parameters that were captured from the various experimental data sets included the experimental conditions/processes, type of reservoir, fluid parameters which include pH, TDS, ionic composition, rock properties and mineral composition, oil composition and the ultimate

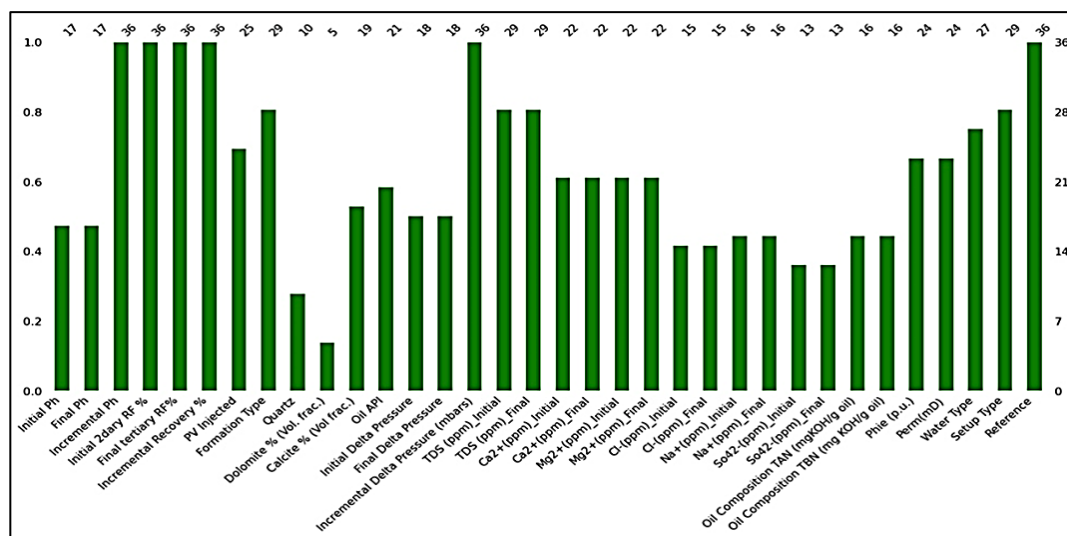


Figure 6-10: Parameter Matrix

recovery. The comprehensiveness of the data sets collected are shown in Figure 6-10 highlighting the missing parameters and what needs to be acquired in the future.

Table 6-2: Data Matrix of different parameters impacting the DCWF

	count	mean	std	min	0.25	0.50	0.75	max
Initial Ph	36.00	7.33	0.55	6.31	7.30	7.33	7.33	9.50
Final Ph	36.00	7.81	1.01	6.00	7.50	7.81	7.81	10.00
Incremental Ph	36.00	0.23	0.80	-1.10	0.00	0.00	0.13	2.50
Initial 2dary RF %	36.00	49.62	26.71	0.00	31.00	56.45	70.15	85.00
Final tertiary RF%	36.00	60.99	20.39	0.00	43.88	63.75	80.10	85.70
Incremental Recovery %	36.00	11.36	16.35	0.00	3.03	5.90	10.13	80.40
PV injected	36.00	11.03	6.44	2.00	7.00	11.03	11.03	33.00
Calcite % (Vol frac.)	19.00	85.39	22.63	0.40	75.00	95.00	97.00	97.00
Oil API	21.00	38.68	5.42	32.00	37.40	38.90	39.60	50.60
INITIAL delta PRESSURE	18.00	1792.67	2301.18	20.00	85.00	460.00	4214.50	5900.00
Final delta Pressure	18.00	1603.89	2021.38	33.00	100.00	546.00	3510.25	5516.00
Incremental delta Pressure (mbars)	36.00	-94.39	887.18	4008.00	0.00	0.00	14.75	2758.00
TDS (ppm)_initial	29.00	92561.84	89879.13	-142.60	15000.00	57670.00	194450.00	252738.00
TDS (ppm)_final	29.00	16829.18	31651.18	33.39	564.00	1500.00	12840.00	107013.80
Ca2+(ppm)_initial	22.00	11180.74	13292.79	32.50	650.00	6276.05	16085.00	35840.00
Ca2+(ppm)_final	22.00	2183.29	4843.27	0.00	77.00	247.35	340.75	16085.00
Mg2+(ppm)_initial	22.00	4931.10	5995.41	34.00	1215.00	1919.75	7350.00	18010.00
Mg2+(ppm)_final	22.00	1479.08	2644.22	0.00	45.05	265.05	1186.03	9005.00
Cl-(ppm)_initial	15.00	68731.47	63395.58	1610.00	15579.35	32200.00	145550.00	160430.00
Cl-(ppm)_final	15.00	10397.23	17616.55	80.50	369.00	1582.00	15579.35	65202.00
Na+(ppm)_initial	16.00	28843.61	30639.76	915.00	7383.78	15643.05	37669.63	84293.00
Na+(ppm)_final	16.00	4843.84	8440.96	45.75	110.00	891.50	7158.83	32439.50
So42-(ppm)_initial	13.00	1539.09	1689.07	0.00	70.00	869.60	2145.00	4290.00
So42-(ppm)_final	13.00	989.39	1270.24	0.00	82.10	214.50	2049.80	4098.80
phie (p.u.)	24.00	0.20	0.05	0.08	0.19	0.22	0.23	0.25
perm(mD)	24.00	101.00	137.11	2.00	3.00	24.15	190.25	432.00

The parameter check matrix Figure 6-10 has the bottom and top of the X axes as the features and their counts respectively; the left and right Y axes are the normalized scaling count of the features and the number of experiments respectively (Thomas, Sharma, Dharmendra, et al., 2023). The data assimilation results in the creation of a correlation matrix Figure 6-11 for narrowing down on the critical parameters and ranking them. The dark blue and red colours on the correlation matrix depict the positively and negatively correlated parameters respectively.

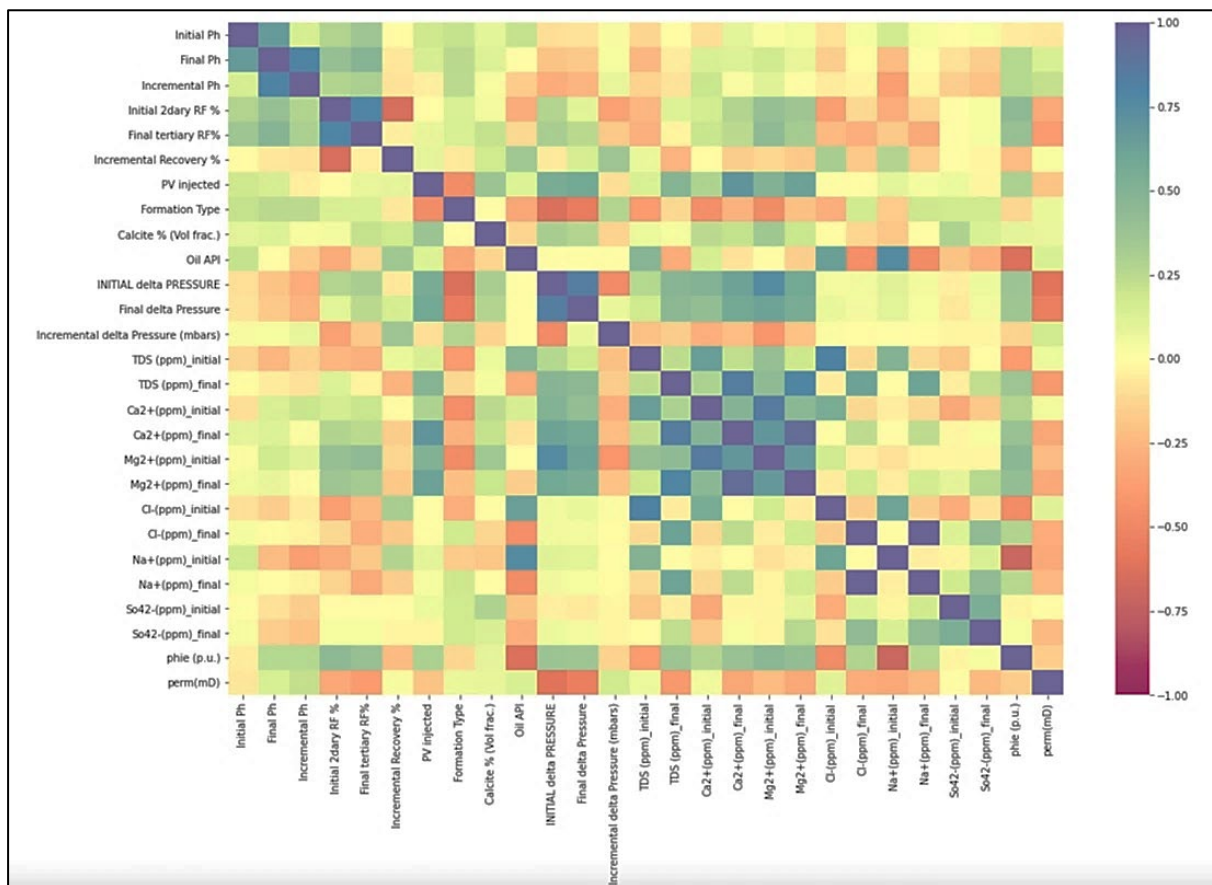


Figure 6-11: Correlation Matrix

The detailed analysis identifies two categories of parameters. The parameters that have a positive impact on the recovery and the parameters that have negative impact on the recovery. These are listed as follows. Na+(ppm)_initial, Cl-(ppm)_initial, Incremental delta pressure(mbars) and Oil API are the positive impact parameters. Porosity (p.u), Na+(ppm)_final, Cl-(ppm)_final, TDS (ppm)_final, Initial 2dary RF% are the negative impact parameters. The research work was executed by Jackson et al (Jackson et al., 2016) and its results are congruent with the aforementioned findings of positive and negative impact

parameters. Random Forest was applied first to the curated data set where the training process utilized 320 points of data and the testing process utilized 80 points of data. The workflow using Random Forest is depicted through Figure 6-12. The metrics used for assessing the reliability of the Random Forest are the Root Mean Square Error (RMSE), Mean Absolute Error (MAE), R-squared, Symmetric Mean Absolute Percentage Error (SMAPE). The lower these metrics the improved model confidence.

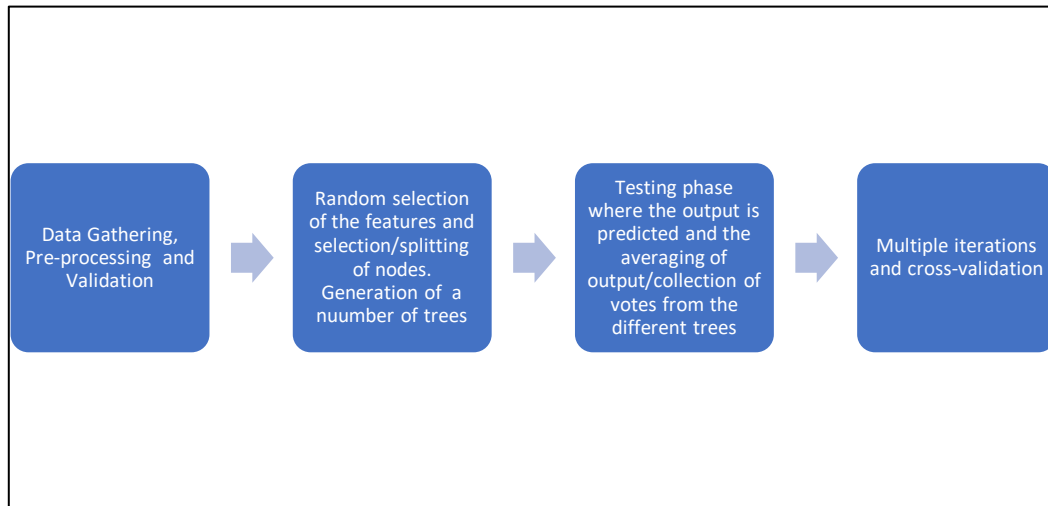


Figure 6-12: Random Forest Workflow

Table 6-3 and Table 6-4 illustrate Random Forest training and testing results respectively.

Table 6-3: Random Forest Training Metrics

Training Performance for Random Forest				
RMSE	MAE	R-squared	Adj. R-squared	SMAPE
2.354087	1.788879	0.97543	0.973431	3.125537

Table 6-4: Random Forest Testing Metrics

Testing Performance for Random Forest				
RMSE	MAE	R-squared	Adj. R-squared	SMAPE
6.346122	4.991092	0.765955	0.715802	8.205874

The Random Forest algorithm modelling also outputs the importance of the various features considered for DCW. The main parameters are the recovery status at the start of the DCW EOR, the type of water used for flooding process, the pH and also ionic compositions of water initial and final, oil API, pore volume injected and delta pressure Table 6-5.

Table 6-5: Random Forest Feature Importance

Features	Feature Importance
Initial 2dary RF %	0.7611
PV injected	0.0624
Incremental delta Pressure (mbars)	0.0335
Ca2+(ppm)_final	0.0187
Incremental Ph	0.0130
WATER TYPE	0.0116
TDS (ppm)_final	0.0107
Mg2+(ppm)_final	0.0100
Calcite % (Vol frac.)	0.0089
So42-(ppm)_initial	0.0083
Mg2+(ppm)_initial	0.0081
perm(mD)	0.0075
TDS (ppm)_initial	0.0064
Na+(ppm)_initial	0.0062
So42-(ppm)_final	0.0060
Oil API	0.0058
Ca2+(ppm)_initial	0.0051
Cl-(ppm)_initial	0.0044
Cl-(ppm)_final	0.0044
Na+(ppm)_final	0.0041
Formation Type	0.0038

The supervised Gradient Boosting machine learning model is applied next and simple workflow using this is shown in Figure 6-13. The Gradient Boosting model metrics for training and testing are depicted through two tables,

Table 6-6 and Table 6-7 respectively. Table 6-8 shows the importance of the various features in the outcome of DCW through the Gradient Boosting modelling. The main parameters are the recovery at the start of the DCW, final TDS of the system, ionic composition of initial and final water, oil API, rock permeability, rock composition, PV injected and delta pressure.

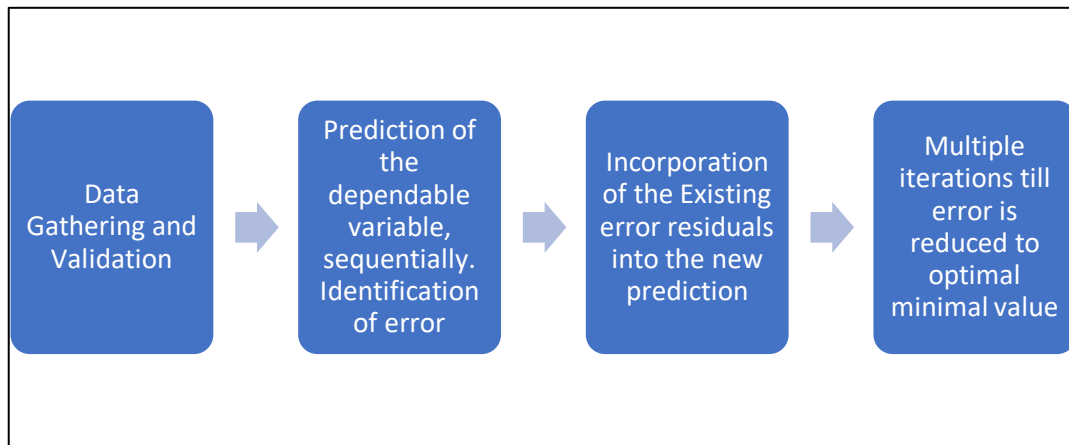


Figure 6-13: Gradient Boosting Workflow

Table 6-6: Gradient Boosting Training Metrics

Gradient Boost Training Performance				
RMSE	MAE	R-squared	Adj. R-squared	SMAPE
4.884448	4.233638	0.894226	0.885616	7.320418

Table 6-7: Gradient Boosting Testing Metrics

Gradient Boost Testing Performance				
RMSE	MAE	R-squared	Adj. R-squared	SMAPE
6.46449	5.299639	0.757142	0.705102	8.734157

Table 6-8: Gradient Boost model Feature Importance

Features	Feature Importance
Initial 2dary RF %	0.537
PV injected	0.117
Ca2+(ppm)_final	0.088
WATER TYPE	0.064
Incremental delta Pressure (mbars)	0.059
Incremental Ph	0.026
TDS (ppm)_final	0.023
Calcite % (Vol frac.)	0.015
So42-(ppm)_initial	0.013
perm(mD)	0.012
Mg2+(ppm)_initial	0.009
Mg2+(ppm)_final	0.008
TDS (ppm)_initial	0.008
Formation Type	0.007
Oil API	0.004
Na+(ppm)_final	0.003
Cl-(ppm)_final	0.002
Na+(ppm)_initial	0.001
Cl-(ppm)_initial	0.001
Ca2+(ppm)_initial	0.001
So42-(ppm)_final	0.000

The prediction of recovery from DCW lab/field work and AI/ML models, Table 6-9 , are within the +/- 6% recovery range except for two cases where the AI/ML predicts over +/- 7%. This is an efficient approach towards screening of DCW before undertaking resource intensive screening tests in the lab and implementation of projects in the field.

ANN was used for the modelling of the recovery factor for the DCW and it was built using 4 hidden layers, each layer contained 64 neurons and RELU activation function. The ANN training and validation versus the Epoch is depicted in Figure 6-14. The recovery factor prediction from the ANN model vis-à-vis the model data is depicted in Table 6-10 with mean absolute error (MAE) of 3.68%. The oil endpoint relative permeability was also predicted and shown in Table 6-11 with a MAE of 0.047

Table 6-9: Comparison of Recovery Factor between lab/field work and AI/ML models

Actual Final tertiary RF%	Predicted Final tertiary RF%
36.00	42.34
51.80	50.07
78.80	71.19
65.00	58.82
62.40	64.36
45.80	46.03
80.20	77.24
63.50	67.47
56.70	61.89
60.00	50.96

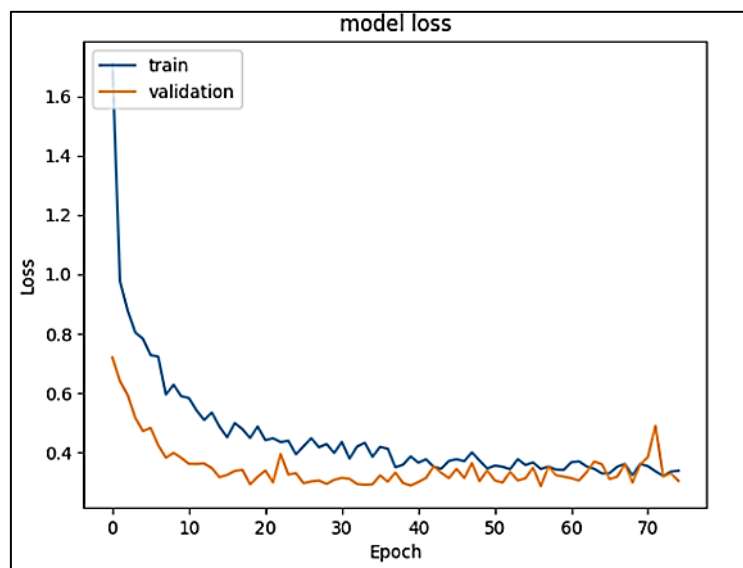


Figure 6-14: ANN Training & Validation

Table 6-10: RF% Prediction Vs Original Simulation

Prediction	Original Values	Error %
70.26	68.86	2.04
75.27	76.06	-1.04
73.21	75.29	-2.76
72.42	73.39	-1.31
74.38	75.32	-1.25
72.30	72.49	-0.26
70.64	72.21	-2.18
72.41	75.53	-4.14
71.28	70.53	1.05
74.25	78.10	-4.94
71.99	70.09	2.72
73.05	71.41	2.30
72.58	71.00	2.22
72.02	69.65	3.40
73.79	70.91	4.07
71.85	71.63	0.31
71.06	70.95	0.15
72.48	71.43	1.48
70.42	67.95	3.64
73.66	76.03	-3.12

Table 6-11: RelPerm Kromax

Prediction_EO	OriginalValues_EO	Error %
0.899292	0.88301	1.84394
0.887453	0.94447	-6.036878
0.895537	0.88399	1.306191
0.825995	0.82754	-0.186723
0.897544	0.97996	-8.410136
0.904743	0.97236	-6.953935
0.87076	0.83386	4.425178
0.890403	0.83753	6.31295
0.878624	0.87895	-0.037121
0.917218	0.95571	-4.027572

CHAPTER 7

SUMMARY, CONCLUSIONS AND RECOMMENDATIONS

The integrated experimental analysis of multiple different corefloods summarises that the predominant mechanisms can be narrowed down to two. The two mechanisms are the interplay between the rock-fluid and fluid-fluid which results in wettability alteration, interfacial tension alteration, or both. The rest of the main mechanisms which are more likely to be the effects rather than the causes for DCWF effects can be summed up as follows: changes in pH, migration of fines, exchanges of ions resulting in double layer expansion, reduction of salt leading to dissolution of hydrocarbon which is termed as salting in and creation of microemulsions.

Elaborate and intensive research and development has been carried out on the subject of DCWF and yet identification of the major mechanisms are still an area of further investigation and ongoing research. This research work highlights the exchange of ion as a significant underlying factor for all the researched and reported major interaction mechanisms. The rest of the interaction mechanisms are all the resulting effects due to the exchange of the ions. Additional driving factors that are proportional to the magnitude of the DCWF impact are temperature of the system and initial wettability condition. The incremental recovery in the range of 2-17% has been reported as the impact of the DCWF. All the experiments and their associated data reported warrant analysis for their underlying premise and the source of the recovery factors reported. As evidenced from various experiments, it should be noted that the coreflood recovery factors are lower compared to that from the imbibition tests, highlighting the impact of heterogeneity and the impact of the flooding processes.

This research has narrowed down on the predominant input parameters with respect to the interactions between the rock, brine (connate and injected) and oil system, which are identified and listed. The expert system workflow, Figure 5-2, developed and presented enables efficient comprehensive screening of the DCW feasibility and is an essential step prior to proceeding with elaborate experiments and modelling that are both resource and time intensive. It provides initial screening methodology and can be used as the basis for further development of advanced screening and modelling specific to DCW. The comprehensive table, Table 3-1, is presented which captures the main interaction mechanisms, their pre-requisites and their corresponding

effects. An improved and comprehensive understanding of the interaction mechanisms in DCW leads to efficient decision making in implementation of the DCW, which is more sustainable in the current economic climate. This will also meet the objectives of lower carbon intensity related energy production while moving towards the overall goals of carbon neutrality and net zero.

The main conclusions that are arrived at based on this research are the following.

1. The critical mechanisms impacting DCW can be categorised into 2 primary interactions (rock-fluid & fluid-fluid) which alters wettability, interfacial tension, or both.

2. A comprehensive experimentation and measurement is recommended which will alleviate the lack of comprehensive data sets and varying approaches being followed for reporting out DCW EOR experiments, which hinders the understanding of the inherent principal mechanisms and their associated parameters. A minimum requirement of experiments is to conduct the corefloods at full reservoir conditions (insitu pressure and temperature) using live oil and formation brine. This needs to be coupled with in-situ saturation monitoring utilizing gamma ray detectors and semi dynamic Pc measurement techniques that are able to capture the full cycle of drainage and imbibition Pc curves. From these curves we can measure the area under the spontaneous imbibition to evaluate the change in the wettability of the ‘core plug’. Additionally the ‘core plug’ should be taken from the full core after the X-ray CT scan/X-ray diffraction (XRD) and the evaluation of the core plug for the level of heterogeneity based on pore throat size distribution needs to be done (Webb et al., 2005). The experiments should also include atomic force microscopy and zeta potential measurement at the different interfaces which are measured in mV and provide indication of the change in the charges at the interface as the DCW is performed through the cores. Additionally, to understand the effect caused due to DCW experiments evaluation of the liquid-liquid interactions through microscopic photographs need to be conducted.

3. Experimental measurements and monitoring should be performed at both the initial and final conditions and specific phase appropriate measurements for each component rock (mineral composition through ‘SEM-EDX’ (‘Scanning Electron Microscopy- Energy Dispersive X-ray’), ‘XRD’ (‘X-ray Diffraction’), ‘XRF’ (‘X-ray Fluorescence’)), brine (pH, Ionic compositions, TDS), oil (API, TAN, TBN) and total system (System temperature, Delta

Pressure, Capillary Pressure, Relative permeability, Wettability, IFT, Recovery Factors, ‘XES’ (‘X-ray Emission Spectroscopy’), ‘AES’ (‘Atomic Emission Spectroscopy’), Zeta Potential at interfaces and CEC).

4. For the different components in the DCW interaction there are specific tests/experiments to be done as follows:

For the oil: TAN/TBN/SARA, mass spectrometry, viscosity, PVT.

For the oil-water interface: AES, XPS (X-ray photoelectron spectroscopy, to determine the surface composition by measuring the surface carbon content), Zeta-potential analyser and CEC.

For the water: Brine analysis, PHREEQC, pH.

For the water-rock interface: AES, XPS, Zeta-potential analyser, CEC.

For the bulk rock: SEM-EDX, XRD, XRF.

5. The aforementioned measurements and modelling requirements are time consuming and resource intensive and therefore it is prudent to have a pre-screening technique (Thomas et al., 2022) that will ensure efficiency and greater value added for the time and effort as researchers and investigators move from initial screening and understanding to the field implementation. The sustainable and efficient approach of AIT/ML has been presented which shows that better screening of DCW EOR process and the determination of critical parameters can be achieved. In the sustainable approach the cycle from data gathering/collection, cleaning/screening, correlation/analysis, application and evaluation of AIT/ML enables better predictability and hence screening of the DCW EOR. As demonstrated and presented in Table 5-14.

6. A sustainable process workflow is implemented for application of AI/ML (comparison between multi-variate Linear Regression, Random Forest and AdaBoost) which ensures improved screening of the DCW EOR process. The Random Forest algorithm and AdaBoost provide better predictability as compared to the initial multi-variate linear regression. This provides a sustainable approach for screening of the DCW EOR before proceeding to more resource intensive experimental data gathering to piloting and full field implementation.

7. The feature importance analysis identified additional parameters of the displacement pressure, oil API and the PV injected that are critical to the DCWF success.

8. A better accuracy is obtained from AI/ML as compared to multi-variate Linear Regression with error in the prediction of the Cumulative Oil production being narrowed down to the range of -0.4% to 1.07% . This demonstrates the capability of the AIT/ML models to reproduce with accuracy the results comparable to computationally intensive 3-D physics-based models for DCW.

9. The data analysis performed led to two categories of parameters being identified based on their positive and negative correlation to the recovery.

10. The initial and final ion concentration in addition to TDS and initial recovery factor at the start of the DCWF are identified as some of the key parameters critical to the success of the DCWF.

11. The ML models of 'Random Forest' and 'Gradient Boosting' have further substantiated the main features that impact DCWF EOR and their predictive capabilities which fall under the explainable AI category.

12. The prediction of the DCWF EOR recovery from lab/field work and the AI/ML models are within the $\pm 7\%$ recovery range except for two cases where the AI/ML predicts upto $\pm 10\%$.

The limitations of the AIT/ML based modelling is that it is specific to the model and data set used. This can be addressed by incorporating data containing other parameters such as the rock mineral composition (clay type, clay %, calcite %, dolomite%). Furthermore, the AIT/ML models can be cross investigated with physics based models for further corroboration of their validity in screening for DCWF EOR.

The future work involves further development of the AIT/ML from the current stage to the next stage inclusive of further models and data sets from multiple sources. This would also involve creation of multiple modelling scenarios with variation in different parameters and the impact of these parameters on the recovery. This can further lead to identification of the critical parameters from the modelling perspective. Additionally, based on the comprehensive experiment data collection and measurements identified through this work, further lab

coreflood/pilot/field experiments can be performed, analysed and screened for enhanced understanding and reporting of the critical mechanism and its associated parameters.

Future experiments need to have a comprehensive reporting which includes the following:

1. Conducted at reservoir conditions with reservoir rock and fluids being used (or as similar as possible to replicate the real reservoir conditions), this should be reported.
2. Reporting details on the ionic composition and TDS of the connate, flooding water and effluent. The API of the oil also needs to be reported. These need to be reported both at initial and final conditions.
3. The IFT, contact angle and CT scans of the sample need to be performed and reported both at the initial and final conditions.
4. The rock sample mineral analysis should also be performed and reported at both initial and final conditions along with system pressure and temperature.

These data collated based on the recommendation of comprehensive experiments need to be updated into the data base, following which additional data analysis and AI/ML modelling performed to understand the important features, evaluate the model prediction and reliability.

REFERENCES

- Abdulla, F., Hashem, H. S., Abdulraheem, B., Al-naqi, M., Al-qattan, A., & John, H. (2013). First EOR Trial using Low Salinity Water Injection in the Greater Burgan. *SPE Middle East Oil and Gas Show and Conference*. <https://www.onepetro.org/download/conference-paper/SPE-164341-MS?id=conference-paper%2FSPE-164341-MS>
- Akhmetgareev, V., & Khisamov, R. (2015). 40 Years of Low-Salinity Waterflooding in Pervomaiskoye Field, Russia: Incremental Oil. *SPE European Formation Damage Conference and Exhibition*. <https://doi.org/10.2118/174182-MS>
- Al-Harrasi, A. S., Al-Maamari, R. S., & Masalmeh, S. (2012, November 11). Laboratory Investigation of Low Salinity Waterflooding for Carbonate Reservoirs. *All Days*. <https://doi.org/10.2118/161468-MS>
- Al-Ibadi, H., Stephen, K., & Mackay, E. (2020, December 1). Heterogeneity Effects on Low Salinity Water Flooding. *Day 1 Tue, December 01, 2020*. <https://doi.org/10.2118/200547-MS>
- Al-saedi, H. N., & Flori, R. E. (2020). *Investigation of Smart Waterflooding in Sandstone Reservoirs : Experimental and Simulation Study Part 2*. September 2019, 12–15.
- Al-Shalabi, E. W., Sepehrnoori, K., & Delshad, M. (2013). Does the double layer expansion mechanism contribute to the LSWI effect on hydrocarbon recovery from carbonate rocks? *SPE Reservoir Characterisation and Simulation Conference and Exhibition: New Approaches in Characterisation and Modelling of Complex Reservoirs, RCSC 2013, 1*, 319–335. <https://doi.org/10.2118/165974-MS>
- Al-Shalabi, E. W., Sepehrnoori, K., Delshad, M., & Pope, G. (2015). A Novel Method To Model Low-Salinity-Water Injection in Carbonate Oil Reservoirs. *SPE Journal*, 20(05), 1154–1166. <https://doi.org/10.2118/169674-PA>
- Al-Shalabi, E. W., Sepehrnoori, K., & Pope, G. (2016). Mechanistic Modeling of Oil Recovery

- Caused by Low-Salinity-Water Injection in Oil Reservoirs. *SPE Journal*, 21(03), 0730–0743. <https://doi.org/10.2118/172770-PA>
- Al-Shalabi, E. W., Sepehrnoori, K., Pope, G., & Mohanty, K. (2014). A Fundamental Model for Predicting Oil Recovery Due to Low Salinity Water Injection in Carbonate Rocks. *SPE Energy Resources Conference*. <https://doi.org/10.2118/169911-MS>
- Aladasani, A., Bai, B., Wu, Y. S., & Salehi, S. (2014). Studying low-salinity waterflooding recovery effects in sandstone reservoirs. *Journal of Petroleum Science and Engineering*, 120, 39–51. <https://doi.org/10.1016/j.petrol.2014.03.008>
- Alshakhs, M. J., BuKhamseen, N. Y., & AlGarni, S. A. (2020). Paradigm shift in smartwater simulation methods. *International Petroleum Technology Conference 2020, IPTC 2020, January*, 13–15. <https://doi.org/10.2523/iptc-19796-ms>
- Austad, T., Rezaeidoust, A., & Puntervold, T. (2010). SPE 129767 Chemical Mechanism of Low Salinity Water Flooding in Sandstone Reservoirs. *Spe*, 129767(September), 19–22. <https://doi.org/10.2118/129767-MS>
- Austad, T., Shariatpanahi, S. F., Strand, S., Black, C. J. J., & Webb, K. J. (2012). Conditions for a low-salinity Enhanced Oil Recovery (EOR) effect in carbonate oil reservoirs. *Energy and Fuels*, 26(1), 569–575. <https://doi.org/10.1021/ef201435g>
- Awolayo, A., Sarma, H., & AlSumaiti, A. M. (2014). A laboratory study of ionic effect of smart water for enhancing oil recovery in carbonate reservoirs. *SPE EOR Conference at Oil and Gas West Asia 2014: Driving Integrated and Innovative EOR*, 46–69. <https://doi.org/10.2118/169662-MS>
- Bernard, G. G. (1967). Effect Of Floodwater Salinity on Recovery of Oil from Cores Containing Clays. *Society of Petroleum Engineers Journal*, 1725, 1–8.
- Bourbiaux, B. (2020). Low salinity effects on oil recovery performance: Underlying physical mechanisms and practical assessment. *Oil and Gas Science and Technology*, 75.

<https://doi.org/10.2516/ogst/2020030>

- Boussour, S., Cissokho, M., Cordier, P., Bertin, H., & Hamon, G. (2009). Oil Recovery by Low Salinity Brine Injection: Laboratory Results on Outcrop and Reservoir Cores. *All Days, 2005*. <https://doi.org/10.2118/124277-MS>
- Cissokho, M., Boussour, S., Cordier, P., Bertin, H., & Hamon, G. (2010). Low salinity oil recovery on clayey sandstone: Experimental study. *Petrophysics, 51*(5), 305–313.
- Dang, C., Nghiem, L., Nguyen, N., Chen, Z., & Nguyen, Q. (2015). Modeling and Optimization of Low Salinity Waterflood. *The SPE Reservoir Simulation Symposium, 23–25*. <https://doi.org/10.2118/173194-MS>
- Egbe, D. I. O., Jahanbani Ghahfarokhi, A., Nait Amar, M., & Torsæter, O. (2021). Application of Low-Salinity Waterflooding in Carbonate Cores: A Geochemical Modeling Study. *Natural Resources Research, 30*(1), 519–542. <https://doi.org/10.1007/s11053-020-09712-5>
- El-M Shokir, E. M., Goda, H. M., Sayyouh, M. H., & Fattah, K. A. (2002, August 5). Selection and Evaluation EOR Method Using Artificial Intelligence. *All Days*. <https://doi.org/10.2118/79163-MS>
- Emadi, A., & Sohrabi, M. (2012). Visual Investigation of Low Salinity Waterflooding. *International Symposium of the Society of Core Analyst, 1–6*.
- Emadi, A., & Sohrabi, M. (2013). Visual Investigation of Oil Recovery by LowSalinity Water Injection: Formation of Water Micro-Dispersions and WettabilityAlteration. *SPE Annual Technical Conference and Exhibition, 1999, 1–15*. <https://doi.org/10.2118/166435-MS>
- Farajzadeh, R., Matsuura, T., van Batenburg, D., & Dijk, H. (2011). *Modeling of Alkali Surfactant Polymer Process by Coupling a Multi-purpose Simulator to the Chemistry Package PHREEQC. April 2011, 12–14*. <https://doi.org/10.3997/2214-4609.201404789>
- Fogden, A., Kumar, M., Morrow, N. R., & Buckley, J. S. (2011). Mobilization of fine particles

- during flooding of sandstones and possible relations to enhanced oil recovery. *Energy and Fuels*, 25(4), 1605–1616. <https://doi.org/10.1021/ef101572n>
- Hadia, N. J., Ashraf, A., Tweheyo, M. T., & Torsæter, O. (2013). Laboratory investigation on effects of initial wettabilities on performance of low salinity waterflooding. *Journal of Petroleum Science and Engineering*, 105, 18–25. <https://doi.org/10.1016/j.petrol.2013.03.014>
- Jackson, M. D., Vinogradov, J., Hamon, G., & Chamerois, M. (2016). Evidence, mechanisms and improved understanding of controlled salinity waterflooding part 1: Sandstones. *Fuel*, 185, 772–793. <https://doi.org/10.1016/j.fuel.2016.07.075>
- Javadi, A., Moslemizadeh, A., Sheikhol Moluki, V., Fathianpour, N., Mohammadzadeh, O., & Zendehboudi, S. (2021). A combination of artificial neural network and genetic algorithm to optimize gas injection: A case study for EOR applications. *Journal of Molecular Liquids*, 339, 116654. <https://doi.org/10.1016/j.molliq.2021.116654>
- Jerauld, G. R., Webb, K. J., Lin, C.-Y., & Secombe, J. C. (2008). Modeling Low-Salinity Waterflooding. *SPE Reservoir Evaluation & Engineering*, 11(06), 1000–1012. <https://doi.org/10.2118/102239-PA>
- Kang, P.-S., Lim, J.-S., & Huh, C. (2014). Integrated Screening Criteria for Offshore Application of Enhanced Oil Recovery. *All Days*, 27–29. <https://doi.org/10.2118/170795-MS>
- Lager, A., Webb, K. J., & Black, C. J. J. (2007). Impact of Brine Chemistry on Oil Recovery. *EAGE - 14th European Symposium on Improved Oil Recovery, April 2007*, 22–24.
- Lager, A., Webb, K. J., Collins, I. R., & Richmond, D. M. (2008, April 20). LoSal Enhanced Oil Recovery: Evidence of Enhanced Oil Recovery at the Reservoir Scale. *All Days*. <https://doi.org/10.2118/113976-MS>
- Lee, S. Y., Webb, K. J., Collins, I., Lager, A., Clarke, S., Sullivan, M., Routh, A., &

- Wang, X. (2010). Low Salinity Oil Recovery: Increasing Understanding of the Underlying Mechanisms. *SPE Improved Oil Recovery Symposium*. <https://doi.org/10.2118/129722-MS>
- Ligthelm, D. J., Gronsveld, J., Hofman, J., Brussee, N., Marcelis, F., & van der Linde, H. (2009). Novel Waterflooding Strategy By Manipulation Of Injection Brine Composition. *EUROPEC/EAGE Conference and Exhibition, June 2009*, 8–11. <https://doi.org/10.2118/119835-MS>
- Mahani, H., Keya, A. L., Berg, S., Global, S., & International, S. (2015). *Driving Mechanism of Low Salinity Flooding in Carbonate Rocks*.
- Mahani, H., Sorop, T. G., Ligthelm, D. ., Brooks, A. D., Vledder, P., Mozahem, F., & Ali, Y. (2011, May 23). Analysis of Field Responses to Low-Salinity Waterflooding in Secondary and Tertiary Mode in Syria. *All Days*. <https://doi.org/10.2118/142960-MS>
- Mahmoud, A. A., Elkatatny, S., Chen, W., & Abdulraheem, A. (2019). Estimation of oil recovery factor for water drive sandy reservoirs through applications of artificial intelligence. *Energies*, *12*(19), 1–13. <https://doi.org/10.3390/en12193671>
- Mahzari, P., & Sohrabi, M. (2014). Crude Oil/Brine Interactions and Spontaneous Formation of Micro-Dispersions in Low Salinity Water Injection. *SPE Improved Oil Recovery Symposium, 2006*. <https://doi.org/10.2118/169081-MS>
- Mcguire, P. L. L., Chatham, J. R. R., Paskvan, F. K. K., Sommer, D. M. M., Carini, F. H. H., & Exploration, B. P. (2005). Low Salinity Oil Recovery: An Exciting New EOR Opportunity for Alaska's North Slope. *SPE Western Regional Meeting*, 1–15. <https://doi.org/10.2118/93903-MS>
- Morrow, N., & Buckley, J. (2011a). Improved Oil Recovery by Low-Salinity Waterflooding. *Journal of Petroleum Technology*, *63*(05), 106–112. <https://doi.org/10.2118/129421-JPT>
- Morrow, N., & Buckley, J. (2011b). Improved Oil Recovery by Low-Salinity Waterflooding.

- Journal of Petroleum Technology*, 63(05), 106–112. <https://doi.org/10.2118/129421-JPT>
- Nande, S. B., & Patwardhan, S. D. (2022). A review on low salinity waterflooding in carbonates: challenges and future perspective. *Journal of Petroleum Exploration and Production Technology*, 12(4), 1037–1055. <https://doi.org/10.1007/s13202-021-01361-5>
- Nasralla, R. A., & Nasr-El-Din, H. A. (2014). Double-Layer Expansion: Is It a Primary Mechanism of Improved Oil Recovery by Low-Salinity Waterflooding? *SPE Reservoir Evaluation & Engineering*, 17(01), 49–59. <https://doi.org/10.2118/154334-PA>
- Ng, C. S. W., Jahanbani Ghahfarokhi, A., & Nait Amar, M. (2021). Application of nature-inspired algorithms and artificial neural network in waterflooding well control optimization. *Journal of Petroleum Exploration and Production*, 11(7), 3103–3127. <https://doi.org/10.1007/s13202-021-01199-x>
- Nguyen, N., Chen, J., & Nghiem, L. (2013). State-of-the Art Low Salinity Waterflooding for Enhanced Oil Recovery. *SPE Asia Pacific Oil & ...* <https://doi.org/10.2118/165903-MS>
- Okabe, H. (2005). Bridging Pore To Core-Scale Flow Properties Using Pore-Scale Modeling and Coreflood. *International Symposium of the Society of Core Analysts*, 1–12.
- Ramos, G. (2017). Application of artificial intelligence for technical screening of enhanced oil recovery methods. *Journal of Oil, Gas and Petrochemical Sciences*, 1, 1–12. <https://doi.org/10.30881/jogps.00002>
- Rezaeidoust, A., Puntervold, T., Strand, S., & Austad, T. (2009). Smart water as wettability modifier in carbonate and sandstone: A discussion of similarities/differences in the chemical mechanisms. *Energy and Fuels*, 23(9), 4479–4485. <https://doi.org/10.1021/ef900185q>
- Rivet, S., Lake, L. W., & Pope, G. A. (2010). A Coreflood Investigation of Low-Salinity Enhanced Oil Recovery. *SPE Annual Technical Conference and Exhibition, September*, 19–22. <https://doi.org/10.2118/134297-MS>

- Robbana, E., Buikema, T. A., Mair, C., Williams, D., Mercer, D. J., Webb, K. J., Hewson, A., & Reddick, C. E. (2012). Low Salinity Enhanced Oil Recovery - Laboratory to Day One Field Implementation - LoSal EOR into the Clair Ridge Project. *Abu Dhabi International Petroleum Exhibition and Conference, April 2011*, 12–14. <https://doi.org/10.2118/161750-MS>
- Romanuka, J., Hofman, J., Ligthelm, D. J., Suijkerbuijk, B., Marcelis, F., Oedai, S., Brussee, N., van der Linde, H., Aksulu, H., & Austad, T. (2012). Low Salinity EOR in Carbonates. *SPE Improved Oil Recovery Symposium*. <https://doi.org/10.2118/153869-MS>
- Rotondi, M., Callegaro, C., Masserano, F., & Bartosek, M. (2014). Low Salinity Water Injection: eni' s experience. *Abu Dhabi International Petroleum Exhibition and Conference, SPE171794-MS*, 10–13. <https://doi.org/http://dx.doi.org/10.2118/171794-MS>
- Sarkar, A. K., & Sharma, M. M. (1990). Fines Migration in Two-Phase Flow. *Journal of Petroleum Technology*, 42(05), 646–652. <https://doi.org/10.2118/17437-PA>
- Schumi, B., Clemens, T., Wegner, J., Ganzer, L., Kaiser, A., Hincapie, R. E., & Leitenmüller, V. (2020). Alkali/Cosolvent/Polymer Flooding of High-TAN Oil: Using Phase Experiments, Micromodels, and Corefloods for Injection-Agent Selection. *SPE Reservoir Evaluation & Engineering*, 23(02), 463–478. <https://doi.org/10.2118/195504-PA>
- Secombe, J., Lager, A., Jerauld, G., Jhaveri, B., Buikema, T., Bassler, S., Denis, J., Webb, K., Cockin, A., & Fueg, E. (2010). Demonstration of Low-Salinity EOR at Interwell Scale, Endicott Field, Alaska. *SPE Improved Oil Recovery Symposium, 2008*. <https://doi.org/10.2118/129692-MS>
- Shafiei, A., Tatar, A., Rayhani, M., Kairat, M., & Askarova, I. (2022). Artificial neural network, support vector machine, decision tree, random forest, and committee machine intelligent system help to improve performance prediction of low salinity water injection

- in carbonate oil reservoirs. *Journal of Petroleum Science and Engineering*, 219(November 2021), 111046. <https://doi.org/10.1016/j.petrol.2022.111046>
- Sheng, J. J. (2014). Critical review of low-salinity waterflooding. *Journal of Petroleum Science and Engineering*, 120, 216–224. <https://doi.org/10.1016/j.petrol.2014.05.026>
- Singh, N., & Sarma, H. K. (2021, April 10). Successful in the Lab, Not as Effective in the Field? Uncertainties in the Field Observations of Low Salinity Water Flooding in Sandstone and Carbonate Reservoirs-A Critical Analysis. *Day 2 Wed, April 21, 2021*. <https://doi.org/10.2118/200803-MS>
- Skauge, A. (2013). Low Salinity Flooding - A Critical Review. *Proceedings of SPE IOR Symposium, St. Petersburg, Russia, April 2013*, 16–18.
- Skrettingland, K., Holt, T., Tweheyo, M. T. . T., & Skjevrak, I. (2011). Snorre Low-Salinity-Water Injection—Coreflooding Experiments and Single-Well Field Pilot. *SPE Reservoir Evaluation & Engineering*, 14(02), 182–192. <https://doi.org/10.2118/129877-PA>
- Sorbie, K. S., & Collins, I. (2010). A Proposed Pore-Scale Mechanism for How Low Salinity Waterflooding Works. *SPE Improved Oil Recovery Symposium*, 1–18. <https://doi.org/10.2118/129833-MS>
- Sorop, T. G., Suijkerbuijk, B. M. J. M., Masalmeh, S. K., Looijer, M. T., Parker, A. R., Dindoruk, D. M., Goodyear, S. G., & Al-Qarshubi, I. S. M. (2013). Integrated Approach in Deploying Low Salinity Waterflooding. *All Days*, 1–9. <https://doi.org/10.2118/165277-MS>
- Strand, S., Høgnesen, E. J., & Austad, T. (2006). Wettability alteration of carbonates - Effects of potential determining ions (Ca²⁺and SO₄²⁻) and temperature. *Colloids and Surfaces A: Physicochemical and Engineering Aspects*, 275(1–3), 1–10. <https://doi.org/10.1016/j.colsurfa.2005.10.061>
- Suijkerbuijk, B. M. J. M., Kuipers, H. P. C. E., Van Kruijsdijk, C. P. J. W., Berg, S., Van

- Winden, J. F., Ligthelm, D. J., Mahani, H., PingoAlmada, M., Van Den Pol, E., Joekar Niasar, V., Romanuka, J., Vermolen, E. C. M., & Al-Qarshubi, I. S. M. (2013). The development of a workflow to improve predictive capability of low salinity response. *International Petroleum Technology Conference 2013: Challenging Technology and Economic Limits to Meet the Global Energy Demand, IPTC 2013*, 7, 5480–5490. <http://www.scopus.com/inward/record.url?eid=2-s2.0-84883432517&partnerID=40&md5=6e59fb46e91700c3d050bd9843a6dad2>
- Sun, Q., & Ertekin, T. (2018, April 23). Development and Application of an Artificial-Neural-Network Based Expert System for Screening and Optimization of Polymer Flooding Projects. *All Days*. <https://doi.org/10.2118/192236-MS>
- Syed, F. I., Muther, T., Dahaghi, A. K., & Negahban, S. (2021). AI/ML assisted shale gas production performance evaluation. *Journal of Petroleum Exploration and Production Technology*, 11(9), 3509–3519. <https://doi.org/10.1007/s13202-021-01253-8>
- Taber, J. J., Martin, F. D., & Seright, R. S. (1997). EOR Screening Criteria Revisited - Part 1: Introduction to Screening Criteria and Enhanced Recovery Field Projects. *SPE Reservoir Engineering*, 12(03), 189–198. <https://doi.org/10.2118/35385-PA>
- Tang, G.-Q., & Morrow, N. R. (1999). Influence of brine composition and fines migration on crude oil/brine/rock interactions and oil recovery. *Journal of Petroleum Science and Engineering*, 24(2–4), 99–111. [https://doi.org/10.1016/S0920-4105\(99\)00034-0](https://doi.org/10.1016/S0920-4105(99)00034-0)
- Tang, G. Q., & Morrow, N. R. (1997). Salinity, Temperature, Oil Composition, and Oil Recovery by Waterflooding. *SPE Reservoir Engineering*, 12(04), 269–276. <https://doi.org/10.2118/36680-PA>
- Tariq, Z., Aljawad, M. S., Hasan, A., Murtaza, M., Mohammed, E., El-Husseiny, A., Alarifi, S. A., Mahmoud, M., & Abdulraheem, A. (2021). A systematic review of data science and machine learning applications to the oil and gas industry. *Journal of Petroleum*

Exploration and Production Technology, 11(12), 4339–4374.

<https://doi.org/10.1007/s13202-021-01302-2>

Tatar, A., Askarova, I., Shafiei, A., & Rayhani, M. (2021). Data-Driven Connectionist Models for Performance Prediction of Low Salinity Waterflooding in Sandstone Reservoirs. *ACS Omega*, 6(47), 32304–32326. <https://doi.org/10.1021/acsomega.1c05493>

Thomas, T., Sharma, P., & Gupta, D. K. (2022). Meta-analysis of rock, brine, oil interactions and expert system development. *Materials Today: Proceedings*, 50, 969–976. <https://doi.org/10.1016/j.matpr.2021.07.140>

Thomas, T., Sharma, P., & Gupta, D. K. (2023a). Sustainable application of ML/AI methods in DCW understanding & screening. *Materials Today: Proceedings*, xxxx. <https://doi.org/10.1016/j.matpr.2023.06.010>

Thomas, T., Sharma, P., & Gupta, D. K. (2023b). Understanding & Screening of DCW through Application of Data Analysis of Experiments and ML/AI. *Energies*, 16(8), 3376. <https://doi.org/10.3390/en16083376>

Thomas, T., Sharma, P. P., Dharmendra, P., & Gupta, K. (2023). Use of AI tools to Understand surface-interaction based EOR processes. *Applied Computing and Geosciences*, 17(July 2022), 100111. <https://doi.org/10.1016/j.acags.2022.100111>

Vledder, P., Gonzalez, I. E., Carrera Fonseca, J. C., Wells, T., & Ligthelm, D. J. (2010). Low Salinity Water Flooding: Proof Of Wettability Alteration On A Field Wide Scale. *SPE Improved Oil Recovery Symposium*, Lil, 1–10. <https://doi.org/10.2118/129564-MS>

Webb, K. J., Black, C. J. J., Tjetland, G., & Exploration, B. P. (2005). A Laboratory Study Investigating Methods for Improving Oil Recovery in Carbonates. *International Petroleum Technology Conference*, 1–7. <https://doi.org/10.2523/IPTC-10506-MS>

Yildiz, H. O., & Morrow, N. R. (1996). Effect of brine composition on recovery of Moutray crude oil by waterflooding. *Journal of Petroleum Science and Engineering*, 14(3–4), 159–

168. [https://doi.org/10.1016/0920-4105\(95\)00041-0](https://doi.org/10.1016/0920-4105(95)00041-0)

- Yousef, A. A., Al-Saleh, S., & Al-Jawfi, M. S. (2012). Improved/Enhanced Oil Recovery from Carbonate Reservoirs by Tuning Injection Water Salinity and Ionic Content. *SPE Improved Oil Recovery Symposium*. <https://doi.org/10.2118/154076-MS>
- Yousef, A. A., Al-Saleh, S. H., Al-Kaabi, A., & Al-Jawfi, M. S. (2011). Laboratory Investigation of the Impact of Injection-Water Salinity and Ionic Content on Oil Recovery From Carbonate Reservoirs. *SPE Reservoir Evaluation & Engineering*, 14(05), 578–593. <https://doi.org/10.2118/137634-PA>
- Yousef, A. A., Liu, J., Blanchard, G., Al-Saleh, S., Al-Zahrani, T., Al-Zahrani, R., Al-Tammar, H., & Al-Mulhim, N. (2012). SmartWater flooding: Industry's first field test in carbonate reservoirs. *Proceedings - SPE Annual Technical Conference and Exhibition*, 3, 2469–2494. <https://doi.org/10.2118/159526-ms>
- Zahid, A., Stenby, E. H., & Shapiro, A. A. (2012). Smart Waterflooding (High Sal/Low Sal) in Carbonate Reservoirs. *All Days*, 21. <https://doi.org/10.2118/154508-MS>
- Zhang, P., & Austad, T. (2005). Waterflooding in chalk: Relationship between oil recovery, new wettability index, brine composition and cationic wettability modifier. *SPE Europec/EAGE Annual Conference*. <https://doi.org/10.2118/94209-MS>
- Zhang, T., Li, Y., Li, C., & Sun, S. (2020). Effect of salinity on oil production: Review on low salinity waterflooding mechanisms and exploratory study on pipeline scaling. *Oil and Gas Science and Technology*, 75. <https://doi.org/10.2516/ogst/2020045>

Appendix A

```
##Initial Screening Code
init_wet=int(input("the initial wetting state is: choose 1 for WW, -1 OW, 0 IW: "))
if init_wet >0:
    print("Not suitable for LSL")
elif init_wet <=0:
    salt_conc=int(input("1 if formation_brine salt_conc >inj_brine salt_conc: "))
    if salt_conc!=1:
        print ("Not suitable for LSL")
    elif salt_conc==1:
        micro_disp=int(input("1 if surface active materials present in oil: "))
        if micro_disp!=1:
            print ("Not suitable for LSL")
        elif micro_disp==1:
            formation_type=int(input("1 if carbonate and -1 if sandstone: "))
            if formation_type==-1:
                monoval_ion=int(input("1 if mono_val ion present in inj_brine: "))
                salinity_injbrine=int(input("salinity of inj_brine in ppm: "))
                if monoval_ion !=1 and salinity_injbrine>3500: #this line needs to be checked
                    print ("Not suitable for LSL")
            else:
                print ("Suitable for LSL, Proceed to Detailed screening")
        elif formation_type==1:
            divalent_ion=int(input("1 if di_val ion present in inj_brine: "))
            if divalent_ion !=1:
                print ("Not suitable for LSL")
            else:
                print ("Suitable for LSL, Proceed to Detailed screening")

##Data Analysis & Comparison between various AI/ML Models
```

```

import numpy as np
import pandas as pd
import seaborn as sns
import matplotlib.pyplot as plt
DCW_data = pd.read_csv('DCW_LSL.csv')
DCW_data
DCW_data.columns
DCW_data.rename({'PV injected':'PV Injected'}, axis=1, inplace=True)
DCW_data.rename({'INITIAL delta PRESSURE':'Initial Delta Pressure', 'Final delta
Pressure':'Final Delta Pressure'}, axis=1, inplace=True)
DCW_data.rename({'Incremental delta Pressure (mbars)':'Incremental Delta Pressure
(mbars)', 'TDS (ppm)_initial':'TDS (ppm)_Initial'}, axis=1, inplace=True)
dt = DCW_data.copy()
dt.columns
DCW_data['Formation Type'].value_counts()
DCW_data.duplicated().count()
DCW_data['Formation Type'].replace(np.nan,'To be determined', inplace=True)
DCW_data['Formation Type'].isnull().count()
DCW_data['Formation Type'].head(10)
import missingno as msno
import numpy as np
import pandas as pd
import seaborn as sns
import matplotlib.pyplot as plt

DCW_data = pd.read_csv('DCW_LSL.csv')

msno.bar(dt, color='green')
from sklearn.impute import SimpleImputer
## Defning the Simple Imputer funtion to use 'mean' as a strategy of imputation

Imp = SimpleImputer(missing_values=np.nan, strategy='mean')
Imp = Imp.fit(DCW_data[['Initial Ph']])
DCW_data['Initial Ph'] = Imp.transform(DCW_data[['Initial Ph']]).ravel()
Imp = Imp.fit(DCW_data[['Final Ph']])
DCW_data['Final Ph'] = Imp.transform(DCW_data[['Final Ph']]).ravel()
Imp = Imp.fit(DCW_data[['PV injected']])
DCW_data['PV injected'] = Imp.transform(DCW_data[['PV injected']]).ravel()
DCW_data.drop(['Quartz'], axis=1, inplace=True)
DCW_data.drop(['Dolomite % (Vol. frac.)'], axis=1, inplace=True)
Imp = Imp.fit(DCW_data[['Calcite % (Vol frac.)']])
DCW_data['Calcite % (Vol frac.)'] = Imp.transform(DCW_data[['Calcite % (Vol
frac.)']]).ravel()
Imp = Imp.fit(DCW_data[['Oil API']])
DCW_data['Oil API'] = Imp.transform(DCW_data[['Oil API']]).ravel()
Imp = Imp.fit(DCW_data[['INITIAL delta PRESSURE']])
DCW_data['INITIAL delta PRESSURE'] = Imp.transform(DCW_data[['INITIAL delta
PRESSURE']]).ravel()
Imp = Imp.fit(DCW_data[['Final delta Pressure']])

```

```

DCW_data['Final delta Pressure'] = Imp.transform(DCW_data[['Final delta
Pressure']]).ravel()
Imp = Imp.fit(DCW_data[['TDS (ppm)_initial']])
DCW_data['TDS (ppm)_initial'] = Imp.transform(DCW_data[['TDS (ppm)_initial']]).ravel()
Imp = Imp.fit(DCW_data[['TDS (ppm)_final']])
DCW_data['TDS (ppm)_final'] = Imp.transform(DCW_data[['TDS (ppm)_final']]).ravel()
Imp = Imp.fit(DCW_data[['Ca2+(ppm)_initial']])
DCW_data['Ca2+(ppm)_initial'] = Imp.transform(DCW_data[['Ca2+(ppm)_initial']]).ravel()
Imp = Imp.fit(DCW_data[['Ca2+(ppm)_final']])
DCW_data['Ca2+(ppm)_final'] = Imp.transform(DCW_data[['Ca2+(ppm)_final']]).ravel()
Imp = Imp.fit(DCW_data[['Mg2+(ppm)_initial']])
DCW_data['Mg2+(ppm)_initial'] = Imp.transform(DCW_data[['Mg2+(ppm)_initial']]).ravel()
Imp = Imp.fit(DCW_data[['Mg2+(ppm)_final']])
DCW_data['Mg2+(ppm)_final'] = Imp.transform(DCW_data[['Mg2+(ppm)_final']]).ravel()
Imp = Imp.fit(DCW_data[['Cl-(ppm)_initial']])
DCW_data['Cl-(ppm)_initial'] = Imp.transform(DCW_data[['Cl-(ppm)_initial']]).ravel()
Imp = Imp.fit(DCW_data[['Cl-(ppm)_final']])
DCW_data['Cl-(ppm)_final'] = Imp.transform(DCW_data[['Cl-(ppm)_final']]).ravel()
Imp = Imp.fit(DCW_data[['Na+(ppm)_initial']])
DCW_data['Na+(ppm)_initial'] = Imp.transform(DCW_data[['Na+(ppm)_initial']]).ravel()
Imp = Imp.fit(DCW_data[['Na+(ppm)_final']])
DCW_data['Na+(ppm)_final'] = Imp.transform(DCW_data[['Na+(ppm)_final']]).ravel()
Imp = Imp.fit(DCW_data[['So42-(ppm)_initial']])
DCW_data['So42-(ppm)_initial'] = Imp.transform(DCW_data[['So42-(ppm)_initial']]).ravel()
Imp = Imp.fit(DCW_data[['phie (p.u.)']])
DCW_data['phie (p.u.)'] = Imp.transform(DCW_data[['phie (p.u.)']]).ravel()
Imp = Imp.fit(DCW_data[['perm(mD)']])
DCW_data['perm(mD)'] = Imp.transform(DCW_data[['perm(mD)']]).ravel()
Imp = Imp.fit(DCW_data[['So42-(ppm)_final']])
DCW_data['So42-(ppm)_final'] = Imp.transform(DCW_data[['So42-(ppm)_final']]).ravel()
plt.figure(figsize=(18, 10))
sns.barplot(y="Initial Ph", x="Final tertiary RF%", data=DCW_data)
plt.show()
sns.histplot(x=DCW_data['Final tertiary RF%'], kde=True);
plt.figure(figsize=(18, 15))
sns.heatmap(correlation, annot=False, vmin=-1, vmax=1, cmap="Spectral")
plt.show()
# to split the data into train and test
from sklearn.model_selection import train_test_split

# to build linear regression model
from sklearn.linear_model import LinearRegression

# to check model performance
from sklearn.metrics import mean_absolute_error, mean_squared_error, r2_score
import sdv
from sdv.tabular import GaussianCopula
model = GaussianCopula()
model.fit(dt_new)
sample = model.sample(400)

```

```

sample.head()
X = sample.drop(["Initial Ph", "Final Ph", "Final tertiary RF%", "phie (p.u)", "Setup type",
"Incremental Recovery %", "INITIAL delta PRESSURE", "Final delta Pressure"], axis=1) #
Independent variables
y = sample["Final tertiary RF%"] # Dependent variable
from sklearn.model_selection import train_test_split

x_train, x_test, y_train, y_test = train_test_split(X, y, test_size=0.2, random_state=1)
lin_reg_model = LinearRegression()
lin_reg_model.fit(x_train, y_train)
coef_df = pd.DataFrame(
    np.append(lin_reg_model.coef_, lin_reg_model.intercept_),
    index=x_train.columns.tolist() + ["Intercept"],
    columns=["Coefficients"],
)
coef_df # Extracting coefficients and intercept
# function to compute adjusted R-squared

def adj_r2_score(predictors, targets, predictions):
    r2 = r2_score(targets, predictions)
    n = predictors.shape[0]
    k = predictors.shape[1]
    return 1 - ((1 - r2) * (n - 1) / (n - k - 1))

# function to compute MAPE
def mape_score(targets, predictions):
    # return np.mean(np.abs((targets - predictions) / targets)) * 100
    return 100 / len(targets) * np.sum(2 * np.abs(predictions - targets) / (np.abs(targets) +
np.abs(predictions)))

# function to compute different metrics to check performance of a regression model
def model_performance_regression(model, predictors, target):
    """
    Function to compute different metrics to check regression model performance

    model: regressor
    predictors: independent variables
    target: dependent variable
    """

    # predicting using the independent variables
    pred = model.predict(predictors)

    r2 = r2_score(target, pred) # to compute R-squared
    adjr2 = adj_r2_score(predictors, target, pred) # to compute adjusted R-squared
    rmse = np.sqrt(mean_squared_error(target, pred)) # to compute RMSE
    mae = mean_absolute_error(target, pred) # to compute MAE

```

```

mape = mape_score(target, pred) # to compute MAPE

# creating a dataframe of metrics
df_perf = pd.DataFrame(
    {
        "RMSE": rmse,
        "MAE": mae,
        "R-squared": r2,
        "Adj. R-squared": adjr2,
        "SMAPE": mape,
    },
    index=[0],
)

return df_perf
# Checking model performance on train set
print("Training Performance\n")
lin_reg_model_train_perf = model_performance_regression(lin_reg_model, x_train, y_train)
lin_reg_model_train_perf
# Checking model performance on test set
print("Test Performance\n")
lin_reg_model_test_perf = model_performance_regression(lin_reg_model, x_test, y_test)
lin_reg_model_test_perf

y_Final_tertiary_RF = lin_reg_model.predict(x_test)
Final_tertiary_RF_difference = pd.DataFrame({'Actual Finaltertiary RF% ': y_test, 'Predicted
Finaltertiary RF% ': y_Final_tertiary_RF})
Final_tertiary_RF_difference

#Decision Tree

from sklearn.tree import DecisionTreeRegressor
from sklearn.ensemble import BaggingRegressor,RandomForestRegressor,
GradientBoostingRegressor, AdaBoostRegressor, StackingRegressor
from xgboost import XGBRegressor
from sklearn import metrics
from sklearn.model_selection import GridSearchCV, train_test_split

dtree=DecisionTreeRegressor(random_state=1)
dtree.fit(x_train,y_train)
from sklearn.metrics import r2_score, mean_squared_error, mean_absolute_error
dtree_model_train_perf=model_performance_regression(dtree, x_train,y_train)
print("Training performance \n",dtree_model_train_perf)
dtree_model_test_perf=model_performance_regression(dtree, x_test,y_test)
print("Testing performance \n",dtree_model_test_perf)

#Hyperparameter Tuning

# Choose the type of classifier.

```

```

dtree_tuned = DecisionTreeRegressor(random_state=1)

# Grid of parameters to choose from
parameters = {'max_depth': list(np.arange(2,20)) + [None],
              'min_samples_leaf': [1, 3, 5, 7, 10],
              'max_leaf_nodes': [2, 3, 5, 10, 15] + [None],
              'min_impurity_decrease': [0.001, 0.01, 0.1, 0.0]
              }

# Type of scoring used to compare parameter combinations
scorer = metrics.make_scorer(metrics.r2_score)

# Run the grid search
grid_obj = GridSearchCV(dtree_tuned, parameters, scoring=scorer,cv=5)
grid_obj = grid_obj.fit(x_train, y_train)

# Set the clf to the best combination of parameters
dtree_tuned = grid_obj.best_estimator_

# Fit the best algorithm to the data.
dtree_tuned.fit(x_train, y_train)

dtree_tuned_model_train_perf = model_performance_regression(dtree_tuned,
x_train,y_train)
print("Training performance \n",dtree_model_train_perf)
dtree_tuned_model_test_perf = model_performance_regression(dtree_tuned, x_test,y_test)
print("Testing performance \n",dtree_tuned_model_test_perf)
print(pd.DataFrame(dtree_tuned.feature_importances_, columns = ["Imp"], index =
x_test.columns).sort_values(by = 'Imp', ascending = False))
feature_names = x_test.columns
importances = dtree_tuned.feature_importances_
indices = np.argsort(importances)

plt.figure(figsize=(12,12))
plt.title('Feature Importances')
plt.barh(range(len(indices)), importances[indices], color='violet', align='center')
plt.yticks(range(len(indices)), [feature_names[i] for i in indices])
plt.xlabel('Relative Importance')
plt.show()

y_FinaltertiaryRF_DT = dtree_tuned.predict(x_test)
Final_tertiary_RF_difference = pd.DataFrame({'Actual Finaltertiary RF% ': y_test, 'Predicted
Finaltertiary RF% ': y_FinaltertiaryRF_DT})
Final_tertiary_RF_difference

rf_estimator=RandomForestRegressor(random_state=1)
rf_estimator.fit(x_train,y_train)

```

```

rf_estimator_model_train_perf = model_performance_regression(rf_estimator,
x_train,y_train)
print("Training performance \n",rf_estimator_model_train_perf)
rf_estimator_model_test_perf = model_performance_regression(rf_estimator, x_test,y_test)
print("Testing performance \n",rf_estimator_model_test_perf)
# Choose the type of classifier.
rf_tuned = RandomForestRegressor(random_state=1)

# Grid of parameters to choose from
parameters = {
    'max_depth':[4, 6, 8, 10, None],
    'max_features': ['sqrt','log2',None],
    'n_estimators': [80, 90, 100, 110, 120]
}

# Type of scoring used to compare parameter combinations
scorer = metrics.make_scorer(metrics.r2_score)

# Run the grid search
grid_obj = GridSearchCV(rf_tuned, parameters, scoring=scorer,cv=5)
grid_obj = grid_obj.fit(x_train, y_train)

# Set the clf to the best combination of parameters
rf_tuned = grid_obj.best_estimator_

# Fit the best algorithm to the data.
rf_tuned.fit(x_train, y_train)
rf_tuned_model_train_perf = model_performance_regression(rf_tuned, x_train, y_train)
print("Training performance \n",rf_tuned_model_train_perf)
rf_tuned_model_test_perf = model_performance_regression(rf_tuned, x_test, y_test)
print("Testing performance \n",rf_tuned_model_test_perf)
# importance of features in the tree building ( The importance of a feature is computed as the
#(normalized) total reduction of the criterion brought by that feature. It is also known as the
Gini importance )

print(pd.DataFrame(rf_tuned.feature_importances_, columns = ["Imp"], index =
x_train.columns).sort_values(by = 'Imp', ascending = False))
feature_names = x_train.columns
importances = rf_tuned.feature_importances_
indices = np.argsort(importances)

plt.figure(figsize=(12,12))
plt.title('Feature Importances')
plt.barh(range(len(indices)), importances[indices], color='violet', align='center')
plt.yticks(range(len(indices)), [feature_names[i] for i in indices])
plt.xlabel('Relative Importance')
plt.show()
y_FinaltertiaryRF_RFor = rf_tuned.predict(x_test)

```

```
Final_tertiary_RF_difference = pd.DataFrame({'Actual Finaltertiary RF% ': y_test, 'Predicted
Finaltertiary RF% ': y_FinaltertiaryRF_RFfor, 'Error%':(y_FinaltertiaryRF_RFfor-
y_test)*100/y_test})
Final_tertiary_RF_difference
```

```
#Boosting models
```

```
ab_regressor=AdaBoostRegressor(random_state=1)
ab_regressor.fit(x_train,y_train)
ab_regressor_model_train_perf = model_performance_regression(ab_regressor,
x_train,y_train)
print("Training performance \n",ab_regressor_model_train_perf)
ab_regressor_model_test_perf = model_performance_regression(ab_regressor, x_test,y_test)
print("Testing performance \n",ab_regressor_model_test_perf)
# Choose the type of classifier.
ab_tuned = AdaBoostRegressor(random_state=1)
```

```
# Grid of parameters to choose from
parameters = {'n_estimators': np.arange(10,100,10),
              'learning_rate': [1,0.1, 0.5, 0.01],
              }
```

```
# Type of scoring used to compare parameter combinations
scorer = metrics.make_scorer(metrics.r2_score)
```

```
# Run the grid search
grid_obj = GridSearchCV(ab_tuned, parameters, scoring=scorer,cv=5)
grid_obj = grid_obj.fit(x_train, y_train)
```

```
# Set the clf to the best combination of parameters
ab_tuned = grid_obj.best_estimator_
```

```
# Fit the best algorithm to the data.
ab_tuned.fit(x_train, y_train)
ab_tuned_model_train_perf = model_performance_regression(ab_tuned, x_train,y_train)
print("Training performance \n",ab_tuned_model_train_perf)
ab_tuned_model_test_perf = model_performance_regression(ab_tuned, x_test,y_test)
print("Testing performance \n",ab_tuned_model_test_perf)
print(pd.DataFrame(ab_tuned.feature_importances_, columns = ["Imp"], index =
x_train.columns).sort_values(by = 'Imp', ascending = False))
```

```
feature_names = x_train.columns
importances = ab_tuned.feature_importances_
indices = np.argsort(importances)
```

```
plt.figure(figsize=(12,12))
plt.title('Feature Importances')
plt.barh(range(len(indices)), importances[indices], color='violet', align='center')
plt.yticks(range(len(indices)), [feature_names[i] for i in indices])
```

```
plt.xlabel('Relative Importance')
plt.show()
```

```
y_FinaltertiaryRF_ab = ab_tuned.predict(x_test)
Final_tertiary_ab_difference = pd.DataFrame({'Actual Finaltertiary RF% ': y_test, 'Predicted
Finaltertiary RF% ': y_FinaltertiaryRF_ab, 'Error%':(y_FinaltertiaryRF_ab-
y_test)*100/y_test})
Final_tertiary_ab_difference
```

```
# training performance comparison
```

```
models_train_comp_df = pd.concat(
    [dtree_model_train_perf.T, dtree_tuned_model_train_perf.T,
    rf_estimator_model_train_perf.T, rf_tuned_model_train_perf.T,
```

```
ab_regressor_model_train_perf.T, ab_tuned_model_train_perf.T, gb_estimator_model_train_p
perf.T, gb_tuned_model_train_perf.T,
```

```
xgb_estimator_model_train_perf.T, xgb_tuned_model_train_perf.T, stacking_estimator_model
_train_perf.T],
    axis=1,
)
```

```
models_train_comp_df.columns = [
    "Decision Tree",
    "Decision Tree Tuned",
    "Random Forest Estimator",
    "Random Forest Tuned",
    "Adaboost Regressor",
    "Adaboost Tuned",
    "Gradient Boost Estimator",
    "Gradient Boost Tuned",
    "XGB",
    "XGB Tuned",
    "Stacking Classifier"
]
```

```
print("Training performance comparison:")
models_train_comp_df
```

```
# testing performance comparison
```

```
models_test_comp_df = pd.concat(
    [dtree_model_test_perf.T,
    dtree_tuned_model_test_perf.T,
    rf_estimator_model_test_perf.T,
    rf_tuned_model_test_perf.T,
    ab_regressor_model_test_perf.T,
```

```

ab_tuned_model_test_perf.T,
gb_estimator_model_test_perf.T,
gb_tuned_model_test_perf.T,
xgb_estimator_model_test_perf.T,
xgb_tuned_model_test_perf.T,
stacking_estimator_model_test_perf.T],
axis=1,
)

```

```

models_test_comp_df.columns = [
    "Decision Tree",
    "Decision Tree Tuned",
    "Random Forest Estimator",
    "Random Forest Tuned",
    "Adaboost Regressor",
    "Adaboost Tuned",
    "Gradient Boost Estimator",
    "Gradient Boost Tuned",
    "XGB",
    "XGB Tuned",
    "Stacking Classifier"
]

```

```

print("Test performance comparison:")
models_test_comp_df

```

#ANN Model and prediction of various Relative Permeability End Points in addition to Recovery Factor.

```

from sklearn.preprocessing import StandardScaler

```

```

sc_x = StandardScaler()
sc_y = StandardScaler()
x_train_sc = sc_x.fit_transform(x_train)
y_train_sc = sc_y.fit_transform(y_train.reshape(-1,1))
x_test_sc = sc_x.fit_transform(x_test)
y_test_sc = sc_y.fit_transform(y_test.reshape(-1,1))

```

```

from sklearn import preprocessing

```

```

scaler_Y = preprocessing.StandardScaler().fit(y.reshape(-1,1))

```

```

model = Sequential()

```

```

# Initializing the ANN
model1 = Sequential()

```

```

# This adds the input layer
model1.add(Dense(activation = 'relu', kernel_initializer='he_uniform',input_dim =
x_train_sc.shape[1], units=128))
model1.add(Dropout(0.3))

#Add 2nd hidden layer
model1.add(Dense(64, activation='relu', kernel_initializer='he_uniform'))

#Add 3rd hidden layer
model1.add(Dense(64, activation='relu', kernel_initializer='he_uniform'))
model1.add(Dropout(0.3))

#Add 4th hidden layer
model1.add(Dense(64, activation='relu', kernel_initializer='he_uniform'))
model1.add(Dropout(0.2))

#Add 5th hidden layer
model1.add(Dense(32, activation='relu', kernel_initializer='he_uniform'))

model1.add(Dense(1, activation='linear'))

#Compiling the ANN with SGD optimizer and binary cross entropy loss function
#MAE : loss=tf.keras.losses.MeanAbsoluteError(name="mean_absolute_error"), metrics
=[tf.keras.metrics.MeanAbsoluteError()]

optimizer = tf.keras.optimizers.SGD(0.01)
model1.compile(optimizer=optimizer, loss='mean_squared_error', metrics=['mae'])
model1.summary()

from keras.callbacks import EarlyStopping

early_stopping_monitor = EarlyStopping(monitor='val_loss',min_delta=0.001, patience=5)

history=model1.fit(x_train_sc, y_train_sc,
validation_split=0.3,
epochs=75, verbose=1, batch_size = 20)

#Plotting Train Loss vs Validation Loss
plt.plot(history.history['loss'])
plt.plot(history.history['val_loss'])
plt.title('model loss')
plt.ylabel('Loss')
plt.xlabel('Epoch')
plt.legend(['train', 'validation'], loc='upper left')
plt.show()

```

```

y_pred_scale = model1.predict(x_test_sc)
final_pred = scaler_Y.inverse_transform(y_pred_scale)
final_pred_original_df =
pd.concat([pd.Series(final_pred.flatten()),pd.Series(y_test.flatten())], axis=1)
final_pred_original_df.columns = ['Prediction', 'Original Values']

final_pred_original_df['percent_diff'] = ((final_pred_original_df['Original Values']-
final_pred_original_df['Prediction'])/final_pred_original_df['Original Values'])*100

final_pred_original_df.head(20)

from sklearn.metrics import explained_variance_score, mean_squared_error, r2_score,
mean_absolute_error

def adj_r2_score(predictors, targets, predictions):
    r2 = r2_score(targets, predictions)
    n = predictors.shape[0]
    k = predictors.shape[1]
    return 1 - ((1 - r2) * (n - 1) / (n - k - 1))
def model_performance_regression(predictors,target,pred):
    r2 = r2_score(target, pred) # to compute R-squared
    adjr2 = adj_r2_score(predictors, target, pred) # to compute adjusted R-squared
    rmse = np.sqrt(mean_squared_error(target, pred)) # to compute RMSE
    mae = mean_absolute_error(target, pred) # to compute MAE

    df_perf = pd.DataFrame(
        {
            "RMSE": rmse,
            "MAE": mae,
            "R-squared": r2,
            "Adj. R-squared": adjr2,
        },
        index=[0],
    )

    return df_perf

# Checking model performance on train set
print("Training Performance\n")
model_train_perf = model_performance_regression(x_test,pd.Series(y_test.flatten()),
pd.Series(final_pred.flatten()))
model_train_perf

X = data_deck.drop(['$EO', '$EW'], axis = 1)
y = data_deck[['$EO', '$EW']]

x_train, x_test, y_train, y_test = train_test_split(X, y, test_size=0.2, random_state = 1)

```

```
from sklearn.preprocessing import StandardScaler
```

```
sc_x = StandardScaler()
sc_y = StandardScaler()
x_train_sc = sc_x.fit_transform(x_train)
y_train_sc = sc_y.fit_transform(y_train)
x_test_sc = sc_x.fit_transform(x_test)
y_test_sc = sc_y.fit_transform(y_test)
```

```
from sklearn import preprocessing
```

```
scaler_Y = preprocessing.StandardScaler().fit(y)
```

```
backend.clear_session()
np.random.seed(42)
import random
random.seed(42)
tf.random.set_seed(42)
```

```
# Initializing the ANN
```

```
model1 = Sequential()
# This adds the input layer
model1.add(Dense(activation = 'relu', kernel_initializer='he_uniform',input_dim =
x_train_sc.shape[1], units=128))
model1.add(Dropout(0.3))
```

```
#Add 2nd hidden layer
```

```
model1.add(Dense(64, activation='relu', kernel_initializer='he_uniform'))
```

```
#Add 3rd hidden layer
```

```
model1.add(Dense(32, activation='relu', kernel_initializer='he_uniform'))
model1.add(Dropout(0.3))
```

```
#Add 4th hidden layer
```

```
model1.add(Dense(32, activation='relu', kernel_initializer='he_uniform'))
```

```
model1.add(Dense(2, activation='linear'))
```

```
optimizer = tf.keras.optimizers.SGD(0.001)
model1.compile(optimizer=optimizer, loss='mean_squared_error', metrics =['mae'])
model1.summary()
```

```
from keras.callbacks import EarlyStopping
```

```
early_stopping_monitor = EarlyStopping(monitor='val_loss',min_delta=0.001, patience=5)
```

```

history=model1.fit(x_train_sc, y_train_sc,
                  validation_split=0.3,
                  epochs=75, verbose=1, batch_size = 10)
#Plotting Train Loss vs Validation Loss
plt.plot(history.history['loss'])
plt.plot(history.history['val_loss'])
plt.title('model loss')
plt.ylabel('Loss')
plt.xlabel('Epoch')
plt.legend(['train', 'validation'], loc='upper left')
plt.show()

y_pred_scale = model1.predict(x_test_sc)
final_pred = scaler_Y.inverse_transform(y_pred_scale)
pred_df = pd.DataFrame(final_pred, columns=['$EO_pred', '$NO_pred'])
df_compare = pd.concat([pred_df, y_test], axis=1)

#Checking model performance on train set
print("Training Performance\n")
model_train_perf = model_performance_regression(x_test,y_test, pred_df)
model_train_perf"

```

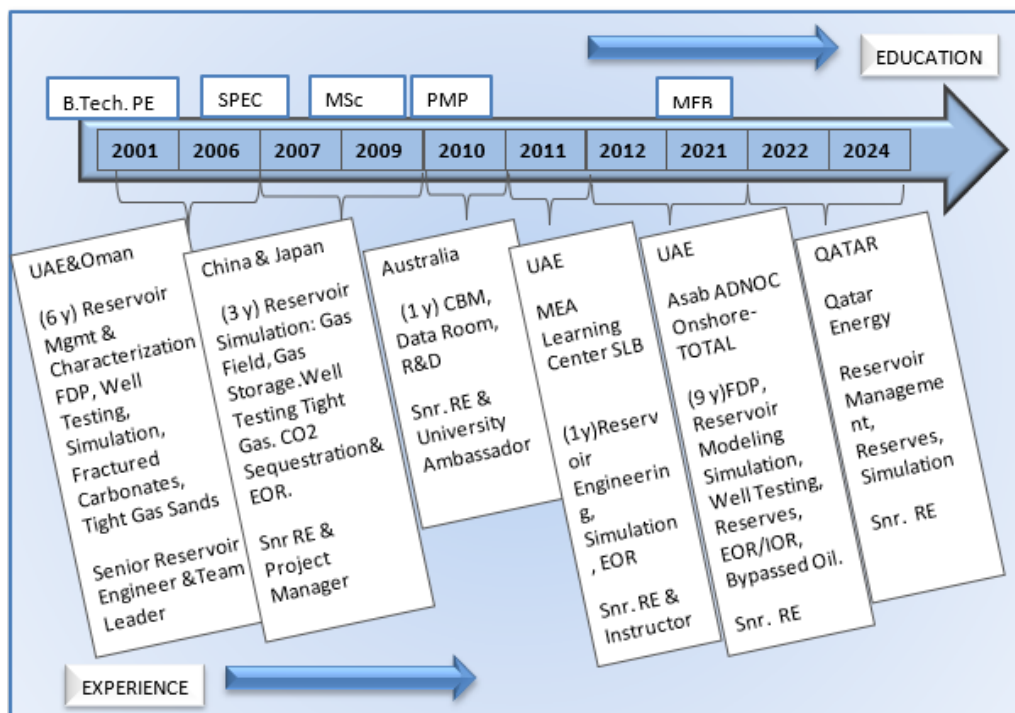
LIST OF PUBLICATIONS

1. Tony Thomas, Pushpa Sharma, Dharmendra K. Gupta, Meta-analysis of Rock, Brine, Oil Interactions and Expert System Development, MATPR-D-21-04934R1, Materials Today: Proceedings ,2022 DOI:[10.1016/J.MATPR.2021.07.140](https://doi.org/10.1016/J.MATPR.2021.07.140)
2. Tony Thomas, Pushpa Sharma, Dharmendra K. Gupta, “Use of AI tools to Understand surface-interaction based EOR processes,” Applied Computing and Geosciences., vol. 17, 2023, 100111, ISSN 2590-1974, DOI: [10.1016/j.acags.2022.100111](https://doi.org/10.1016/j.acags.2022.100111)
3. Tony Thomas, Pushpa Sharma and Dharmendra K. Gupta, “Understanding & Screening of DCW through Application of Data Analysis of Experiments and ML/AI,” Energies, vol. 16, no. 8, p. 3376, Apr. 2023, DOI: [10.3390/en16083376](https://doi.org/10.3390/en16083376)



TONY THOMAS - RESUME

A multi-faceted petroleum engineer; 20+ years of diverse experience in reservoir engineering & simulation, field development, project gate reviews, resource maturation, eor, ccus, reserves, data analysis/ml, renewable energy, certified by society of petroleum engineers & project management institute



TECHNICAL SKILL SET

- Highly varied experience (reservoir modeling, static/dynamic data integration, classical analysis: Volumetrics/Reserves, Material Balance, Decline Curve Analysis, history matching, forecast and sensitivity analysis) in the Exploration, Development (Resource Maturation) , Production Optimization studies(Water Flood/EOR) of different fields (clastic, carbonates, tight gas, heavy oil). FDP update, optimization and well planning and delivery. CO2 Sequestration feasibility studies.
- Well Test Analysis-Analytical and Numerical methods-fractured reservoirs and hydraulically fractured wells for Tight gas fields.
- EOR mechanisms assessment through application of compositional simulations.

- Comprehensive Reservoir Characterization(Matrix/Fault/Fracture) through using Logging data, Well Test Analysis, Reservoir Simulation and Modeling
- Reservoir Surveillance and Monitoring of Performance – involving Well-wise Analysis through Production Logging, Pulsed Neutron Logging, Formation Testing and Sampling and integration of static and dynamic data
- CO2 Sequestration through EOR and storage in Oil & Gas fields, deep saline aquifers and CBM – Site Screening and Conceptual Design.
- Performing reservoir simulation and surface network modeling in unconventional reservoirs-CBM.
- Reserves Estimation as per SPE Standard Guidelines
- Energy Policy Development & Analysis
- Decision Risk Analysis using @Risk and Precision Tree.
- Training and mentoring of junior reservoir engineers

EDUCATION

- University of Petroleum and Energy Studies. India
(Ongoing) Research on AI applications in EOR Screening
- Heriot Watt University, Edinburgh, Scotland, UK
MSc in Petroleum Engineering
- SPE Certified **Petroleum Professional**
- University of TULSA, Oklahoma, USA
Masters in Energy Business (Beta Gamma Sigma)
- Certified **Project Management Professional**
- Indian School of Mines, Dhanbad, India
B.Tech. in Petroleum Engineering

Email: tonythomasa@gmail.com



PLAGIARISM CERTIFICATE

1. We **Dr. Pushpa Sharma** (Internal Guide) and **Dr. D.K. Gupta** (Co-Guide) certify that the Thesis titled **Modeling of Low Salinity Enhanced Oil Recovery Applying Artificial Intelligence** submitted by Scholar **Mr. Tony Thomas** having SAP ID **500065488** has been run through a Plagiarism Check Software and the Plagiarism Percentage is reported to be **10%**
2. Plagiarism Report generated by the Plagiarism Software is attached.

Pushpa Sharma
19/07/2024

Signature of the Internal Guide

D.K. Gupta
19/07/24

Signature of Co Guide

Tony Thomas
19/07/2024

Signature of the Scholar

MODELING OF LOW SALINITY ENHANCED OIL RECOVERY APPLYING ARTIFICIAL INTELLIGENCE

ORIGINALITY REPORT

10%

SIMILARITY INDEX

8%

INTERNET SOURCES

7%

PUBLICATIONS

4%

STUDENT PAPERS

PRIMARY SOURCES

1

www.researchgate.net

Internet Source

1%

2

Tarek Ahmed. "Principles of Waterflooding",
Elsevier BV, 2019

Publication

<1%

3

doi.org

Internet Source

<1%

4

utpedia.utp.edu.my

Internet Source

<1%

5

Submitted to University of Adelaide

Student Paper

<1%

6

"Proceedings of the International Field
Exploration and Development Conference
2019", Springer Science and Business Media
LLC, 2020

Publication

<1%

7

link.springer.com

Internet Source

<1%